Xinquan Zhou
PhD Student
UMR8148 GEOPS
xinquan.zhou@universite-paris-saclay.fr
Paris Saclay University
91405 ORSAY Cedex, France

Dear Dr. Yin,

Please, find attached our revised manuscript entitled "Dynamics of primary productivity in the northeastern Bay of Bengal over the last 26,000 years" by Zhou et al., which I would like to resubmit as an Article to Climate of the Past. We truly thank the 2 reviewers for their constructive remarks. Their expertise in the field gave us a chance to take some aspects of our work a step further and provide, what we feel is a much improved manuscript. Particularly, we followed the proposition made by Reviewer #1 regarding the structure of our manuscript and as previously explained in our reply to reviewers, an entire chapter is now devoted to the results that are now discussed regarding the three time-intervals highlighted by Reviewer #1 (the last glacial period, the last deglaciation and the Holocene). Besides, model outputs are now fully integrated with proxy data which help better setting our arguments up and present our findings in a clearer way.

In the current revised manuscript, all the fundamental changes mentioned in our previous responses to reviewers have been carefully added, so that the message remains unchanged. We have however merged some figures and removed a few supplementary ones to provide what we feel is a much clearer manuscript. You will find below our previous response to the reviewers with changes marked.

Based on the positive feedbacks we received from the referees, highlighting the novelty of our study, we are further confident that our manuscript, will be of interest to the broad climate science community and will provide a novel insight into a yet overlooked aspect of the relationship that exists between the Indian Monsoon and Primary Productivity in the past.

Our resubmission consists of a central text, eight colour figures and five supplementary figures.

On behalf of the co-authors,
Yours sincerely,
Xinquan Zhou

Response to Reviewer #1

Dear reviewer,
Please find below our answers to the constructive remarks you raised regarding our manuscript. They all have been carefully considered and will provide what we feel is a much improved manuscript. You will also find all of the modified figures of the new manuscript and Supplementary Material.

Comment #1 (C1): *The overall structure of the manuscript and occasional lack of clarity in some sections is a major shortcoming of the manuscript. For example, results from the model outputs are not fully integrated with proxy data and are rather independently summarized. Although, this manuscript presents an important dataset, which is of interest for the scientific community, some of the interpretations need to be significantly refined and I find few of them not convincing at all (see my comments on the discussion section below). The fact that only figures are provided as the supplementary information is also unhelpful and I believe a short text summary is warranted. To summarize, the manuscript in its present form does not meet the following CP peer review guidelines/criteria:*
1. Are substantial conclusions reached? Needs to be improved (see detailed comments below). 2. Are the results sufficient to support the interpretations and conclusions? In general yes but some of the interpretations need to be improved. 3. Is the overall presentation well structured and clear? Needs to be improved. 4. Is the language fluent and precise? In general yes but there is occasional lack of clarity in some sections. 5. Should any parts of the paper (text, formulae, figures, tables) be clarified, reduced, combined, or eliminated? Some discussion sections can be combined to improve clarity and train of thought. 6. Is the amount and quality of supplementary material appropriate? The supplementary information lack sufficient information and needs to be significantly improved.

Reply #1 (R1): We agree with Reviewer #1 that despite the important dataset we provide in the manuscript, some changes in the structure of the manuscript might help describing our results more clearly, and improving our interpretations and conclusions. Now we clearly separate the result and discussion sections (new sections 4 and 5, respectively), and fully discuss the model outputs together with the empirical data in subsections 5.1 to 5.3 (see our Reply 6). This change relies on the relocation of figures from the Supplementary Material to the main core of the manuscript, and on the addition of new figures related to simulated Primary productivity (PP) and oceanic profiles in the results. The number of figures in the supplementary Material is thus reduced, and we significantly improved the explaining text for all of the remaining figures.

C2: *Line 30: The way the monsoon is currently defined need to be improved.*
Here, the monsoon is practically presented as a giant sea breeze that is responsive to changes in the land-sea thermal contrast alone and excludes the more complex aspects of the monsoon and its relation with the tropical ocean on seasonal to interannual to decadal timescales (e.g. ENSO and IOD).

R2: In addition to the simple 'sea-breeze' description of the monsoon, there is, indeed, a description that focuses on its energetic aspects and provides a broader overview of the mechanisms behind monsoon variability (Schneider et al., 2014). In the revised manuscript, we now mention both aspects, and added a few sentences to mention the interannual and decadal changes of monsoon related to ENSO and IOD variability, an important aspect of Indian Monsoon natural variability. It also echoes the seasonal and interannual PP changes we describe in the introduction. However, since the present manuscript chiefly deals with orbital to millennial climate changes, we chose to not fully detail this aspect in the introduction.

C3: *Line 40–53: The subsequent section provides a detailed summary of the oceanographic setting in the Bay of Bengal and Andaman Sea. To be more articulate and improve clarity, it's probably best that comparisons within the Arabian Sea and differences with in the broader Northern Indian Ocean oceanography are presented in the introduction section.*

R3: We totally agree with Reviewer #1. Indeed, in this section, we highlight the specific patterns of PP in the Bay of Bengal and the Andaman Sea compared to the Arabian Sea. PP in the Arabian Sea is particularly high compared to the Bay of Bengal and the Andaman Sea during Summer Monsoon, due to the occurrence of important coastal upwelling that bring nutrients into the photic zone. To the contrary, summer monsoon is associated with important freshwater inputs in the Bay of Bengal that cause salinity-driven, water column stratification, resulting in a reduced nutrient input to the upper water column, and thus subdued PP. Such broad PP difference is an important aspect that we also highlight when discussing about past evolution (new section 5) and compare our results with previous works (Schulz et al., 1998; Ivanochko et al., 2005). It seems therefore very important to mention such modern pattern in the introduction.

Lines 40-53 might not be clear enough, particularly when dealing with acronyms such as the Andaman Sea or Arabian Sea. Since we don't refer to the Andaman Sea very often in the manuscript, we only use diminutives for the Bay of Bengal and the Arabian Sea. We also describe more clearly the relationship that actually exists between the upwelling system and PP in the Arabian Sea, adding a few sentences and references (~~Bartolacci and Luther, 1999~~ Anderson and Prell, 1992; Madhupratap et al., 1996; Gardner et al., 1999; Wiggert et al., 2005~~; Liao et al., 2016~~) on this aspect. We are aware that in the western Arabian Sea, the summer upwelling system is quite complex, with for example, a branch that can transport nutrient to the central part of the Arabian Sea. However, we prefer to not mention PP distribution in a very detailed way, because we are not able to discuss its evolution and distribution with such details in the past due to a lack of high-resolution PP.

C4: *2) Site description and oceanographic setting*
This section provides a detailed summary of the oceanographic setting of the studied site and is well written.
Are there any notable differences in seasonal PP variability between the Bay of Bengal and the Andaman Sea? Perhaps a sentence or two addressing the above question will be helpful.

R4: Geographically and oceanographically speaking, our site is located at the junction between the northeastern Bay of Bengal and the northern Andaman Sea. These two parts represent open oceanic settings and are both influenced today by low SSS seawaters originating from the Irrawaddy-Salween river system (Figs. 1g, f). They are both characterized by annual rates of PP around 100-140 gC m^{-2} yr^{-1} (Fig. 1h, i). Very high annual PP (up to 340 gC m^{-2} yr^{-1}) can be observed in coastal settings that are under the direct influence of river-driven nutrients, but these nutrients are actually consumed in these proximal environments and do not reach the studied site. Such configuration may have changed in the past particularly during the LGM when sea-level was relatively low (see Reply 8). However, ~~there is no reason why the northeastern Bay of Bengal and the northern Andaman sea should behave in a completely different way under such conditions (Fig. 1), and~~ the most likely forcing factor that might drive orbital and millennial PP changes is monsoon, modulated by sea-level, insolation and/or AMOC dynamics. Our core location is therefore suitable to test the relationships between these parameters. As suggested by Reviewer #1, we added a sentence to highlight such similarities between the northeastern Bay of Bengal and the northern Andaman Sea, in the new version of the manuscript.

C5: *3) Materials and Methods*
This section provides a detailed summary of the methodology and is generally well written. However, information provided on age model reconstruction is insufficient and citation of Figure 2 is not very useful either. I suggest that the authors provide a summary of the age model including changes in the rate of sedimentation etc. This can be included in the same section or in the form of a supplementary material.

R5: The age model used herein has originally been described in Marzin et al., (2013), and has latterly been used by Yu et al., (2018) and Ma et al., (2019). Indeed, Marzin et al. (2013) devoted an entire chapter to this chronological aspect (in their chapter 2.1), and already described all of the important information required herein, such as the sedimentation rate (represented in their Fig. 3). Therefore, we decided to refer to Marzin et al. (2013) but we added a figure including the sedimentation rates of the core within the Supplementary Material (new Figure S1). We discuss this part with extreme caution to avoid any confusions regarding the age model, and clearly demonstrate its robustness. The Figure 2 has been modified compared to the initial submission. It is now new Figure 2~~3~~ that includes relative abundance of coccoliths and reconstructed PP.

C6: *4) Results and discussions*
This section of the manuscript is poorly structured and in my opinion, the weakest part of the manuscript. For example, a large chunk of the text (e.g. section 4.3, section 4.3.1: lines 300 – 317) should have been included in the methodology section. This has made the discussion section overall very descriptive and lacking in substance, and most crucially hard to follow. One way of overcoming this predicament is to divide this section in to two separate sections (i.e., Results and Discussions). For example, the proxy data and model data results can be grouped into two subsections and the discussion section should focus on the dynamics of PP variability over the studied time interval. The Discussion section should also integrate both proxy data and model inferences to build a more coherent understanding of PP variability over the last 26 kyrs.
Looking at the PP record, it is clear that there are three distinct time intervals that can be discussed separately including the highly variable LGM (?), the last deglaciation period marked by an abrupt shift in PP centered around the BA and the Holocene period, which displays a more gradual change. Therefore, dividing the discussion section accordingly and zooming on these three distinct periods will significantly improve clarity

R6: We believe that the proposition made by Reviewer #1 regarding the structure of our manuscript will certainly clarify it, therefore helping to improve the description of our results as well as the interpretations. Therefore, we changed our manuscript in the light of the suggestions. An entire chapter is now devoted to the results. In the discussion, empirical data and model outputs are interpreted simultaneously, which is helpful to build a more coherent scheme behind PP variability. Our results are now discussed regarding the three time-intervals highlighted by Reviewer #1.

Below is the new structure of chapters 4 and 5:

4. Results

4.1. Coccolith abundances and reconstructed primary productivity over the last 26 kyr~~s~~

4.2. Simulated primary productivity and physicochemical profiles ~~in the northeastern Bay of Bengal~~

5. ~~Forcing factors behind PP variations over the last 26 kyrs: the inputs of model-data comparisons~~Discussion: Forcing factors behind PP variations over the last 26 kyr as revealed by a model-data comparison

5.1. ~~During t~~The glacial period

5.2. ~~During t~~The last deglaciation

5.3. ~~During t~~The Holocene

In detail:

- In section 4.1, we present and describe coccolith species abundances and reconstructed PP (~~Figure 1 of Author Response (Fig. AC1)~~new Fig. 2).
- Section 4.2. relies on new IPSL-CM5A-LR figures dedicated to model results, that help understanding and improving model output interpretations i.e. i) simulated PP maps (~~Fig. AC2~~new Fig. 3), and ii) simulated vertical profiles of potential temperature, salinity, potential density, and nitrate content of the Ganges-Brahmanputra-Meghna and Irrawaddy-Salween river mouth systems (new Figure 4) and of the northeastern Bay of Bengal under four experimental runs (~~Fig. AC3~~new Fig. 5), under two and four experimental runs, respectively. It~~that~~ helps discussing climate conditions for the LGM (LGMc), the Heinrich Stadial 1 (LGMf), and the Mid-Holocene (MH), compared to preindustrial (CTRL). We show the results of annual mean, summer seasons mean (from June to August, JJA) and winter seasons mean (from December to February) for all these specific time intervals, in order to evaluate PP changes during the monsoonal seasons.
- In sections 5.1 to 5.3., we compare our reconstructed PP signal with the published empirical records ~~previously documented in Fig. AC4~~, and with TraCE-21 transient simulations of the upper water column stratification, SSS, SST and net precipitation (P-E)~~, previously documented in Fig. 5~~(new Fig. 6). We have mMerg~~eding~~ our previous Figures 4 and 5 into the~~a~~ new Figure 6 ~~(Fig. AC4), allows~~ to better discuss PP variations in the monsoonal context. We also combine atmospheric and oceanic outputs of the four experiments run together with the simulated PP obtained by the IPSL-CM5A-LR model (new Fig. 7) in order to better discuss and interpret our reconstructed PP during the last glacial period (section 5.1~~; Fig. AC5, AC6~~), the last deglaciation (section 5.2~~; Fig. AC7, AC8~~) and the Holocene (section 5.3~~; Fig. AC9~~), as proposed by Reviewer #1. A new Figure 8 merged from our previous Figures 6 and 8, has been put in section 5.2.

At last, we moved lines 300 – 317 and all the parts referring to the description of the chosen simulated variables to the section 3 (Material and Methods).

***C7:** Lines 205 – 208: the authors write 'at millennial-scale, large magnitude PP oscillations, are observed during the deglaciation (19–11 kyr BP), showing similar features than those found in the Greenland ice core δ18O record, representing the rapid climatic changes in north hemispheric high-latitude areas (Fig. 2; Stuiver and Grootes, 2000).'*
But it is stated in section 3.1 that the age model, although primarily based on 31 AMS 14C dates, it was still tuned to GISP2 Greenland ice core δ18O curve. Can this be considered circular reasoning?

R7: We thank Reviewer # 1 for highlighting this peculiar aspect. Indeed, it might be seen as a circular reasoning. However, our micropalaeontological data are well in phase with numerous geochemical data obtained elsewhere in the Tropical Indian Ocean and the Chinese continent, based on sediment cores and speleothems with totally independent age models, respectively. They also match very well TraCE-21 and IPSL-CM5A-LR outputs. Besides, as mentioned above (Reply 5), the age model of core MD77-176 has already been used by Marzin et al., (2013), Yu et al. (2018), and Ma et al. (2019), i.e. papers discussing geochemical data at regional and global scales. All these highlights point to a robust age model and demonstrate that our micropalaeontological data can ~~be~~ properly be discussed in the light of the rapid climatic changes recorded in the northern high latitudes. To avoid any confusion, we rephrased this part of the manuscript focusing on the relationship that exists between PP and SSS of MD77-176.

***C8:** Lines 255 – 229: the authors write, 'Several pieces of evidence suggest that millennial- scale variations of PP between 26 and 19 kyr (i.e. before the LGM) chiefly resulted from wind-driven mixing. First, high PP values are reached during intervals of low surface water salinity. If these PP variations (and upper water column stratification) were primarily driven by precipitation–evaporation changes, the opposite relationship would be expected, and PP would peak at periods of higher salinity because of the weaker barrier layer effect'.*

a) Can you independently verify if the wind-driven mixing in the Northern Indian Ocean was enhanced during the LGM?
b) Which are the intervals of low salinity during the LGM?
c) Isn't the LGM Andaman Sea significantly more saline compared to other periods such as the Holocene?
d) How does precipitation minus evaporation impact PP variability in general?
e) What inferences can be made on LGM PP variability from the LGM experiments?

R8: We appreciate these remarks that rise further questions and clearly help us improving our interpretations. We first answer your questions one by one and then develop a more detailed response that echoes question a–e.
a) We checked the modeling outputs of surface winds during the both monsoonal seasons. It shows stronger summer wind and weaker winter wind intensities over the Bay of Bengal and Andaman Sea during the LGM (~~Fig. AC6~~new Fig. 7i, j).

b) The short intervals of low salinity are shown by the SSS record of MD77-176. They are recorded at ~21 kyr BP and ~23 kyr BP (~~Fig. AC4~~new Fig. 6h). However, it is not possible to test such specific short-term intervals with model outputs that give mean states of chosen parameters during the LGM.
c) The modeling outputs show that generally, Bay of Bengal and Andaman Sea behave the same way. That is only in the northeastern Bay of Bengal, close to the coasts, that a significant difference may be seen. Indeed, according to these model outputs, they are both getting saltier during the LGM, while the northeastern BoB is unchanged or a little fresher (~~Fig. AC5~~new Fig. 7h). The Andaman Sea doesn't appear specifically more saline than the BoB during that time interval.
d) According to IPSL-CM5A-LR outputs, it appears that if the net precipitation is lower during the LGM, the Bay of Bengal and Andaman Sea might get saltier and PP might increase due to weaker salinity stratification.
e) The LGMc experiment gives a mean state of PP during LGM. Generally, it shows higher PP in the BoB and the Andaman Sea. Under weaken AMOC condition, LGMf experiment shows higher PP compared to LGMc matching our reconstructed PP results from the LGM to the Heinrich 1.

General reply:

During glacial times (26–19 kyrs), high (low) PP intervals do match low (high) SSS ones, as shown by low (high) values in seawater oxygen anomalies recorded at the same site (Marzin et al., 2013; ~~Fig. AC4~~new Fig. 6h, i).

There is no doubt that the South Asia and the North Indian Ocean are drier during the LGM due to relatively lower precipitation over the South Asia, as demonstrated by previous empirical data (Dutt et al., 2015; Contreras-Rosales et al., 2014; Kudrass et al., 2001) as well as numerical outputs here (~~Figs. AC4, AC5~~new Fig. 7f, g). However, the outputs of IPSL-CM5A-LR simulations, together with TraCE-21 ones show that, compared to preindustrial, weaker winter winds, stronger summer winds, and saltier sea surface conditions, generally prevailed in the Bay of Bengal and the Andaman Sea during the LGM (LGMc in ~~Fig. AC5~~ new Fig. 7). These results suggest that the interpretation we have made for the last deglaciation and the Holocene, stating that a stronger summer monsoon and/or a weaker winter monsoon, induce increased precipitation, decreased SSS and thus, stronger salinity stratification and subdued PP is not always verified, and particularly during the LGM. In such a case, we cannot exclude that stronger and drier summer winds during that time interval (as suggested by model here), could eventually lead to enhanced sea-surface mixing, thus triggering upper water mixing, higher SSS, and higher PP as observed in the Arabian Sea today. However, as mentioned in the introduction of our manuscript, the Arabian Sea behave in a very different way than the Bay of Bengal, notably thanks to the development of massive upwelling on its western coasts, and the direct comparison of both basins may be questioned. Unfortunately, we cannot test such sea-surface mixing hypothesis with TraCE-21 or IPSL-CM5A-LR outputs, so far.

Spatial discrepancies of SSS are also found with model outputs. This is particularly the case when dealing with the northeastern Bay of Bengal and northern Andaman Sea areas. First, models in PMIP3 (Braconnot et al., 2012) show different results of SSS for the LGM: some models show fresher water, while others depict saltier conditions ~~(Fig. AC10)~~. Second, when dealing with the outputs of IPSL-CM5A-LR, such area (that include our core site) has very limited SSS increases during the LGM, if it doesn't show sometimes SSS decreasing trends (~~Fig. AC5~~new Fig. 7g). Such discrepancies have also been reported once by empirical data. Indeed, Sijinkumar et al. (2016) depict lower SSS in the northern

Andaman Sea during the LGM, i.e. under lower sea-level conditions. It may highlight the complex area that is the northeastern Bay of Bengal and northern Andaman Sea due to the Irrawaddy mouth influence. It might also partly explain the millennial-scale relationship documented at our core between SSS and PP at that time, i.e. under relatively low sea-level when site MD77-176 is located in a more proximal environment. Indeed, one cannot exclude that under such conditions, the PP increases (decreases) observed when SSS decreases (increases), reflect an increases (decreases) of nutrient together with freshwater inputs from the Irrawaddy river, respectively. Such assumption is confirmed in ~~Figures AC2 and AC3~~new Fig. 3g ~~–~~where PP strongly increases ~~(Fig. AC2)~~, and in the new vertical oceanic profiles we provide (Fig. 5e,j), whe~~ren~~ increased PP are accompanied by increased nutrient in surface layers thanks to a more proximal environment at our studied site highlighting a change ~~vertical profiles clearly change~~ from an open ocean type to a more coastal one ~~one (Fig. AC3)~~. Our scenario appears therefore to be a suitable explanation for the PP pattern obtained herein during the LGM.

However, in all cases, it seems difficult at that point, to deeply compare thoroughly (and discuss) the millennial PP changes obtained at our core site, to mean state simulations of local PP and SSS, obtained for the northern Bay of Bengal and Andaman Sea during the LGM. Additional high-resolution PP records and further numerical simulations are required in the area, in order to discuss this issue properly. ~~As an example, a PP record further south in the Andaman Sea, i.e. far away from river mouth influences, (Zhou et al., unpublished) clearly shows higher PP from 30 to 19 ka, under saltier conditions, and does not show strong short-term fluctuations as recorded at site MD77-176.~~

~~The influence of drier and stronger summer winds together with the influence of nutrient and freshwater inputs from the Irrawaddy river behind PP variability during the LGM, are therefore evoked in the manuscript, but with extreme caution.~~In conclusion, we now interpret the reconstructed PP variations observed at site MD77-176 during the last glacial as the result of nutrient conditions changes within the upper layers, thanks to both, lower sea-level and enhanced influence of the Irrawaddy-Salween river mouth system.

C9: *In section 4.1 (line 217): The authors write that, 'PP peaks are related to low SSS intervals before the LGM, and high SSS intervals over the last 19 kyr'.*
Although, PP did not significantly change over the course of the Holocene, there appears to be a clear discrepancy between the gradual monsoon intensification over the Holocene and PP variability. PP variability over the course of the last deglaciation and the Holocene are clearly different. Proxy data shown in Figure 2 suggest that estimated PP has lower valued during the Mid-Holocene (~90 gC m-2 yr-1) compared to late – Holocene (~130 gC m-2 yr-1). This, however, is not discussed in any detail and the way the discussion section is structured is at fault again.

R9: We agree with Reviewer #1. While the mechanisms controlling PP variations during the last deglaciation and the Holocene are similar and related to salinity stratification, PP variability is different over these two time intervals. They are characterized by rapid and large amplitude PP changes during the deglaciation, and rather gradual PP trends during the Holocene. Both periods are under the influence of insolation and AMOC forcing that impact land-sea thermal distribution over low latitudes, thus moderating monsoon strength, and controlling oceanic stratification and PP. However, to the different of the Holocene, rapid changes occur in the AMOC strength during the deglaciation, and they are clearly reflected in the Indian monsoon and PP dynamics at that time.

Therefore, such different PP patterns between the last deglaciation and the Holocene is clearly related to AMOC vs insolation imprints other the last 19 kyrs. Rapid changes in PP patterns during the last deglaciation clearly reflect the rapid changes in the AMOC strength. To the opposite, long-term changes in PP during the Holocene most probably reflect long-term changes in insolation and associated feedbacks with the ocean-atmosphere system. We now discuss the deglacial and Holocene PP variabilities separately, in our revised sections 5.2 and 5.3, respectively.

***C10:** In section 4.1 (lines 204 – 205): it is briefly mentioned that PP variability shows 'an opposite trend compared to insolation (Fig. 4a, h)' and in section 4.3.1 it is stated that 'insolation is the main climate forcing factor during the Holocene'.*
Why do we have the monsoon peaking later during the mid-Holocene lagging maximum Northern Hemisphere summer insolation by few kyrs then? The lagged response of the monsoon to insolation forcing suggests that orbital scale monsoon variability is more complex (see Clemens et al., 2003; Caley et al., 2011; Gebregiorgis et al., 2018). Having this in mind, I would therefore encourage the authors to have a more critical outlook on PP variability over the course of the Holocene. I also recommend including Figure S3 – S6 in the main text body and can be used to gain some unique insights on LGM, deglacial and Holocene PP variability. Perhaps Fig. 3 can be moved to the supplementary section.

R10: During the Holocene, our PP record shows a minimum at ~6–8ka, lagging of about few centuries~~3.5–5.5 kyr~~, the maximum North Hemisphere august insolation curve. However, it is clearly in phase with geochemical records obtained in the area that document high PP in the Arabian sea (Schulz et al., 1998; Ivanochko et al., 2005) and high precipitation over South Asia during that time interval (Dutt et al., 2015; Contreras-Rosales et al., 2014; ~~Fig. AC4~~new Fig. 6). Such results show that during the Holocene, PP from the northeastern Bay of Bengal is highly related to monsoonal dynamic, and more particularly, precipitation. Summer winds triggers strong coastal upwelling and high PP in the Arabian Sea. They also transport moisture to the South Asia where the summer precipitation is strong. Such increase in precipitation causes strong salinity stratification over the northeastern Bay of Bengal and thus low PP.

The references cited in reviewer's comment argue for the hypothesis that tropical monsoon variability is dominated by, and responds directly to the North Hemisphere summer solar radiation, and point out the importance of internal climate forcing and oceanic feedbacks, such as latent heat export from the southern Indian Ocean. Clemens et al., (2003) particularly point out that the minima of SST in the southern subtropical Indian Ocean are synchronous with the maxima of summer monsoon, and the moderating effect of ocean thermodynamic features on monsoon circulation is important. In all cases this aspect is an (usually) inexplicable issue. ~~We have mentioned this lag in the revised section 5.3 of the manuscript, and interpret the Holocene period with caution. The modifications of supplementary figures are explained in Reply 25.~~

***C11:** Line 57: What 'fast changes'? Please rephrase.*

R11: We have rephrased to 'abrupt changes'

***C12:** Line 61: PP record or paleo-PP record. Stick with one for consistency.*

R12: We s~~S~~ticked with ‘PP record’.

***C13:** Line 61: Da Silva et al., 2017 is a relevant reference here.*

R13: We have cited this.

***C14:** Line 62: ‘tropical ocean ecology’ is very broad and I am not sure this is accurate as well. Perhaps Northern Indian Ocean ecology is more appropriate.*

R14: We agree with this suggestion and made the changes in the light of the comment.

***C15:** Line 73: ‘High-time-resolution’ or ‘High-temporal-resolution’? ‘High-resolution’ is a perhaps a better phrase.*

R15: We have rephrased to ‘high-resolution’

***C16:** Line 74: Why is it important that the ‘studied period covers a complete precession cycle’? This sentences need to be qualified or delete otherwise.*

R16: We’ve removed this sentence.

***C17:** Line 80: ‘interpret’ is perhaps a better word here than ‘analyze’.*

R17: We agree with this suggestion and made the changes when necessary.

***C18:** Line 199–200: ‘At orbital scale’ – remove.*

R18: It has been done.

***C19:** Line 202: use ‘maximum or minimum Northern Hemisphere (NH) summer insolation’ instead of low or high insolation with no reference to the latitude or the season.*

R19: It has been done.

***C20:** Line 205: ‘On millennial timescale...’*

R20: It has been done.

***C21:** Line 211: ‘Synchronous vs. asynchronous’ rather than ‘Negatively vs. positively correlated’ and of course ‘correlation’ being a statistical term.*

R21: We agree with this suggestion and made the changes in the light of the comment.

***C22:** Line 290–291: Rephrase or remove*
'During the Holocene, insolation is the main climate forcing factor since other forcing (i.e. greenhouse gas, ice volume, coastlines, vegetation) are relatively stable after the deglaciation.

R22: We have removed this sentence.

***C23:** Line 291–292: Rephrase. Perhaps, a sentence along these lines will do: 'the response of the Indian monsoon to changes in orbital insolation has previously been examined using both AGCMs and ocean–atmosphere general circulation models. . .(Refs).)'*
'The mechanisms that force monsoon climate to change were studied by many modeling works (Refs).'

R23: We have removed this part, because of the new manuscript structure.

***C24:** Figures S1, S5, S6 are not cited in the main text and please add supplementary text to the supplementary information. Also make sure that the figures are in chronological order.*

R24: We ~~decided to keep all of the maps of TraCE-21 outputs in the Supplementary Material, and show all of~~only show the maps ~~from our~~ of IPSL-CM5A-LR results in the main text. ~~They have been slightly modified to match the new structure/discussion of the manuscript. All of the figures presented in the Supplementary Material are summarized, within detailed captions.~~

R25 (modification of supplementary figures 3 to 6):
1) ~~Fig. S3 have been modified and moved to the main text (Figs. AC5, AC6, AC8, AC9)~~The figure showing IPSL-CM5A results have been merged and moved to the main text (new Fig. 8). We show four groups of maps, which are the CTRL results as well as the differences between LGMc and CTRL, LGMf and LGMc, MH and CTRL. The variables are annual net precipitation (precipitation minus evaporation), annual SSS, annual potential gradient between 200 and 5 m, JJA surface wind speed and DJF surface wind speed.
2) ~~For Figs. S4 to S6, we have removed the results of ORB simulation as they are similar to the FULL simulation, and removed the results of MWF_BA minus MWF_HS1 as well, since they are similar to the results of TraCE_LGM minus MWF_HS1. Therefore, for the maps of TraCE-21 simulations, we show five groups of maps in the Supplementary Material which are the LH, and differences between MH and LH, LGM and LH, BA and HS1, MWF_HS1 between LGM. We show the same variables as IPSL-CM5A-LR. The modified supplementary figures can be seen from Fig. AC11 to AC16.~~We have removed the maps of TraCE-21 as they are similar to the IPSL-CM5A results.

References

Anderson, D. M. and Prell, W. L, 1992. The structure of the southwest monsoon winds over the

Arabian Sea during the late Quaternary: observation, simulations, and marine geologic evidence, Journal of Geophysical Research, 97, 15481–15487.

~~**Bartolacci and Luther, 1999.** Patterns of co-variability between physical and biological parameters in the Arabian Sea. Deep-Sea Research II, 46, 1933–1964.~~

Braconnot et al., 2012. Evaluation of climate models using palaeoclimatic data, Nature Climate Change, 2, 417– 424.

Clemens and Prell, 2003. A 350,000 year summer-monsoon multi-prosy stack from the Owen Ridge, North Arabian Sea. Marine Geology, 201, 35–51.

Contreras-Rosales et al., 2014. Evolution of Indian Summer Monsoon and terrestrial vegetation in the Bengal region during the past 18 ka. Quaternary Science Reviews, 102, 133-148.

Dutt et al., 2015. Abrupt changes in Indian summer monsoon strength during 33,800 to 5500 years B.P. Geophysical Research Letter, 42, 5526-5532.

Gardner et al., 1999. The role of seasonal and diel changes in mixed-layer depth on carbon and chlorophyll distributions in the Arabian Sea, Deep-Sea Research Ⅱ, 46, 1833–1858.

Ivanochko et al., 2005. Variations in tropical convection as an amplifier of global climate change at the millennial scale. Earth and Planetary Science Letter, 235, 302-314.

Kudrass et al., 2001. Modulation and amplification of climatic changes in the Northern Hemisphere by the Indian summer monsoon during the past 80 k.y. Geology, 29, 63-66.

Ma et al., 2019. Changes in Intermediate Circulation in the Bay of Bengal since the Last Glacial Maximum as inferred from benthic foraminifera assemblages and geochemical proxies. Geochemistry, Geophysics, Geosystems, 20, 1592-1608.

Madhupratap et al., 1996. Mechanism of the biological response to winter cooling in the northeastern Arabian Sea, Nature, 384, 549–552.

~~Liao et al., 2016. Potential new production in two upwelling regions of the western Arabian Sea: Estimation and comparison. Journal of Geophysical Research: Oceans, 121, 4487–4502.~~

Marzin et al., 2013. Glacial fluctuations of the Indian monsoon and their relationship with North Atlantic climate: new data and modeling experiments, Climate of the Past, 9, 2135–2151.

Schulz et al., 1998. Correlation between Arabian Sea and Greenland climate oscillations of the past 110,000 years. Nature, 393, 54-57.

Schneider et al., 2014. Migrations and dynamics of the intertropical convergence zone. Nature, 513, 45–53.

Sijinkumar et al., 2016. δ18O and salinity variability from the Last Glacial Maximum to Recent un the Bay of Bengal and Andaman Sea. Quaternary Science Reviews, 135, 79–91.

Wiggert et al., 2005. Monsoon-driven biogeochemical processes in the Arabian Sea. Progress in Oceanography, 65, 176–213.

Yu et al., 2018. Antarctic Intermediate Water penetration into the Northern Indian Ocean during the last deglaciation. Earth and Planetary Science Letters, 500, 67–75.

Figures

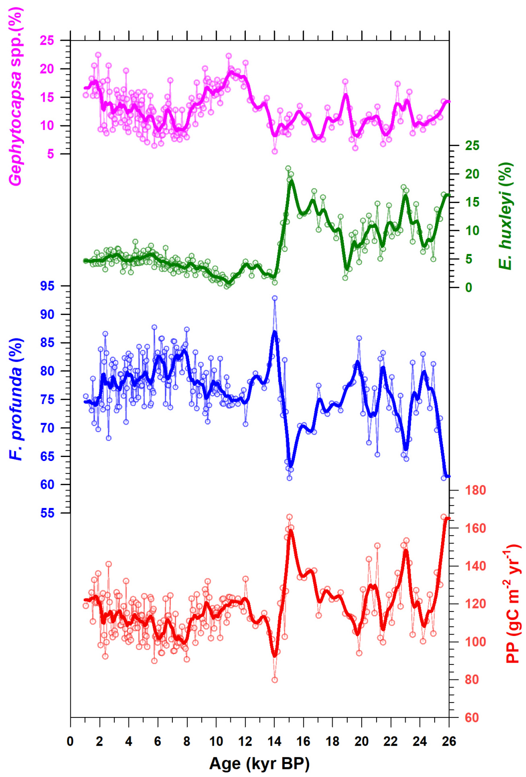

Fig. AC1. Relative abundance changes of main coccolith species and reconstructed PP.

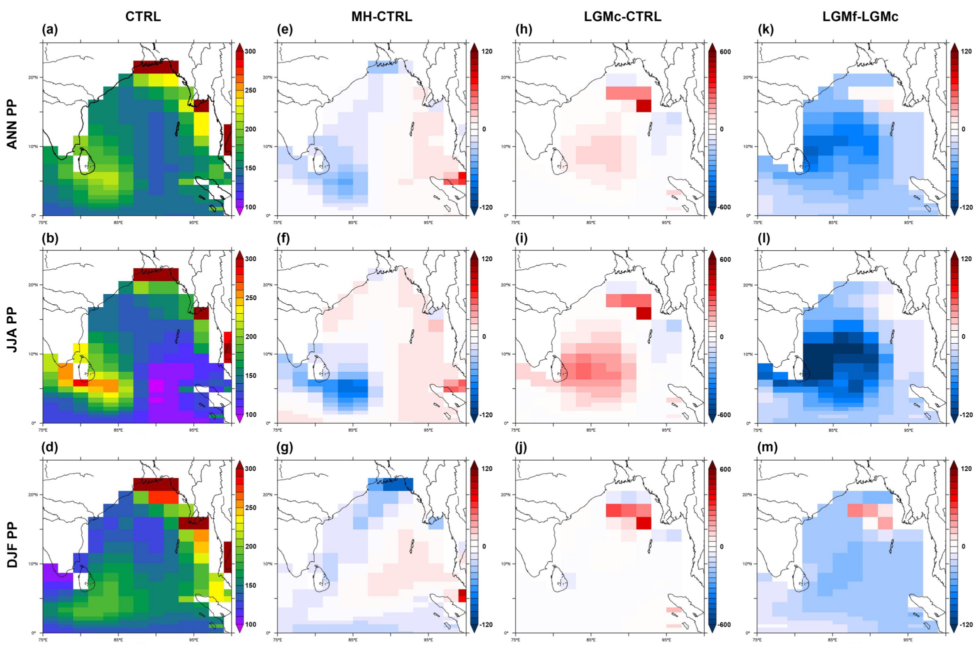

Fig. AC2. Simulated PP of CTRL and PP differences between MH and CTRL, LGMc and CTRL, and LGMf and LGMc. Results of annual mean, JJA mean and DJF mean are shown. PP is in gC m^{-2} yr^{-1}.

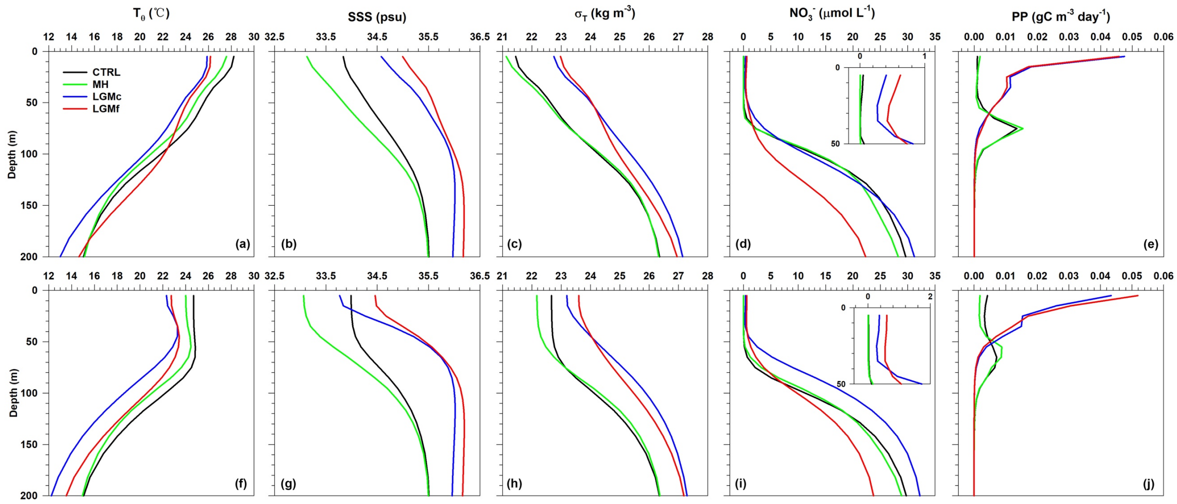

Fig. AC3. Simulated ocean profiles in four experiment run with IPSL-CM5A-LR. (a)–(e) Results of JJA mean. (f)–(j) Results of DJF mean. Grid of data extracting see Fig. AC12. The parameters shown here are potential temperature (T_θ), sea surface salinity (SSS), potential density (sigma-t, σ_T), nitrate content of seawater (NO_3^-) and total primary productivity (PP).

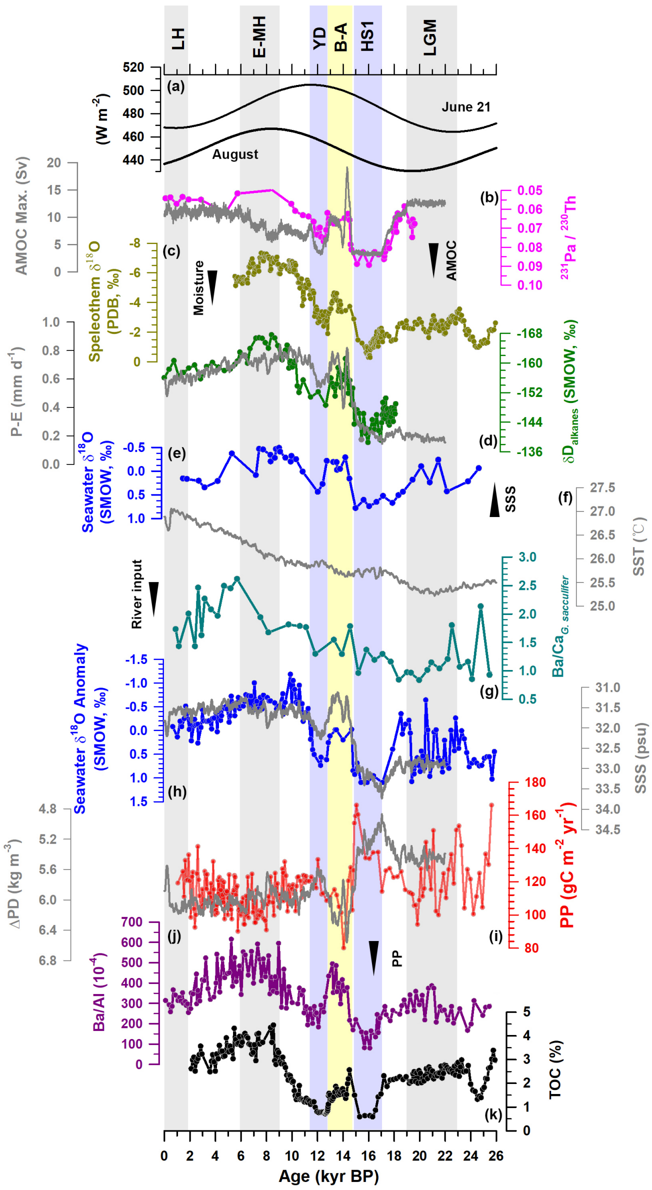

Fig. AC4. (a) August mean insolation and at 25°N. (b) AMOC strength indicated by $^{231}Pa/^{230}Th$ ratio of marine sediment from the western subtropical Atlantic Ocean (in pink, McManus et al., 2004). The changes of the maximum in the AMOC stream function below 500 m (AMOC strength) in TraCE-21 (in gray). (c) Mawmluh Cave speleothem $\delta^{18}O$ (Dutt et al., 2015). (d) Alkane δD in marine sediment, core SO188-342 (in green, Contreras-Rosales et al., 2014) and simulated precipitation minus evaporation of TraCE-21 (in gray). (e) Seawater $\delta^{18}O$ record of core RC12-344 (Rashid et al., 2007). (f) Simulated SST in the NE-BoB. Grids of data extracted see Fig. S2. (g) Ba/Ca ratios derived from mixed layer foraminifer species Globigerinoides sacculifer from core SK 168/GC-1(Gebregiogis et al., 2016). (h) Seawater $\delta^{18}O$ anomaly record of core MD77-176 (Marzin et al., 2013). (i) Estimated PP record of core MD77-176 (this study, in red) and simulated potential density gradient between 200 and 5m of TraCE-21 (in gray). (i) Ba/Al ratio of marine sediment, core 905 (Ivanochko et al., 2005). (j)

Total organic carbon weight percentage of marine sediment, core SO90-136KL (Schulz et al., 1998). Core locations of all these records above are marked in Fig. 1a. TraCE curves are shown using 100-yr averaged results.

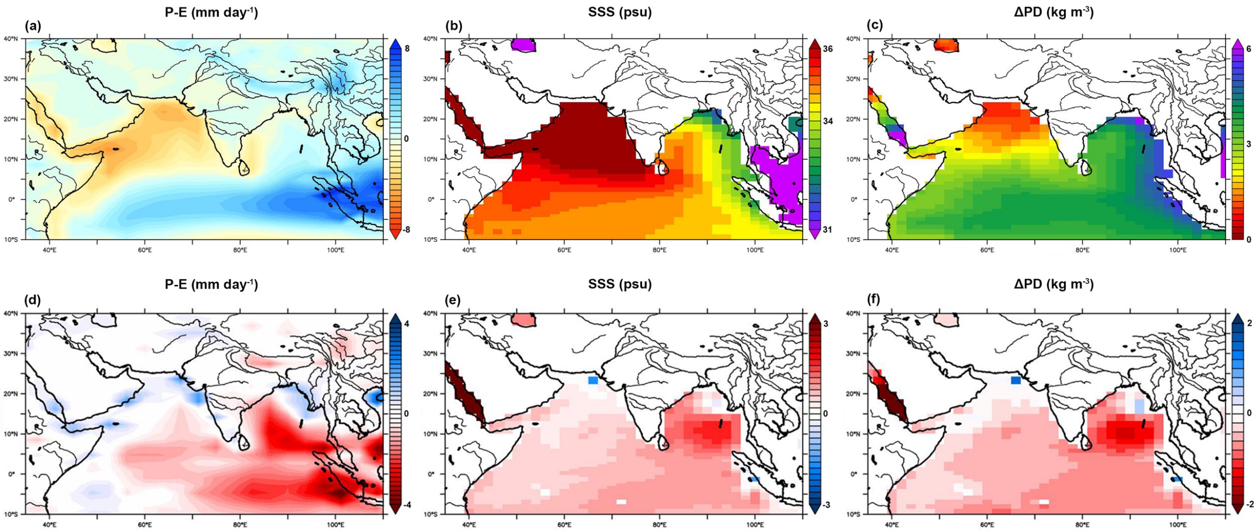

Fig. AC5. (a)–(c) Annual mean precipitation minus evaporation (P-E), sea surface salinity (SSS) and potential density gradient between 200 and 5 m of CTRL. (d)–(f) Differences of the same parameters between LGMc and CTRL.

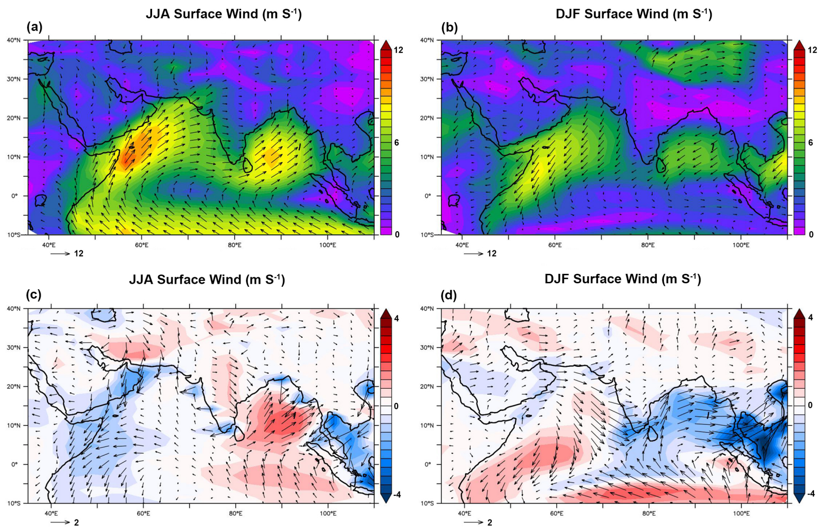

Fig. AC6. (a) and (b) JJA and DJF mean surface wind speed and vectors of CTRL. (c) and (d) Differences of the same parameters between LGMc and CTRL.

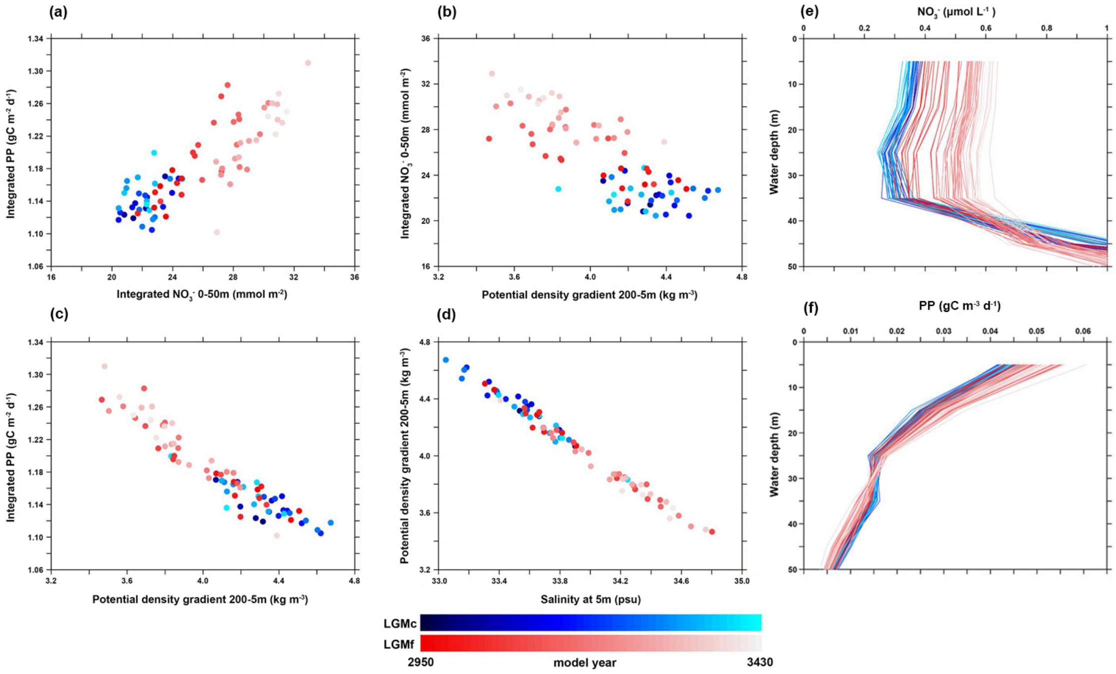

Fig. AC7. (a)–(d) Crossplots between different oceanic parameters of LGMc and LGMf (grids of data extracted see Fig. AC12). (e) and (f) Vertical profiles of nitrate content and PP of LGMc and LGMf (grids of data extracted see Fig. AC12). All the results are DJF mean and every curve represents an average of ten model years.

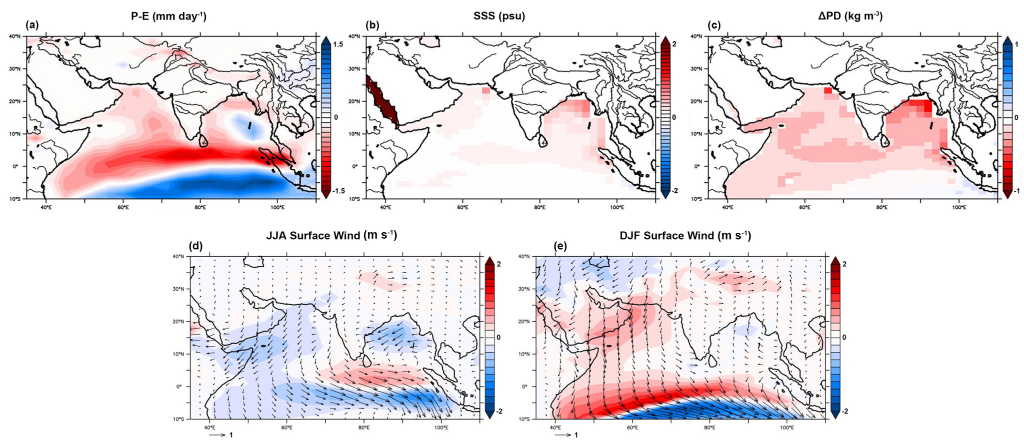

Fig. AC8. As in Fig. AC5 (d)–(f) and Fig. AC6 (c) and (d), but between LGMf and LGMc.

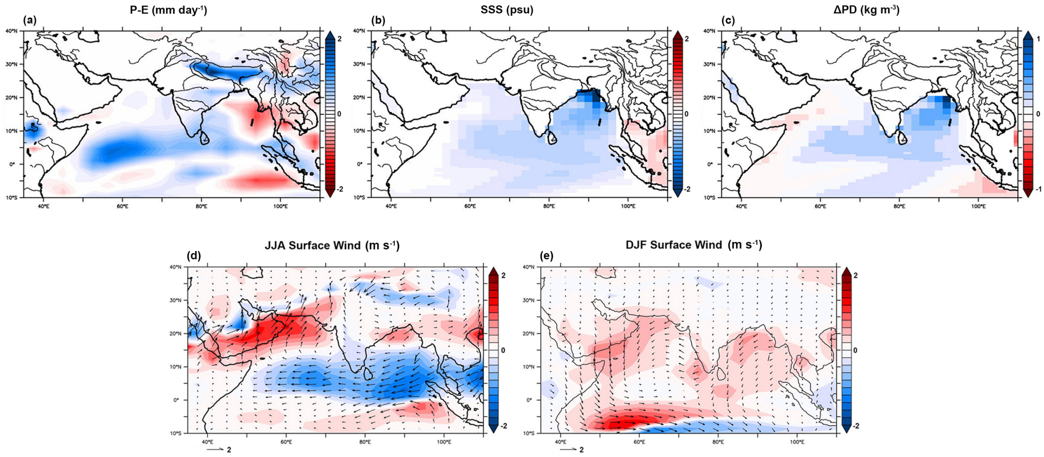

Fig. AC9. As in Fig. AC5 (d)–(f) and Fig. AC6 (c) and (d), but between MH and CTRL.

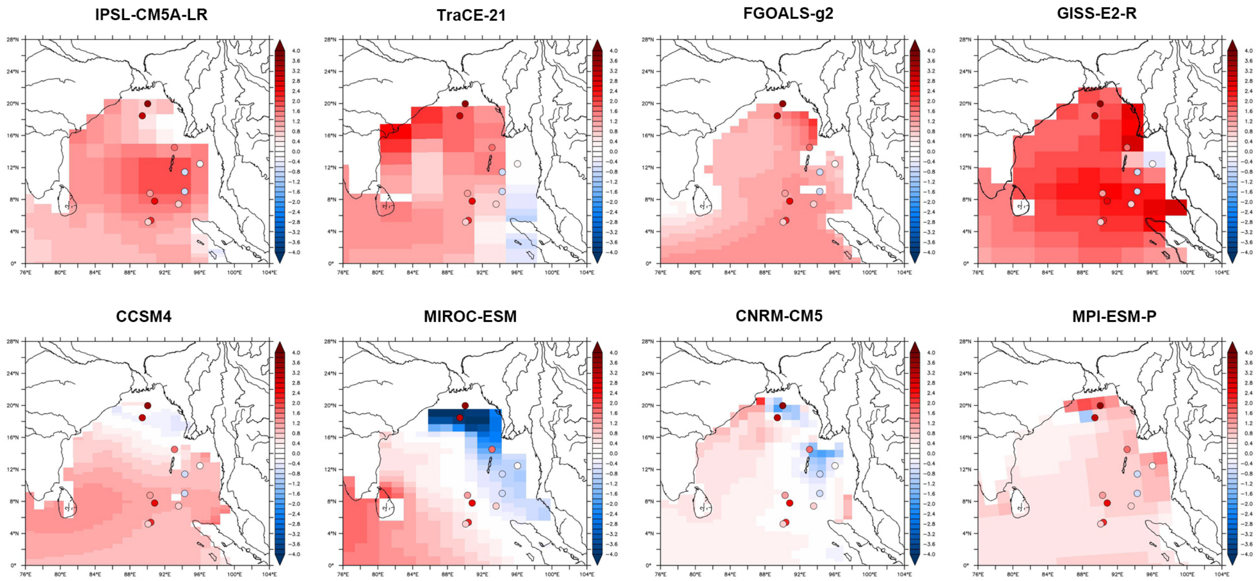

Fig. AC10. PMIP3 models and TraCE-21 outputs. Result of SSS difference between LGM and CTRL (late Holocene for TraCE-21) of PMIP3 models and TraCE-21. PMIP3 data source is Earth System Grid Federation (https://esgf-node.ipsl.upmc.fr/projects/esgf-ipsl/). The dots mark the results of reconstructed SSS (see Sijinkumar et a., 2016)

Supplementary Figures

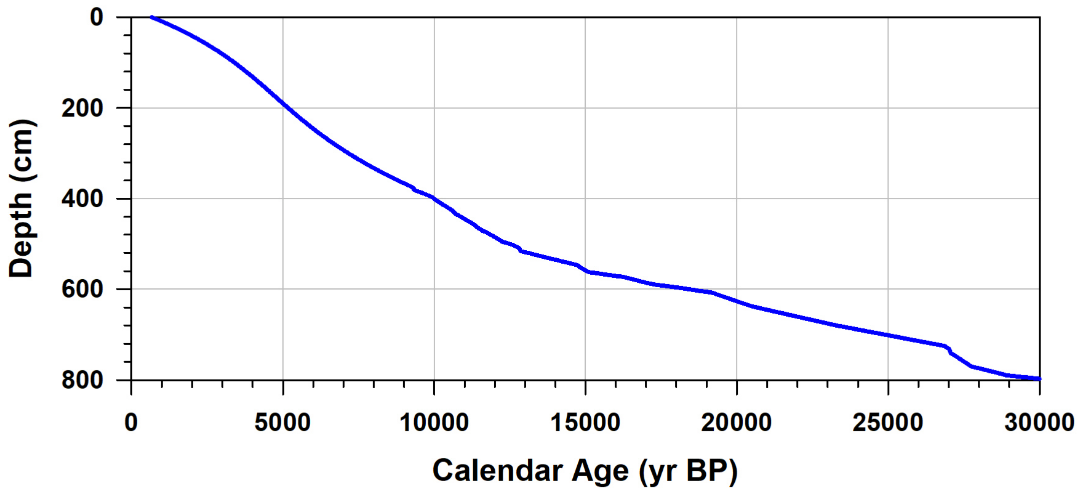

Fig. AC11. Tuned age model of MD77-176. The age model used in this studied is a tuned model constructed by Marzin et al., 2013. Details can be found in that article.

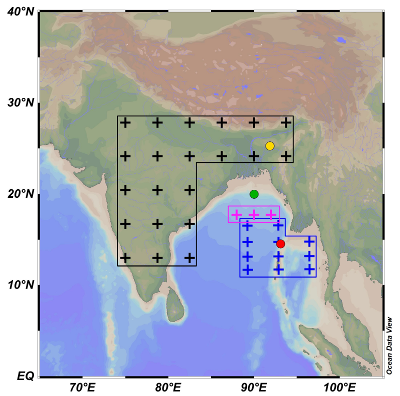

Fig. AC12. The grids of data extracting. Black cross are grids for TraCE-21 atmospheric outputs. Blue grids are for TraCE-21 oceanic outputs. Pink cross are grids for IPSL-CM5A-LR oceanic and biogeochemical outputs

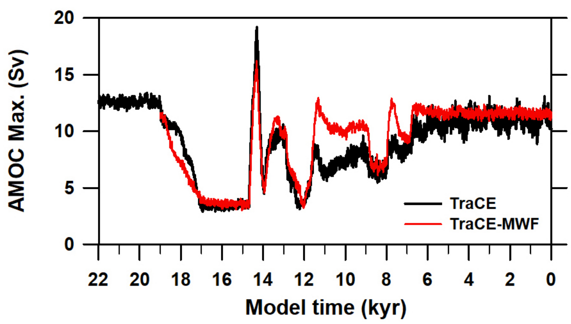

Fig. AC13. Changes of the maximum in the AMOC stream function below 500 m (AMOC strength) in TraCE and melt water of ice sheets single forcing simulation (MWF).

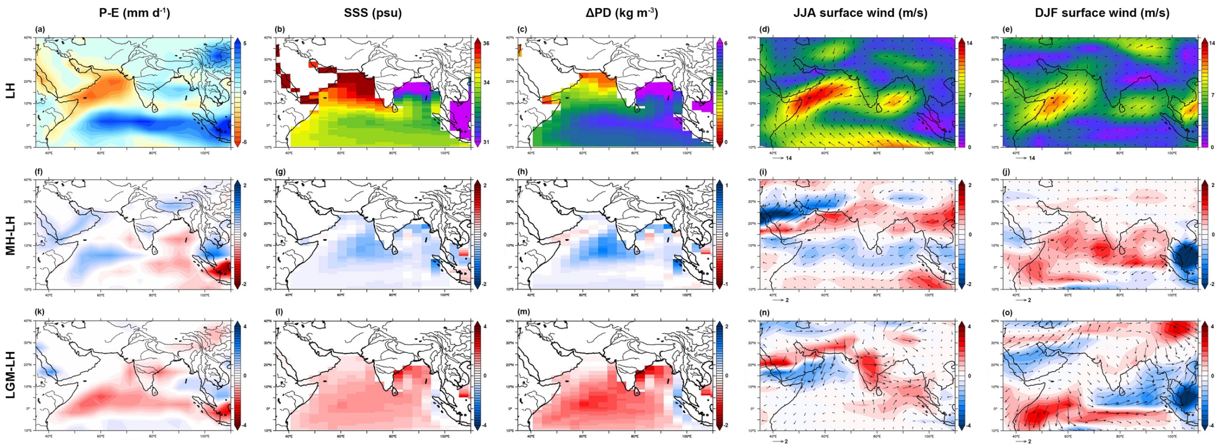

Fig. AC14. Results of TraCE-21 of three periods mean are shown: late Holocene (LH, from 1 kyr BP to presen), middle Holocene (MH, from 6.5 to 5.5 kyr BP), and the Last Glacial Maximum (LGM, from 23 to 19 kyr BP). (a)–(e) Annual mean precipitation minus evaporation (P-E), sea surface salinity (SSS) and potential density gradient between 200 and 5 m, JJA mean and DJF mean surface wind of LH. (f)–(j) Differences of the same parameters between MH and LH. (k) –(o) Differences of the same parameters between LGM and LH.

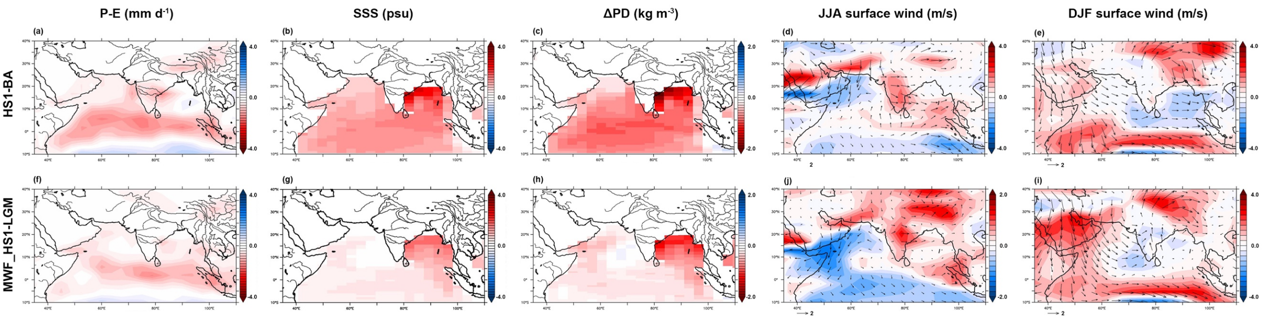

Fig. AC15. Results of TraCE-21 of three periods mean are shown: Bølling-Allerød (BA, from 14.5 to 13 kyr BP), and Heinrich Stadial 1 (HS1, from 17 to 15.5 kyr BP), and the Last Glacial Maximum (LGM, from 23 to 19 kyr BP). (a)–(e) As in Fig. AC13 (f)–(j), but between between BA and HS1. (f)–(j) As in Fig. AC13 (f)–(j), but between HS1 (melt water single forcing simulation) and LGM (full simulation). We can see the results are similar to the differences of the same parameters between LGMf and LGMc (see Fig. AC5, AC6).

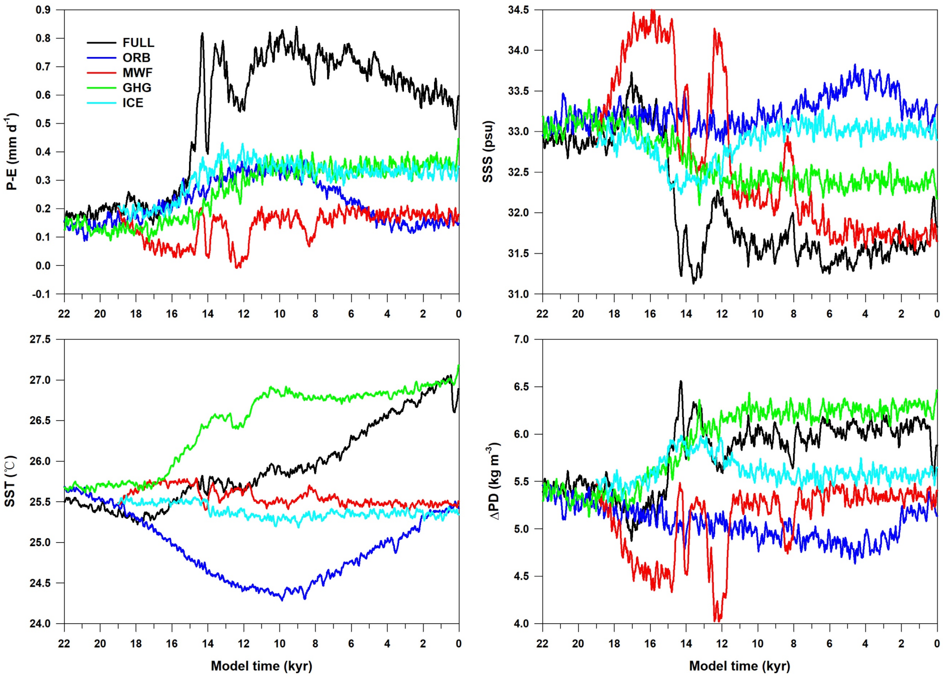

Fig. AC16. Annual mean results of precipitation minus evaporation, SSS, SST and potential density difference between 200 and 5 m (ΔPD) in TraCE-21 simulation (FULL) and single forcing experiments. The single forcing experiments are with other forcing fixed at their values at 19 kyr BP and forced by changing orbital insolation (ORB), green-house gas concentration (GHG), meltwater flux (MWF) and ice sheet (ICE). During the last deglaciation from 19 to 11 kyr BP, we can see that the millennial-scale variations of these parameters are mainly contributed by MWF forcing which moderated AMOC strength. The changes of SST during the deglaciation is very limited.

Response to Reviewer #2

Dear reviewer,

Please find below our answers to the constructive remarks you raised regarding our manuscript below. They all have been carefully considered and will provide what we feel is a much improved manuscript. You will also find, below, all of the modified figures of the new manuscript and Supplementary Material, below.

Comment #1 (C1): *The structure of the manuscript needs some improvement. While the first part (Introduction, Material and Methods) are very well written (although lacking some details about age-model), the discussion relative to the model outputs is not so clear. I find the discussion about model output section very difficult to follow, needs to be simplified in order to improve the understanding and to be better integrated with the proxy data, not to be discussed separately.*

Reply #1 (R1): We agree with Reviewer #2. Therefore, we revised the structure of our manuscript, based (as well) on Reviewer #1' suggestions. An entire chapter is now devoted to the results. In the discussion, empirical data and model outputs are interpreted simultaneously in chapter 5. Particularly, sections 5.1 to 5.3 discuss PP patterns regarding the LGM, the deglaciation, and the Holocene, respectively. We believe that this new structure is helpful to build a more coherent scheme behind PP variability.

Below is the new structure of chapters 4 and 5:

4. Results

4.1. Coccolith abundances and reconstructed primary productivity over the last 26 kyrs

4.2. Simulated primary productivity and physicochemical profiles~~ in the northeastern Bay of Bengal~~

5. ~~Forcing factors behind PP variations over the last 26 kyrs: the inputs of model-data comparisons~~Discussion: Forcing factors behind PP variations over the last 26 kyr as revealed by a model-data comparison

5.1. ~~During t~~The glacial period

5.2. ~~During t~~The last deglaciation

5.3. ~~During t~~The Holocene

In detail:

- In section 4.1, we present and describe coccolith species abundances and reconstructed PP (~~Figure 1 of Author Reponse (Fig. AC1)~~new Fig. 2).
- Section 4.2. relies on new IPSL-CM5A-LR figures dedicated to model results, that help understanding and improving model output interpretations i.e. i) simulated PP maps (~~Fig. AC2~~new Fig. 3), and ii) simulated vertical profiles of potential temperature, salinity, potential density, and nitrate content ~~of~~ near the river mouths and the northeastern Bay of Bengal under four experimental runs (~~Fig. AC3~~new Fig. 4 and 5), that help discussing climate conditions for the LGM (LGMc), the Heinrich Stadial 1 (LGMf), and the Mid-Holocene (MH), compared to preindustrial (CTRL). We show the results of annual mean, summer seasons mean (from June

to August, JJA) and winter seasons mean (from December to February) for all these specific time intervals, in order to evaluate PP changes during the monsoonal seasons.

- In sections 5.1 to 5.3, we compare our reconstructed PP signal with the published empirical records ~~previously documented in Fig. AC4, and~~ with TraCE-21 transient simulations of the upper water column stratification, SSS, SST and net precipitation (P-E)~~, previously documented in Fig. 5~~. and ~~Merging~~have merged our previous Figures 4 and 5 into the~~a~~ new Figure ~~(Fig. AC47), allows~~ to better discuss PP variations in the monsoonal context. We also combine atmospheric and oceanic outputs of the four experiments run together with the simulated PP obtained by the IPSL-CM5A-LR model (new Fig. 7) in order to better discuss and interpret our reconstructed PP during the last glacial period (section 5.1~~; Fig, AC5, AC6~~), the last deglaciation (section 5.2~~; Fig. AC7, AC8~~) and the Holocene (section 5.3~~; Fig, AC9~~). A new Figure 8 merged from our previous Figures 6 and 8, has been put in section 5.2.

***C2:** The figure 2 is not very useful, it repeats data that are shown later in other figures several times. For example, showing the d18Osw and the GISP2 ice-core d18O is not really relevant, as we see the proxy data already tuned to the ice-core data. I assume that Marzin et al., (2013) contains a plot showing this, so these two curves are not needed here. An important point regarding the age-model is that if, despite the large number of radiocarbon ages, the proxy data is tuned to the GISP ice-core d18O, later comparisons between proxy and ice-core data are not very well sustained (circularity). The authors should keep this in mind when discussing about it at L. 205-207.*

R2: The initial Figure 2 does not exist anymore. GISP $\delta^{18}O$ and $\delta^{18}O_{G.ruber}$ obtained on core MD77-169 are now only evoked when dealing with the age model (new Fig. S1). *Florisphaera profunda* distribution and PP reconstructions are presented within the a new figure (~~Fig. AC1~~new Fig. 2), that is entirely devoted to micropalaeontological results (i.e. abundances of *F. profunda, Gephyrocapsa* spp. and *Emiliania huxleyi* together with PP estimates).

We thank Reviewer # 2 for highlighting that our phrasing in lines 205-207 could be seen as a circular reasoning, since proxy data are in part tuned to the GISP $\delta^{18}O$ signal. However, our micropalaeontological data are well in phase with numerous geochemical data obtained elsewhere in the Tropical Indian Ocean and the Chinese continent, based on sediment cores and speleothems with totally independent age models. They also match very well the TraCE 21 and IPSL-CM5A-LR outputs obtained here. Such feature, together with its use in previous works (Marzin et al., 2013; Yu et al., 2017; Ma et al., 2019), point to a robust age model and demonstrate that our micropalaeontological data can be discussed properly in the light of the rapid climatic changes recorded in northern high-latitudes. To avoid any confusion, we rephrased lines 205-207 of the manuscript focusing on the relationship that exists between PP and SSS.

***C3:** I find particularly intriguing the change in the salinity-PP relationship before and after LGM (L. 213-222).. The authors suggest that the higher PP during low salinity between 26-19ka are due to higher wind mixing. Are there independent proxy evidence of this coupling? For example, loess deposits that could record changes in wind intensity which could support their view? And why the wind-forcing gets weaker after the LGM?*

R3: To our knowledge, there is a high-resolution record of loess grain size from the northeastern China which indicates the local winter wind intensity (Sun et al., 2012; Zhang et al., 2016). The record shows that the winter wind is stronger during LGM than during the late Holocene. However, there is no published record of wind intensity for the Bay Bengal and Andaman Sea. We think it might be questionable to use the wind record over the northwestern China to interpret the Bay of Bengal as these two regions are not close to one another and the wind directions are different (Fig. 1c; Sun et al., 2012). We checked the modeling outputs and found that compared to preindustrial (CTRL), stronger summer winds and weaker winter winds prevailed over annually saltier sea surface in the Bay of Bengal during the LGM (~~Fig. AC5, AC6~~new Fig. 7i, j). This implies that the winter wind over the northwestern China and the Bay of Bengal are not strengthened at the same period during the LGM. Therefore, we think if wind-mixing is stronger over the Bay of Bengal during the LGM, it should be related to strengthened summer winds. However, the relationship between PP and SSS of MD77-176 encourages us to explore further mechanisms behind PP (and SSS) variability at that time. We have also found that IPSL-CM5A-LR outputs show spatial differences of SSS in the Bay of Bengal, and particularly, that the studied area could have been associated to low SSS during the LGM (Sijinkumar et al. (2016). Our best explanation is that during the LGM, i.e. under relatively low sea-level, and a more proximal environment for MD77-176, PP and SSS react to the Irrawaddy dynamic in the same way as proximal environment do, today (Fig. 1). Indeed, higher (lower) nutrient and freshwater inputs from the Irrawaddy river, may trigger higher PP and lower SSS, and vice versa. Such assumption is ~~confirmed in~~indicated in ~~Fig. AC2 and AC3~~new Figure 3, where PP strongly increases, and in new Figure 5e and j ~~(Fig. AC2)~~, when PP vertical profiles clearly depict a change from open ocean type to coastal one near the studied core. ~~(Fig. AC3)~~. Our scenario seems therefore to provide a suitable explanation behind the PP pattern reconstructed for the LGM.

Bearing in mind that the LGMc experiment of IPSL-CM5A-LR gives us a mean state of PP and SSS conditions and may not simulate the high-resolution PP changes discussed here, we only evoke the possible Irrawaddy river influence on PP distribution during the LGM, with caution.

***C4:** Finally, in the section Data availability the authors indicate that "Data to this paper can be required. Please contact the X. Zhou or S. Duchamp-Alphonse.". Copernicus journals (including Climate of the Past) have a very clear policy regarding data curation (https://www.climate-of-the-past.net/about/data_policy.html), which "requests depositing data that correspond to journal articles in reliable (public) data repositories, assigning digital object identifiers, and properly citing data sets as individual contributions". Clearly the current statement about data availability does not meet this criteria, and all data and code should be archive somewhere or included as supplementary material.*

R4: Thanks for this reminding. We have added our data in the supplementary materials.

***C5:** Some minor corrections: L. 104. Abbreviate Arabian Sea L. 177. Strange symbol between longitude and latitude.*

R5: We have corrected them.

***C6:** Fig. 1f, why choosing SON instead of JJA as the other panels?*

R6: Because the occupation of the input fresh water is the largest during SON in the northeastern Indian Ocean at modern time, lagging the maximum precipitation over the South Asia.

~~**R7:** modified supplementary figures are Fig. AC10 to AC15~~

References

Marzin et al., 2013. Glacial fluctuations of the Indian monsoon and their relationship with North Atlantic climate: new data and modeling experiments, Climate of the Past, 9, 2135–2151.

Yu et al., 2018. Antarctic Intermediate Water penetration into the Northern Indian Ocean during the last deglaciation. Earth and Planetary Science Letters, 500, 67–75.

Ma et al., 2019. Changes in Intermediate Circulation in the Bay of Bengal since the Last Glacial Maximum as inferred from benthic foraminifera assemblages and geochemical proxies. Geochemistry, Geophysics, Geosystems, 20, 1592-1608.

Sijinkumar et al., 2016. δ18O and salinity variability from the Last Glacial Maximum to Recent un the Bay of Bengal and Andaman Sea. Quaternary Science Reviews, 135, 79–91.

Sun et al., 2012. Influence of Atlantic meridional overturning circulation on the East Asian winter monsoon. Nature Geoscience, 5, 46-49.

Zhang et al., 2016. Dynamics of primary productivity in the northern South China Sea over the past 24,000 years. Geochemistry, Geophysics, Geosystems, 17, 4878-4891.

Figures

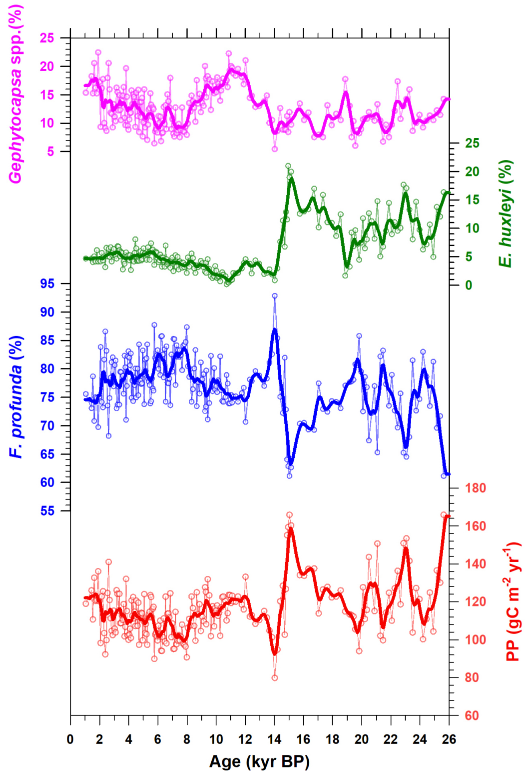

Fig. AC1. Relative abundance changes of main coccolith species and reconstructed PP.

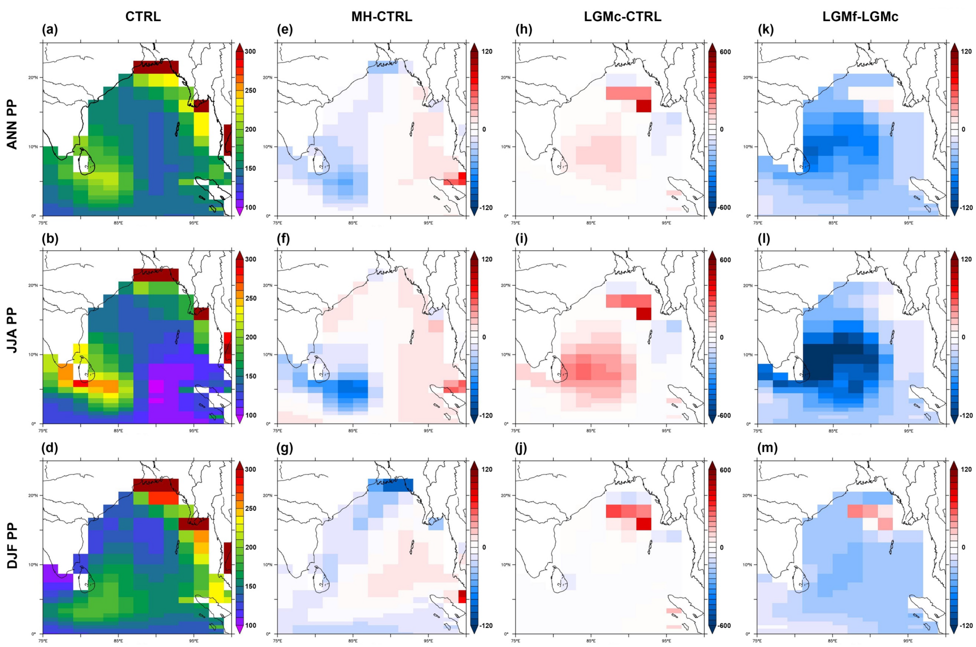

Fig. AC2. Simulated PP of CTRL and PP differences between MH and CTRL, LGMc and CTRL, and LGMf and LGMc. Results of annual mean, JJA mean and DJF mean are shown. PP is in gC m^{-2} yr^{-1}.

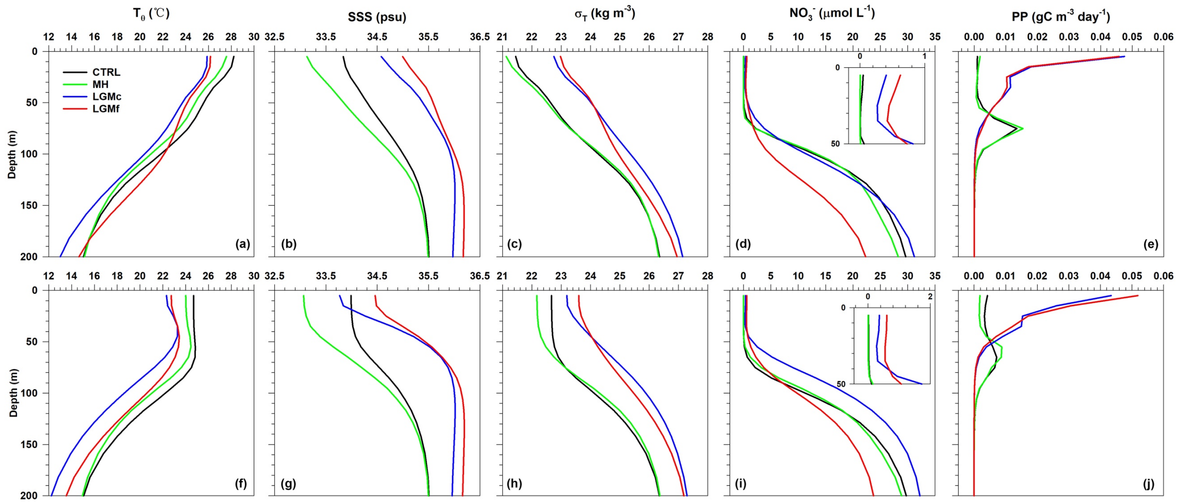

Fig. AC3. Simulated ocean profiles in four experiment run with IPSL-CM5A-LR. (a)–(e) Results of JJA mean. (f)–(j) Results of DJF mean. Grid of data extracting see Fig. AC12. The parameters shown here are potential temperature (T_θ), sea surface salinity (SSS), potential density (sigma-t, σ_T), nitrate content of seawater (NO_3^-) and total primary productivity (PP).

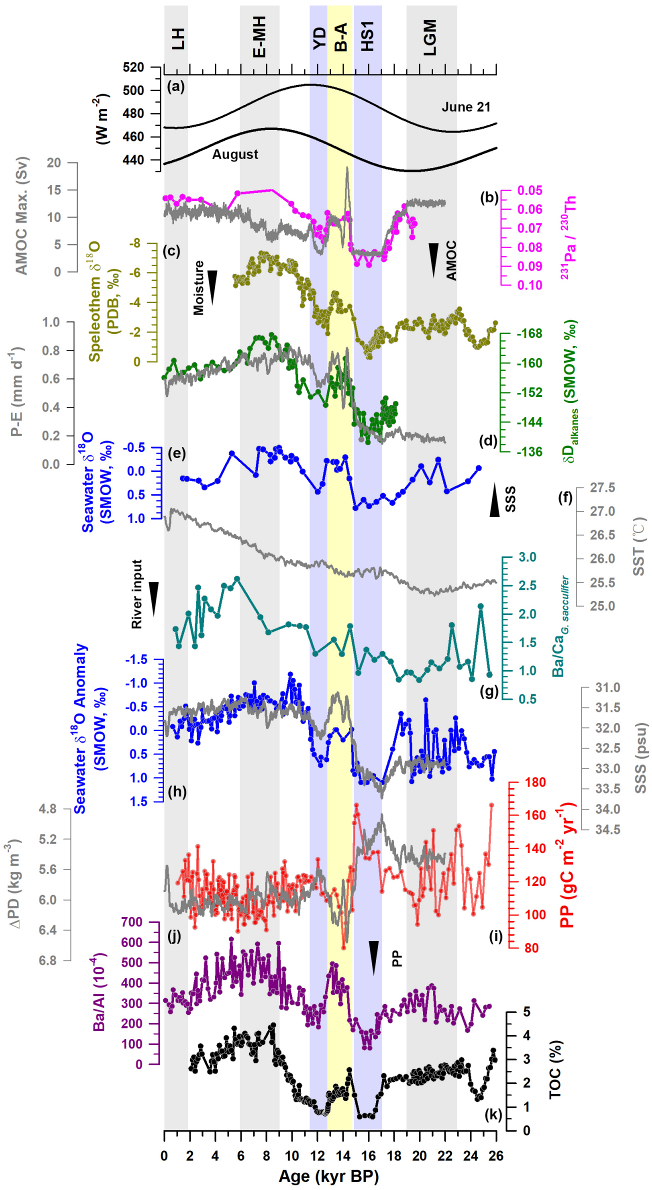

Fig. AC4. (a) August mean insolation and at 25°N. (b) AMOC strength indicated by $^{231}Pa/^{230}Th$ ratio of marine sediment from the western subtropical Atlantic Ocean (in pink, McManus et al., 2004). The changes of the maximum in the AMOC stream function below 500 m (AMOC strength) in TraCE-21 (in gray). (c) Mawmluh Cave speleothem $\delta^{18}O$ (Dutt et al., 2015). (d) Alkane δD in marine sediment, core SO188-342 (in green, Contreras-Rosales et al., 2014) and simulated precipitation minus evaporation of TraCE-21 (in gray). (e) Seawater $\delta^{18}O$ record of core RC12-344 (Rashid et al., 2007). (f) Simulated SST in the NE-BoB. Grids of data extracted see Fig. S2. (g) Ba/Ca ratios derived from mixed layer foraminifer species Globigerinoides sacculifer from core SK 168/GC-1(Gebregiogis et al., 2016). (h) Seawater $\delta^{18}O$ anomaly record of core MD77-176 (Marzin et al., 2013). (i) Estimated PP record of core MD77-176 (this study, in red) and simulated potential density gradient between 200 and 5m of TraCE-21 (in gray). (i) Ba/Al ratio of marine sediment, core 905 (Ivanochko et al., 2005). (j)

Total organic carbon weight percentage of marine sediment, core SO90-136KL (Schulz et al., 1998). Core locations of all these records above are marked in Fig. 1a. TraCE curves are shown using 100-yr averaged results.

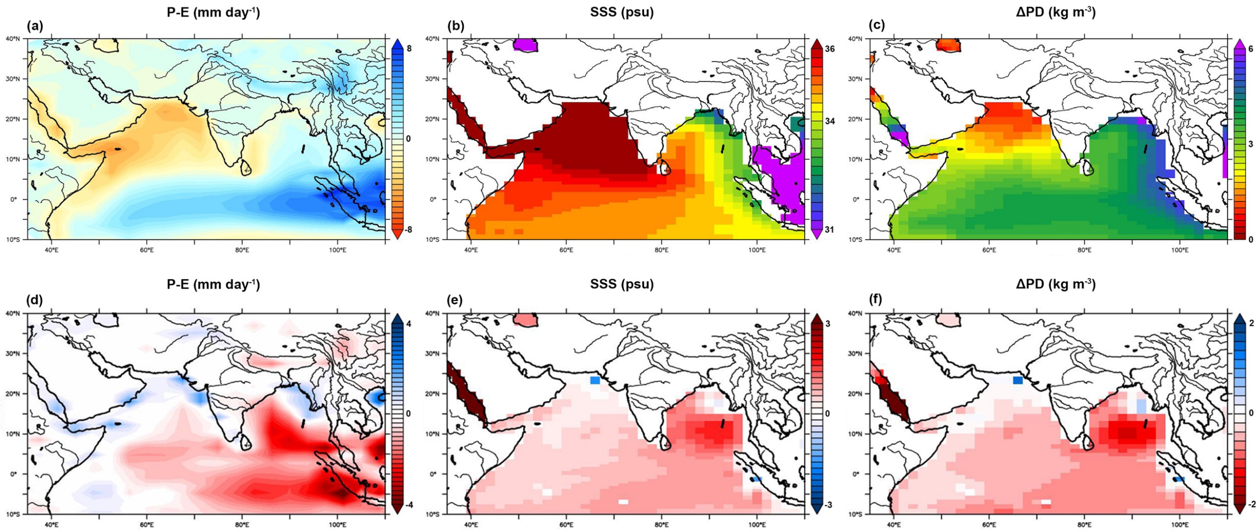

Fig. AC5. (a)–(c) Annual mean precipitation minus evaporation (P-E), sea surface salinity (SSS) and potential density gradient between 200 and 5 m of CTRL. (d)–(f) Differences of the same parameters between LGMc and CTRL.

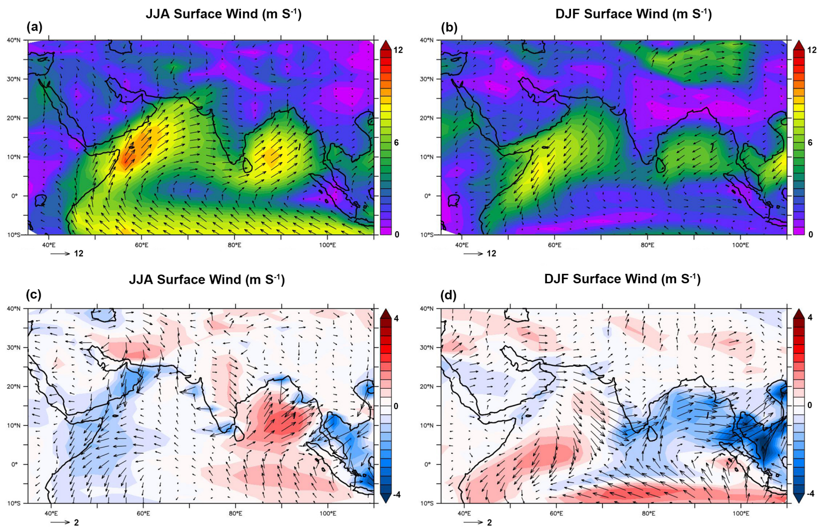

Fig. AC6. (a) and (b) JJA and DJF mean surface wind speed and vectors of CTRL. (c) and (d) Differences of the same parameters between LGMc and CTRL.

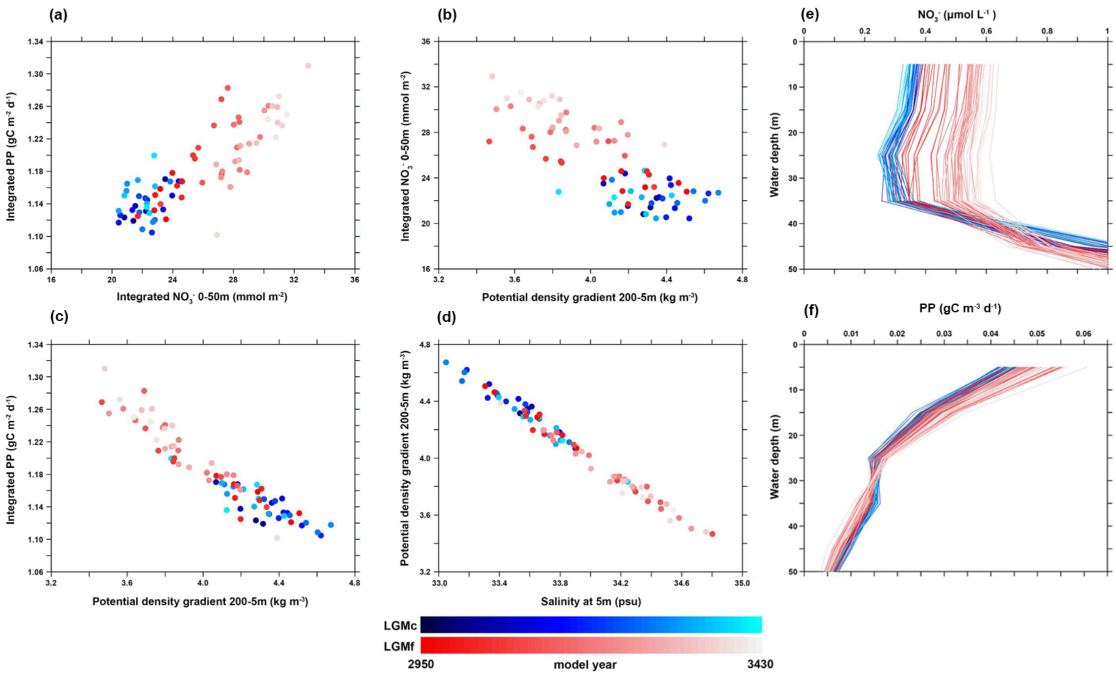

Fig. AC7. (a)–(d) Crossplots between different oceanic parameters of LGMc and LGMf (grids of data extracted see Fig. AC12). (e) and (f) Vertical profiles of nitrate content and PP of LGMc and LGMf (grids of data extracted see Fig. AC12). All the results are DJF mean and every curve represents an average of ten model years.

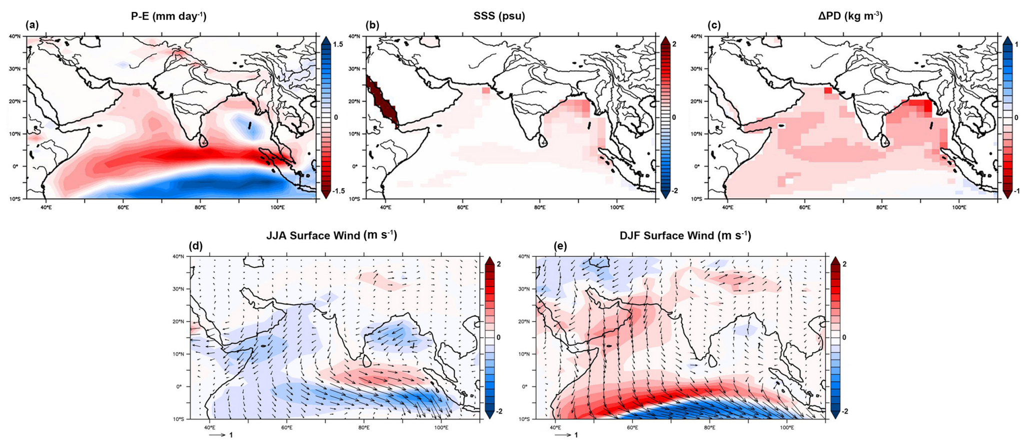

Fig. AC8. As in Fig. AC5 (d)–(f) and Fig. AC6 (c) and (d), but between LGMf and LGMc.

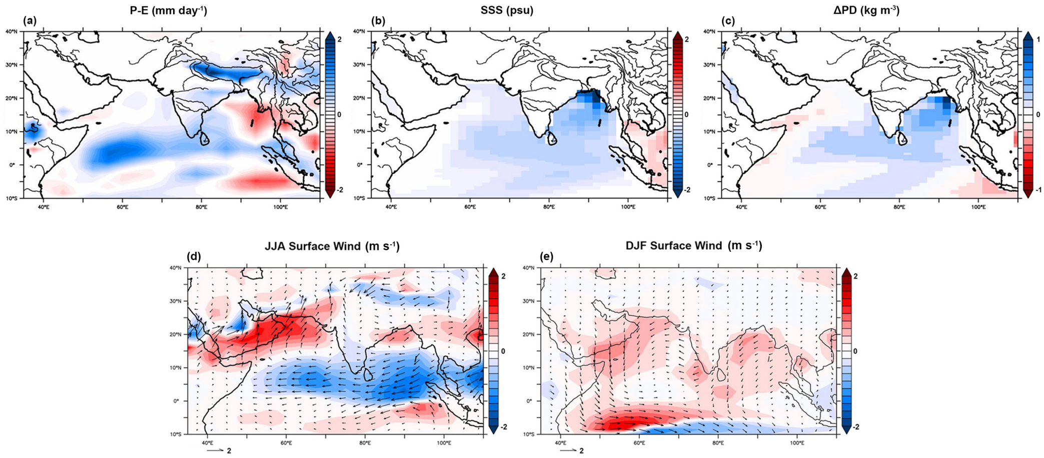

Fig. AC9. As in Fig. AC5 (d)–(f) and Fig. AC6 (c) and (d), but between MH and CTRL.

Supplementary Figures

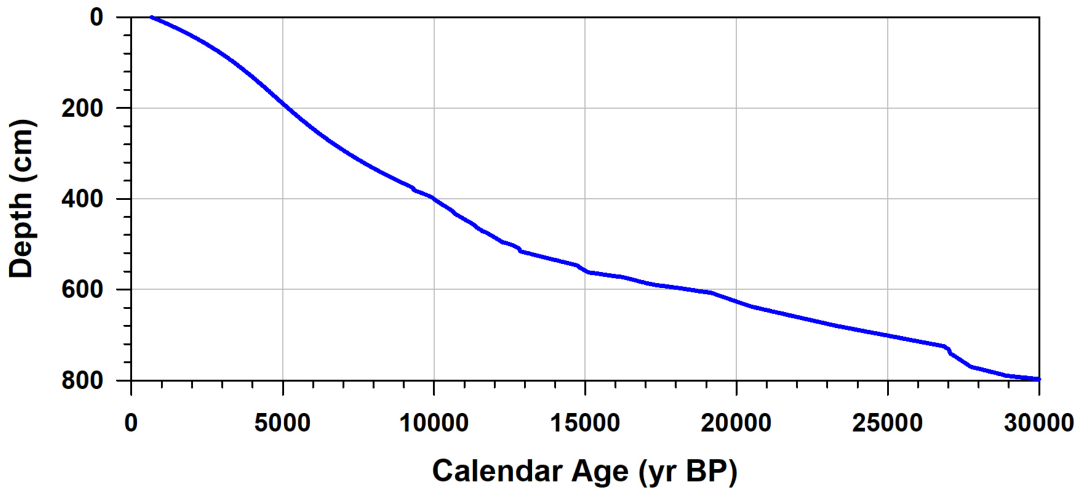

Fig. AC10. Tuned age model of MD77-176. The age mod

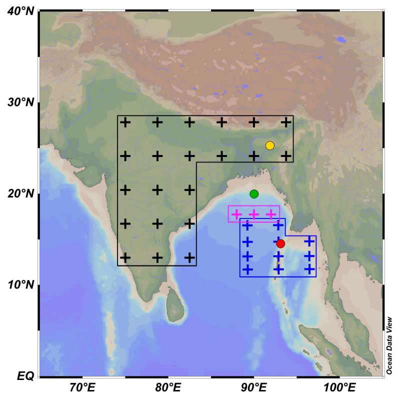

Fig. AC11. The grids of data extracting. Black cross are grids for TraCE-21 atmospheric outputs. Blue grids are for TraCE-21 oceanic outputs. Pink cross are grids for IPSL-CM5A-LR oceanic and biogeochemical outputs

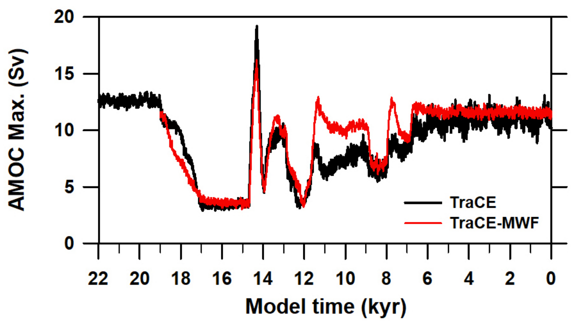

Fig. AC12. Changes of the maximum in the AMOC stream function below 500 m (AMOC strength) in TraCE and melt water of ice sheets single forcing simulation (MWF).

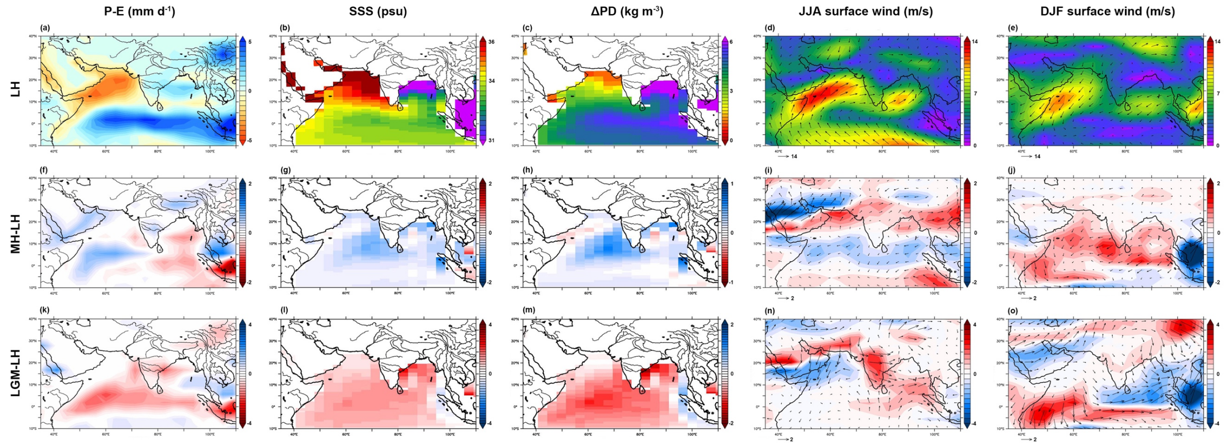

Fig. AC13. Results of TraCE-21 of three periods mean are shown: late Holocene (LH, from 1 kyr BP to presen), middle Holocene (MH, from 6.5 to 5.5 kyr BP), and the Last Glacial Maximum (LGM, from 23 to 19 kyr BP). (a)–(e) Annual mean precipitation minus evaporation (P-E), sea surface salinity (SSS) and potential density gradient between 200 and 5 m, JJA mean and DJF mean surface wind of LH. (f)–(j) Differences of the same parameters between MH and LH. (k) –(o) Differences of the same parameters between LGM and LH.

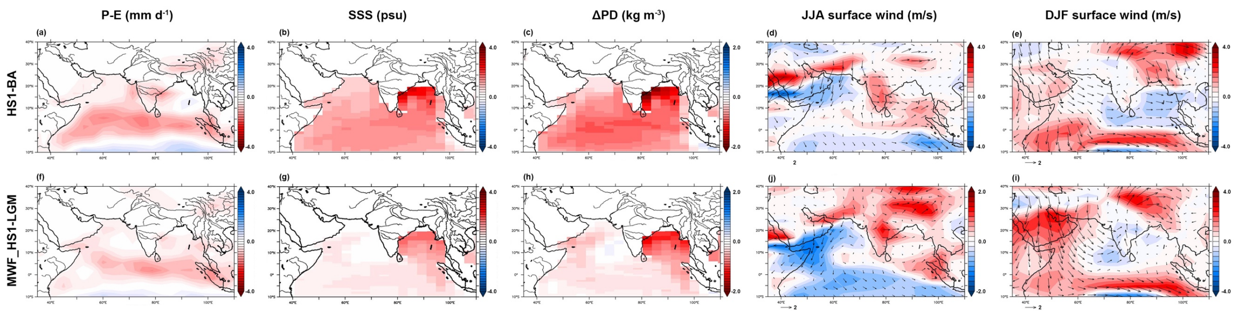

Fig. AC14. Results of TraCE-21 of three periods mean are shown: Bølling-Allerød (BA, from 14.5 to 13 kyr BP), and Heinrich Stadial 1 (HS1, from 17 to 15.5 kyr BP), and the Last Glacial Maximum (LGM, from 23 to 19 kyr BP). (a)–(e) As in Fig. AC13 (f)–(j), but between between BA and HS1. (f)–(j) As in Fig. AC13 (f)–(j), but between HS1 (melt water single forcing simulation) and LGM (full simulation). We can see the results are similar to the differences of the same parameters between LGMf and LGMc (see Fig. AC5, AC6).

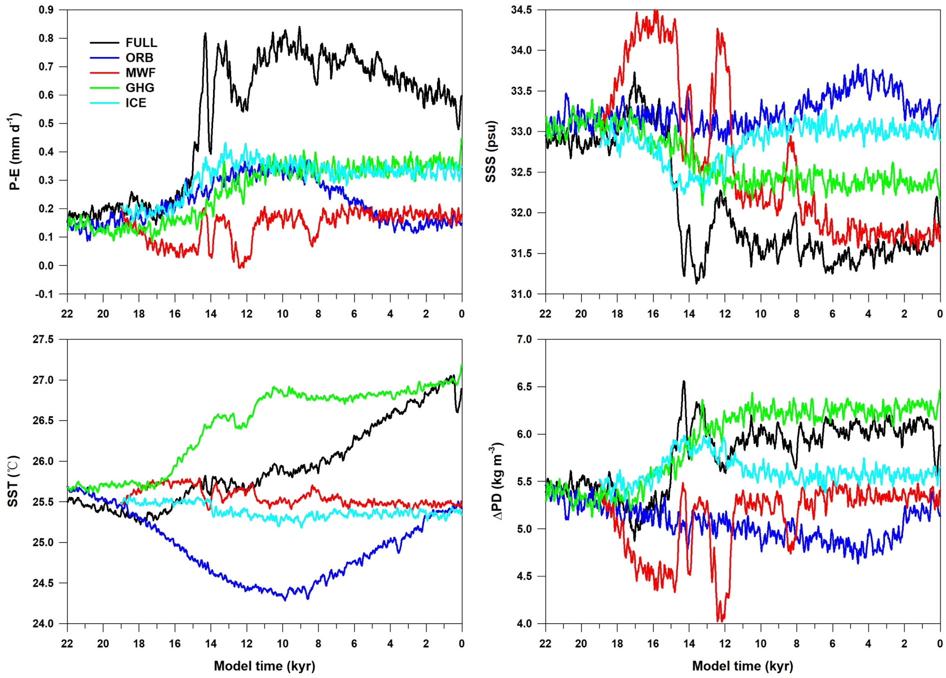

Fig. AC15. Annual mean results of precipitation minus evaporation, SSS, SST and potential density difference between 200 and 5 m (ΔPD) in TraCE-21 simulation (FULL) and single forcing experiments. The single forcing experiments are with other forcing fixed at their values at 19 kyr BP and forced by changing orbital insolation (ORB), green-house gas concentration (GHG), meltwater flux (MWF) and ice sheet (ICE). During the last deglaciation from 19 to 11 kyr BP, we can see that the millennial-scale variations of these parameters are mainly contributed by MWF forcing which moderated AMOC strength. The changes of SST during the deglaciation is very limited.

Dynamics of primary productivity in the northeastern Bay of Bengal over the last 26,000 years

Xinquan Zhou[1], Stéphanie Duchamp-Alphonse[1], Masa Kageyama[2], Franck Bassinot[2], Luc Beaufort[3], Christophe Colin[1]

[1]Université Paris-Saclay, Géosciences Paris Sud, UMR 8148, CNRS, Rue du Belvédère, 91405 Orsay, France

[2]Laboratoire des Sciences du Climat et de l'Environnement, UMR 8112, CEA/CNRS/UVSQ, Université Paris-Saclay, Centre CEA-Saclay, Orme des Merisiers, 91191 Gif-sur-Yvette, France

[3]Centre de Recherche et d'Enseignement de Géosciences de l'Environnement, UMR 7330, CNRS/IRD/Aix-Marseille Université, Av. Louis Philibert, BP80, 13545, Aix-en-Provence, France

Correspondance to: Xinquan Zhou (xinquan.zhou@universite-paris-saclay.fr)

Abstract. At present, variations of primary productivity (PP) in the Bay of Bengal (BoB) are driven by~~are responding to~~ salinity-related-stratification, which is controlled by the Indian Summer Monsoon (ISM). The relationships between PP, precipitation~~ISM~~, and more generally climate in the past, are not clearly understood ~~to a broader scale, North Atlantic climate rapid variability in the past, are not clearly understood~~. Here, we present a new record of PP based on the examination of coccolithophore assemblages in a 26,000-~~-~~year~~s~~ sedimentary series~~record~~, retrieved in the northeastern BoB (core MD77-176). We ~~C~~compare~~isons~~ our PP records ~~with~~ to published climate and monsoon records, as well as outputs from numerical experiments obtained with the Earth System Model IPSL-CM5A-LR, including marine biogeochemical component PISCES, and with the transient climate simulation TraCE-21. ~~and experiments run with the Earth System Model IPSL-CM5A-LR, including marine biogeochemical components, helped us interpret our PP records in the context of ISM and~~Our results show that PP was most probably controlled by nutrient contents and distribution within the upper water column, that were predominantly influenced by (i) regional river systems between 26 and 19 kyr BP, i.e. when sea-level was relatively low, and climate was relatively dry and (ii) salinity-related stratification over the last 19 kyr BP, i.e. when sea level rose and more humid conditions prevailed. During that period, salinity and stratification were directly related to monsoon precipitation dynamics, which were chiefly forced by both insolation and AMOC strength. During Heinrich Stadial 1 and Younger Dryas, i.e. when the AMOC collapsed, weaker South Asian precipitation diminished stratification and enhanced PP. During Bølling-Allerød, i.e. when the AMOC recovered, stronger South Asian precipitation increased stratification and subdued PP. Similarly, the precipitation peak recorded around the middle–early Holocene is consistent with a stronger stratification that drives PP minima. ~~Atlantic Overturning Meridional Circulation (AMOC) changes. We demonstrate that PP is influenced by vertical stratification in the upper water column over the last 26,000 years (26 kyr BP). It is controlled by wind-driven mixing from 26 to 19 kyr BP, i.e., when dry climate conditions and reduced freshwater inputs occurred, and by salinity-related-stratification over the last 19 kyr BP (since the Last Glacial Maximum), i.e., when humid conditions prevailed. During the deglaciation, salinity and stratification are related to monsoon precipitation dynamics, which are chiefly forced by both, insolation and the strength of the AMOC. The collapse (recovery) of the AMOC during Heinrich Stadial 1 (Bølling Allerød) weakened (strengthened) ISM and diminished (increased) stratification, thus enhancing (subduing) productivity.~~

1. Introduction

The climatology and oceanography of ~~the~~ South Asia and the North Indian Ocean are dominated by the Indian Monsoon, which is characterized by strong seasonal contrasts in wind and precipitation patterns (Shankar et al., 2002; Gadgil et al., 2003). During the northern hemisphere summer season, the North Indian Ocean is strongly influenced by the southwesterly winds blowing from the sea toward the Asian continent, thus carrying large amounts of moisture on land. During the winter season, the winds blow over the continent toward the Indian Ocean from the northeast, thus causing relatively dry conditions on land, with precipitations moved over the ocean. Monsoon precipitations are directly associated to the position of the Inter Tropical Convergence Zone (ITCZ; Schneider et al., 2014), whose latitudinal displacement~~The Indian Monsoon is a subsystem of the large-scale Asian Monsoon, which~~ is paced by seasonal changes in insolation due to the obliquity of the Earth's axis and precession, and results from variations in the land-sea thermal contrast caused by differences of heat capacity of the continent and the ocean (Meehl, 1994, 1997; Webster, 1998; Wang et al., 2003). It is also influenced by teleconnections with the El Niño–Southern Oscillation and the Indian Ocean Dipole, two climate modes of interannual variability that develop from air–sea interactions in the tropical Pacific, and drive significant changes within the Indian Ocean (Ashok et al., 2004; Wang et al., 2008; Currie et al., 2013; Jourdain et al., 2013).

Remarkably,~~The North Indian Ocean is strongly influenced by the southwesterly winds blowing from the sea during the northern hemisphere summer season thus carrying large amounts of moisture. T~~the eastern part of the North Indian Ocean, i.e.~~,~~ the Bay of Bengal (BoB) and the Andaman Sea~~ (ADS)~~, receives heavier annual precipitation than its western counterpart, i.e. the Arabian Sea (AS). This pattern,~~This discrepancy~~ together with differences in local evaporation result in hydrological and ecological differences between these two areas (e.g.

Prasanna Kumar et al., 2002; Vinayachandran et al., 2002; Shenoi et al., 2002; Shi W et al., 2002; Dey and Singh, 2003; Rao and Sivakumar, 2003; Prasad, 2004; Currie et al., 2013). A noteworthy characteristic of modern conditions prevailing in the North Indian Ocean is the low PP in the BoB and the Andaman Sea~~ADS~~ compared to the AS (Prasanna Kumar et al., 2002). Previous studies revealed that low annual PP in the BoB results from the important freshwater input by rivers and direct rainfall on the sea, which cause a strong stratification of the upper seawater column and an impoverishment of nutrients in surface layers (Vinayachandran et al., 2002; Madhupratap et al., 2003; Gauns et al., 2005). In contrast, the AS has a high PP which is mainly associated with high nutrient content in the upper layer, thanks to wind driven mixing during winter and coastal upwelling during summer (Schott, 1983; Anderson and Prell, 1992; Madhupratap et al., 1996; Gardner et al., 1999;~~Veldhuis et al., 1997; Keen et al., 1997;~~ Prasanna Kumar et al., 2001; Wiggert et al., 2005). Both, the BoB and AS are characterized by a relatively small sea surface temperature (SST) seasonal cycle. Thus,~~the western and eastern parts of the North Indian Ocean are remarkable examples of tropical ocean dynamics, which is characterized by limited seasonal differences of SST, and for which~~ seasonal and interannual changes in PP result chiefly from variations in the nutricline depth (i.e. variations in nutrient availability in the photic zone) controlled by salinity-related stratification of the upper seawater column in relation to local evaporation-precipitation balance and river runoff, and/or dynamical processes such as wind-driven mixing/upwelling~~, and/or by salinity-related stratificationof the upper seawater column in relation to local evaporation-precipitation balance and river runoff~~ (e.g. Lévy et al., 2001; Vinayachandran et al., 2002; Chiba et al., 2004; Rao et al., 2011; van de Poll et al., 2013; Behara and Vinayachandran, 2016; Spiro Haeger and Mahadevan, 2018).

Past changes of PP at both orbital- and millennial-scales in the western and northern AS have been widely studied, and authors have interpreted PP variations as chiefly reflecting changes in the intensity of Indian Summer Monsoon (ISM) southwesterly winds (e.g. Schultz et al., 1998; Ivanova et al., 2003; Ivanochko et al., 2005; Singh et al., 2011). Far less is known about past changes in PP in the BoB and their link to changes in monsoon precipitation, although reconstructions and climate model simulations have clearly pointed important changes in ISM precipitation driven by~~Proxy reconstructions and climate model simulations have also pointed out that the Indian Summer Monsoon precipitation is sensitive to~~ both, ~~the slow~~ orbital forcing and ~~then~~ fast changes ~~of~~ at high-latitude, ~~processes~~ such as those associated with the Atlantic meridional overturning circulation (AMOC) ~~and the temperature fluctuations in the North Atlantic~~ (e.g. Braconnot et al., 2007a, 2007b; Kageyama et al., 2013; Marzin et al., 2013; Contreras-Rosales et al., 2014). The poorer attention devoted to past PP in the BoB is in part due to the absence of high time-resolution PP records in the BoB and the Andaman Sea~~However, the relationship between PP and monsoon precipitation in the past has been given less attention due to the absence of high time-resolution PP record in the BoB and the ADS~~ (Phillips et al., 2014; Da Silva et al., 2017; Li et al., 2019), which precludes our complete understanding of how monsoon climate changes impact tropical ocean ecology through different mechanisms and at different time-scales. To fill this gap, reliable paleo-PP records are needed for that region.~~a reliable paleo-PP record is needed for the BoB/ADS. On the other hand, the PP record can also indicate the variability of Indian Monsoon strength.~~

Coccolithophores are marine calcifying phytoplankton organisms that constitute one of the most important "functional groups", responsible for primary production and export of carbonate particles (i.e. the coccoliths they produce) to the sedimentary reservoir. The coccoliths preserved in marine sediment are good study material for paleoenvironmental reconstructions. Particularly, *Florisphaera profunda* is a lower photic zone dweller and its relative abundance in marine coccolithophore assemblages obtained from the sediments has been successfully used to reconstruct past changes of the nutricline depth and PP (Molfino and McIntyre, 1990a, 1990b; Beaufort et al., 1997; Zhang et al., 2016; Hernández-Almeida et al., 2019).

In this study, we provide the first record of coccolith assemblage changes in the BoB. The relative abundance of *F. profunda* in the sediment core MD77-176 makes it possible to reconstruct at a high-temporal resolution, paleo-PP over the last 26 kyr BP in the northeastern BoB. The studied period covers a complete precession cycle and the last deglaciation. This time interval is characterized by rapid climate changes remotely controlled by north hemisphere~~ic~~ high-latitude climate and disruptions of the AMOC (McManus et al., 2004; Clement and Peterson, 2008; Liu et al., 2009; Wolff et al., 2010; Clark et al., 2012),~~.~~ as observed during the cold periods Heinrich Stadial 1 (17−14.8 kyr BP) and Younger Dryas (12.9−11.8 kyr BP) when massive collapses of northern hemisphere ice shelves release prodigious volume of icebergs and freshwaters in the North Atlantic Ocean (Heinrich, 1988). In addition, we used the outputs of paleoclimate experiments obtained with the "Institut Pierre Simon Laplace" Earth System Model version 5 (IPSL-CM5A-LR) (Dufresne et al., 2013) in which marine biogeochemistry is represented, and the transient climate simulations run with the Community Climate System Model version 3 (CCSM3) (He et al., 2008; Collins et al., 2006a), ~~and paleoclimate experiments run with the "Institut Pierre Simon Laplace" Earth System Model version 5 (IPSL-CM5A-LR) (Dufresne et al., 2013), in which marine biogeochemistry is represented,~~ to analyze our reconstructed PP results in terms of local evolution of upper seawater stratification, as well as monsoon climate ~~ISM and AMOC~~ dynamics. Based on our reconstructed PP record and modelling results documented through integrated PP maps as well as oceanic parameters profiles and cross plots, we ~~can~~ unravelled the dynamical relationship between PP in the ~~NE~~ northeastern BoB and the Indian Monsoon at both orbital- and millennial- timescales.

2. Site description and oceanographic setting

Core MD77-176 (14°30′5″N, 93°07′6″E) was retrieved from the northeastern BoB, at the junction with the Andaman Sea, during the OSIRIS 3 cruise of the R.V. *Marion Dufresne* in 1977 (Fig. 1a). The site lies ~200 km southwest of the modern Irrawaddy River mouth. ~~and is close to the limit between the northern BoB and the northern ADS.~~ It was retrieved~~is located~~ on the continental slope, at a water depth of 1375 m, i.e.~~which is~~ above the modern lysocline located between ~ 2000 m and ~ 2800 m in the northern BoB~~of the BoB~~ (~~Fig. 1a;~~ Cullen and Prell, 1984; Belyaeva and Burmistrova, 1985). The lithology consists of olive grey terrigenous clay and silty clay layers with foraminifera- ~~or~~ and nannofossil-bearing oozes ~~(Colin et al., 2006)~~.

At our core site, ~~The amplitude of seasonal changes in sea surface temperature (SST) in the BoB and the ADS is relatively small. T~~the lowest ~~(~26 °C)~~ and highest SST ~~(~28−29 °C) are~~ recorded ~~in~~ during winter (~26 °C) and summer (~28−29 °C), respectively, reflect well the relatively low amplitude SST seasonal changes (~ 2-3°C) observed in the area (Locarnini et al., 2010). The oceanic environment ~~surrounding the studied site~~ is under the influence of the Indian Monsoon and shows strong seasonal variations in evaporation/precipitation that is expected under such conditions (Webster et al., 1998; Schott and McCreary, 2001; Shankar et al., 2002; Gadgil, 2003). During the summer, moisture-rich southwesterly surface winds blowing from the Indian Ocean result in heavy precipitation ~~over South Asia, the BoB and the ADS~~ (Fig. 1b, d; Lau et al., 2000; Chen et al., 2003; Randel and Park, 2006). During winter, dry and cool northeasterly surface winds, weaker than the summer winds, blow from Himalayan highlands and result in drier conditions~~to the ocean~~ (Fig. 1c, e).

The summer precipitation rates over the BoB and the Andaman Sea~~ADS~~ and over the surrounding lands (up to 15 mm/day) are much higher than that in the AS (1–3 mm/day; Fig 1d, k). This heavy precipitation area covers the catchments of ~~—~~Ganges-Brahmaputra-Meghna (GBM) and Irrawaddy-Salween (IS) river systems~~river catchments on the land surrounding the BoB and ADS~~, and thus generates massive freshwater discharge (up to 4050 km^3 a year) to the ocean (Sengupta et al., 2006). This input of freshwater depletes~~generates a tongue of low~~ sea surface salinity (SSS) at our core site (lower than 33 psu) in the same way as the entire northern BoB and Andaman Sea~~occupying the northern BoB and ADS~~, that is occupied by a low salinity tongue, with a~~whose extension is~~ largest extension in November, several months later than the peak of summer precipitation (Akhil et al., 2014; Fournier et al., 2017; Fig. 1f, g, l). ~~The low SSS tongue together with the direct rainfall on sea surface cause low SSS in the whole BoB and ADS (Duplessy et al., 1982; Akhil et al., 2014; Fig. 1f, g, l).~~ Low SSS decreases sea surface density, thereby increasing the density gradient of the upper water column, and thus leading to a strong stratification that impedes the transfer of nutrient from the nutrient-rich deep layer into the euphotic zone. Such a “barrier layer” effect results in generally low annual PP (around 100−140 gC m^{-2} yr^{-1}) in this area~~in the BoB and ADS~~ (Prasanna Kumar et al., 2002; Madhupratap et al., 2003; Fig. 1h, i)~~.~~, with maxima being reached during winter, when increased surface wind intensity together with decreased precipitation enhance upper seawater column mixing. The low annual PP at the studied site indicates that this area is not significantly influenced by nutrient inputs from rivers to the difference of the near-shore settings, characterized by annual PP maxima (up to 340 gC m^{-2} yr^{-1}). By contrast, evaporation is high and~~with lower~~ precipitation is lowover the AS. It~~Arabian Sea,~~ generates higher SSS (higher than 35 psu)~~explaining that SSS~~ than in the BoB (Fig. 1f, g, l).~~,~~ Such SSS conditions and therefore, the absence of a strong stratification, makes it possible the development of upwelling and convective mixing during summer and winter respectively, and thus, high PP through the year (up to 320–340 gC m^{-2} yr^{-1}, Fig. 1h)~~with subsurface flows of particularly high salinity waters originating from the Persian Gulf and the Red Sea. This high surface salinity and therefore the absence of a strong stratification make it possible the development of well-developed, wind-driven upwelling cells along the Somalian, Arabian and Indian coasts, which result in high PP in the AS~~ (Anderson and Prell, 1992; Prasanna Kumar et al., 2001, 2009; McCreary et al., 2009). ~~Although PP is generally low in the BoB and the ADS, seasonal variations can be seen at the studied site, with relatively higher PP during winter (Fig. 1m). This increased PP in winter is the result of increased SSS due to decreased precipitation, and increased mixing due to a secondary maximum in surface wind intensity (Fig. 1j, l). The low annual PP at the studied site indicates that this area is not significantly influenced by river input nutrients, which sustain extreme high PP in the near-shore and river mouth areas (Fig. 1h, i). Consequently, changes in the upper seawater column stratification and PP at the studied site are dominated by changes of SSS and wind-driven mixing.~~

3. Materials and Methods

3.1 Age model and sampling

The age model of core MD77-176 was previously established by Marzin et al., (2013) based on 31 Accelerator Mass Spectrometry (AMS) ^{14}C ages combined with the MD77-176 high-resolution oxygen isotope record obtained on planktonic foraminifera *Globigerinoides ruber*, which were correlated to the~~measured on planktonic foraminifera *Globigerinoides ruber*. It was then refined by tuning the seawater oxygen isotope~~ ~~($\delta^{18}O_{SW}$) anomaly curve with the~~ GISP2 Greenland ice core ~~$\delta^{18}O$~~ oxygen isotope curve ~~(Fig. 2)~~. The correlated age model is consistent with the AMS ^{14}C age model, especially after 20 kyr BP (Marzin et al., 2013). The sedimentation rates recorded at site MD77-176 (~25 cm/kyr and up to 40 cm/kyr for the Holocene) provide a good opportunity to study productivity patterns over the last 26 kyr, with millennial to centennial resolutions (Fig. S1).~~For the present study, we sampled the upper 711 cm of core MD77-176, every 3 cm. A total of 212 samples were analyzed, covering an interval ranging between 26 and 1 kyr BP, with temporal resolution varying from ~50 to 400 years.~~

3.2 Coccolith analysis and PP reconstruction

For coccolith data, a total of 212 samples were analyzed, with a temporal resolution of ~50 to 400 years. Slides ~~for coccolith analysis~~ were prepared using ~~a~~ the “settling” technique described in Duchamp-Alphonse et al., (2018) after Beaufort et al., (2014). About 0.004 g of dry sediment was diluted in 28 mL Luchon™ water (pH = 8, bicarbonate = 78.1 mg/L, total dissolved solid = 83 mg/L) within a flat beaker and settled on a 12 × 12 mm coverslip for 4 h. After pumping the clear liquid out, the coverslip was then dried at 60°C in an oven~~,~~ and mounted on slide with NOA74 glue. This technique ensures a homogenous distribution of coccoliths on the coverslip.

Slices were analyzed with a polarized light microscope (Leica DM6000B) at ×1000 magnification. For each slice, at least 500 coccolith specimens were counted by human eyes under at least 3 random fields of view. The relative abundance of *F. profunda* (Fp%) were calculated as: Fp% = 100 × (Fp number / total coccolith number). The 95% confidence interval for Fp% was calculated following the method of Patterson and Fishbein (1984), and corresponds to a reproducibility smaller than ±5 %.

Fp% indicates relative depth of nutricline which is critical for PP (Molfino and McIntyre, 1990a, 1990b). To the difference of most coccolith species that are found in the upper photic zone (< 100 m water depth),~~According to early studies,~~ *F. profunda* ~~thrives in the tropics and~~ dwells in the lower photic zone, at water depth of ~100–200 m~~, in the lower photic zone~~ (Okada and Honjo, 1973). Therefore, ~~W~~when nutricline gets shallower, more nutrient is brought into the upper euphotic zone and primary production increases, while relative abundance of *F. profunda* decreases. ~~leading to production increase of the upper euphotic zone coccolithophores, and thus lowering the relative abundance of the deep dwelling *F. profunda*.~~ By contrast, when nutricline becomes deeper and primary production decreases, the relative abundance of *F. profunda* increases. This relationship between Fp% and nutricline depth is the basement ~~base~~ of~~for~~ PP reconstructions via Fp% in marine sediment. Beaufort et al., (1997) first established a Fp%-PP empirical relationship in the AS based on PP estimates from satellite observations and Fp% in surface sediments.~~the study of surface sediments.~~ In this study, we estimated PP for the last 26 kyr using a recently published Fp%-PP empirical equation suited for tropical Indian Ocean (Hernández-Almeida et al., 2019): PP = [10^ (3.27 ~~–~~ – 0.01 × Fp%)] × 365 / 1000. The unit of estimated PP is gram of carbon per meter square per year (gC m^{-2} yr^{-1}).

3.3 Paleoclimate simulations

3.3.1 Experiments run with IPSL-CM5A-LR~~TraCE-21 simulation~~

IPSL-CM5A-LR (termed “IPSL-CM5A” in the following) is an Earth System Model (ESM) developed at the “Institut Pierre Simon Laplace” (Dufresne et al., 2013) for the Coupled Model Intercomparison Project phase 5 (CMIP5; Taylor et al., 2012) and the Paleoclimate Modelling Intercomparison Project phase 3 (PMIP3; Braconnot et al., 2012)~~ exercises~~. It is composed of several model components representing the atmospheric general circulation and physics~~the~~ (LMDZ5A~~ atmospheric general circulation model (~~;Hourdin et al., 2013), the land-surface (ORCHIDEE; ~~land-surface model (~~Krinner et al., 2005) and the ocean (NEMO v3.2; ~~ocean model (~~Madec, 2008) which includes the ocean general circulation and physics (OPA9)~~ ocean general circulation model~~, sea-ice~~the~~ (LIM-2; Fichefet and Maqueda, 1997)~~ sea-ice model~~, and ~~the~~marine biogeochemistry (PISCES; ~~ biogeochemical model (~~Aumount and Bopp, 2006). The LMDZ atmospheric grid~~The atmospheric grid of this ESM model~~ is regular in the horizontal with 96×95 points in longitude×~~÷~~ latitude (corresponding to a resolution of ~3.75°×1.9°) and 39 irregularly spaced vertical levels. The oceanic grid is curvilinear with 182×149 points, corresponding to a nominal resolution of 2°, and 31 vertical levels. It is refined close to the equator, where the resolution reaches ~0.5°.

Four experiments, set under different boundary conditions, were exploited in this study. Three of them were run for the PMIP3 exercise: the pre-industrial experiment (CTRL), the mid-Holocene experiment (MH), and the Last Glacial Maximum experiment (LGMc). Boundary conditions and ~~more ~~details for these three experiments can be found in Le Mézo et al. (2017). The fourth experiment (LGMf) is a freshwater “hosing” simulation similar to the IPSL-CM4 freshwater “hosing” simulation (~~as in ~~Kageyama et al., 2013), in which ~~which was applied under LGM conditions. Compared to the LGMc experiment, the only difference is that an additional ~~a freshwater flux of 0.2 Sv is applied under LGM (LGMc) conditions~~was added~~ over the North Atlantic Ocean, the ~~ and ~~Nordic Seas, and the Arctic Ocean, ~~in the LGMf experiment. The freshwater flux~~that causes the AMOC to slow down (Fig. S2~~3b~~). Both LGMf and LGMc were run for nearly 500 model years. The monthly outputs averaged over the last 100 years of the four experiments~~each experiment ~~were used to compare their mean states~~in this study~~. In addition,~~Moreover,~~ we focused on~~used~~ monthly results averaged over successive periods of 10 years for the LGMc and LGMf experiments to analyze the transient effects of ~~the changes of ~~AMOC ~~strength~~changes.

In the glacial experiments (LGMc and LGMf) the sea level is lower, resulting in more extensive continents, including in the study area. The core location is then closer to the coast. In these simulations, the river mouth locations, at which fresh water and nutrients from rivers are brought to the ocean, are moved together with the modified coastline. In particular the GBM river mouth is brought to the south of its present location, while the IS river mouth is brought northeastward. These locations have been chosen as they reflect the closest LGM coastal points to the present river mouths, and the most probably river paths during low sea-level conditions. In our relatively simple set up, for the MH, LGMc and LGMf simulations we are using the same nutrient content of river inputs for the CTRL simulations, in which they are prescribed according to Ludwig et al. (1996). However, due to the sea level drop and associated continental extension under glacial conditions, in LGMc and LGMf, the nutrients from rivers are less diluted before reaching a fixed location.

Several parameters were extracted to describe climate conditions: surface wind speed and precipitation minus evaporation rates (P-E), as well as ocean conditions: potential temperature (T_θ), salinity, nitrate content (NO_3^-), upper seawater stratification based on potential density (σ_T) difference between 200 m and 5 m (ΔPD; Behrenfeld et al., 2006), and primary productivity (PP). T_θ and salinity of the top layer of the oceanic model are used as SST and SSS.~~TraCE-21 is a transient simulation of the global climate evolution over the last 22 kyr run with the CCSM3 model, designed by the National Center of Atmosphere Research (He et al., 2008; Collins et al., 2006a; Liu et al., 2009). CCSM3 is a global, coupled ocean-atmosphere-sea ice-land surface climate model, run without flux adjustment (Collins et al., 2006a). It includes four component models: the Community Atmospheric Model version 3 at T31 resolution (CAM3; Collins et al., 2006b), the Community Land Surface Model version 3 (CLM3; Dickinson et al., 2006), the Community Sea Ice Model version 5 (CSIM5; Briegleb et al., 2004), and the Parallel Ocean Program version 1.4.3 (POP; Smith and Gent, 2002). The forcing of the TraCE-21 simulation comprises changes in insolation due to the slow variations of astronomical parameters (ORB), changes in atmospheric greenhouse gases as measured in ice cores (GHG), modification of topography, land surface type and coastlines resulting from the evolution of the continental ice sheets as reconstructed by Peltier (2004) (ICE-5G), and changes in freshwater discharge from melting ice sheets which force the AMOC strength to change (MWF; Fig. 3a). In addition to the full TraCE-21 simulation (termed “TraCE” in the following), there are four single-forcing sensitivity experiments: the ORB, GHG, MWF, and ICE, in which only one of the forcing mentioned above is allowed to evolve through time while all the three others are kept fixed at their 19 kyr BP value. More details about the TraCE can be found in He (2008). The datasets of TraCE and other experiments were downloaded from the website of Earth System Grid: https:// earthsystemgrid.org/project/trace.html. Atmosphere decadal-mean seasonal averaged and ocean decadal-mean annual averaged datasets were used in this study.~~

3.3.2 TraCE-21 simulation~~Experiments run with IPSL-CM5A-LR~~

TraCE-21 (termed “TraCE” in the following) is a transient simulation of the global climate evolution over the last 22 kyr which was run with the CCSM3 model~~,~~ designed by the National Center of Atmosphere Research (He et al., 2008; Collins et al., 2006a; Liu et al., 2009). CCSM3 is a global, coupled ocean-atmosphere-sea ice-land surface climate model, run without flux adjustment (Collins et al., 2006a). It includes four components representing atmosphere ~~models: the Community Atmospheric Model version 3 at T31 resolution~~ (CAM3; Collins et al., 2006b), land surface~~the Community Land Surface Model version 3~~ (CLM3; Dickinson et al., 2006), sea ice~~the Community Sea Ice Model version 5~~ (CSIM5; Briegleb et al., 2004), and ocean~~the Parallel Ocean Program version 1.4.3~~ (POP; Smith and Gent, 2002). The forcing of the TraCE-21 simulation comprises changes in insolation due to the slow variations of astronomical parameters (ORB), ~~changes~~ in atmospheric greenhouse gases as measured in ice cores

(GHG), in topography, land surface type, coastlines~~modification of topography, land surface type and coastlines resulting from the evolution of the continental ice sheets as reconstructed by Peltier (2004)~~ (ICE-5G; Peltier, 2004), and ~~changes~~ in freshwater discharge from melting ice sheets which force the AMOC strength to change (MWF; Fig. S3~~a~~). In addition to the full TraCE-21 simulation ~~(termed "TraCE" in the following)~~, we used the~~there are~~ four single-forcing-sensitivity experiments~~: the~~ (ORB, GHG, MWF, and ICE), in which only one of the forcing mentioned above is allowed to evolve through time while all the three others are kept fixed at their 19 kyr BP value. Atmosphere decadal-mean seasonal averaged and ocean decadal-mean annual averaged datasets were downloaded from the website of Earth System Grid: https://earthsystemgrid.org/project/trace.html. They have been used to provide the same atmospheric and oceanic parameters simulated by the IPSL model, but over the last 26 kyr, and with the exception of marine biogeochemical variables which are not computed in the CCSM3.~~More details about the TraCE can be found in He (2008). The datasets of TraCE and other experiments were downloaded from the website of Earth System Grid: https:// earthsystemgrid.org/project/trace.html. Atmosphere decadal-mean seasonal averaged and ocean decadal-mean annual averaged datasets were used in this study.~~

4. Results ~~and discussion~~

4.1 Coccolith abundances and reconstructed PP over the last 26 kyr~~Paleoproductivity record in the northeastern Bay of Bengal~~

At the studied site, coccolith assemblages mainly consist of~~the main coccolith species are~~ *Florisphaera profunda*, *Emiliania huxleyi*. *Gephyrocapsa* ~~*oceanica*, small *Gephyrocapsa* (*Gephyrocapsa*~~ spp. ~~<3µm) and *Emiliania huxleyi*.~~ *F. profunda* largely dominates the assemblage (> 60%) over the last 26 kyr, while *E. huxleyi* and *Gephyrocapsa* spp. never exceed 23 % (Fig. 2)~~varies between 60 % and 95 % and thus, largely dominates the assemblage over the last 26 kyr (Fig. 2 and S1)~~. Such relative contributions are coherent with coccolith distribution in sediment traps from the northern BoB (Stoll et al., 2007), that shows a high abundance of *F. profunda* due to a strong salinity-related stratification and low surface nutrient concentration (see section 2).~~The high abundance of *F. profunda* in the studied core can be explained by the low surface nutrient concentration caused by strong stratification (section 2). Our results are coherent with high abundances of *F. profunda* observed in sediment trap records from the northern BoB (Stoll et al., 2007).~~

The most striking shifts of coccolith abundances are observed between ~20 and ~11 kyr BP, and particularly around 15-14 kyr BP, when *F. profunda* drastically increases from 60 to 93 %, while *E. huxleyi* decreases from 22 to 1 % and *Gephyrocapsa* spp. slightly decreases from 12 to 5 %. Such patterns subdivide the record into three main time intervals: (i) from ~26 to 19 kyr BP, when *F. profunda* depicts relatively high amplitude variations, ranging from 60 to 85 % with minima at ~ 25, 23 and 21 kyr BP, while *E. huxleyi* and *Gephyrocapsa* spp. both average ~10%; (ii) from 19 to 11 kyr BP, when *F. profunda, E. huxleyi* and *Gephyrocapsa spp.* depicts their highest variations (up to about 33 %, 21 % and 15% in amplitude, respectively) and (iii) from 11 to 1 kyr BP, when *F. profunda* shows a long-term increasing trend up to 8 kyr, a maxima of 85% between 8 and 6 kyr, and a long-term decreasing trend up to 1 kyr, while *Gephyrocapsa* spp. abundances exceed those of *E. huxleyi* despite minima of ~7 % between 8 and 6 kyr BP.~~PP varies between 80 and 160 gC m^{-2} yr^{-1} (Fig. 2). Remarkably, estimated PP values (~125 gC m^{-2} yr^{-1}) of the late Holocene are very close to the modern annual PP mean (~135 gC m^{-2} yr^{-1}) of the studied area (Fig. S2). At orbital-scale, PP variations appear to be anti-phased with the northern hemisphere August insolation. Relatively high PP (~120 gC m^{-2} yr^{-1}) during the Last Glacial Maximum (LGM; 21–19 kyr BP) and the late Holocene (LH; 2 kyr BP to present) match low insolation periods. Conversely, relatively low PP (~100 gC m^{-2} yr^{-1}) during the early-middle Holocene (E-MH; 9–6 kyr BP) matches a high insolation period (Fig. 4a, h). Across the Holocene (11 kyr BP to present), PP first decreases, reaching a minimum between 8 and 6 kyr BP, and then increases upward, therefore showing an opposite trend compared to insolation (Fig. 4a, h). At millennial-scale, large magnitude PP oscillations, are observed during the deglaciation (19–11 kyr BP), showing similar features than those found in the Greenland ice core $\delta^{18}O$ record, representing the rapid climatic changes in north hemispheric high-latitude areas (Fig. 2; Stuiver and Grootes, 2000). High PP up to ~150 gC m^{-2} yr^{-1} and ~120 gC m^{-2} yr^{-1}, are found in the cold periods Heinrich stadial 1 (HS1, 17.0–14.8 kyr BP) and Younger Dryas (YD, 12.9–11.7 kyr BP) respectively. Low PP down to ~100 gC m^{-2} yr^{-1}, is found in the Bølling-Allerød warm period (B-A, 14.8–12.9 kyr BP) (Fig. 4h). In the time interval before the LGM (from 26 to 19 kyr BP), PP peaks with values higher than 140 gC m^{-2} yr^{-1} are observed at ~25, 23 and 21 kyr BP showing a ~2 kyr cycle in this interval (Fig. 4h).~~

Estimated PP varies between 80 and 170 gC m^{-2} yr^{-1} (Fig. 2). Remarkably, values obtained during the late Holocene (~125 gC m^{-2} yr^{-1}) are comparable to those recorded in the study area today (annual PP mean of ~135 gC m^{-2} yr^{-1}). Because estimated PP is inversely related to *F. profunda* percentages (see section 3.2), PP reconstructed over the last 26 kyr mirrors *F. profunda* distribution. It is characterized by peaks higher than 140 gC m^{-2} yr^{-1} at ~25, 23 and 21 kyr BP. Changes with largest amplitude are found over the deglaciation with a maximum (~170 gC m^{-2} yr^{-1}) and a minimum (~80 gC m^{-2} yr^{-1}) observed at ~15 and 14 kyr BP, respectively. Relatively low PP are recorded during the Holocene, with minima of 90 gC m^{-2} yr^{-1} obtained between 8 and 6 kyr BP.~~The PP record of core MD77-176 is negatively correlated with the seawater oxygen isotope ($\delta^{18}O_{SW}$) anomaly obtained on the same core before the LGM, while a positive correlation can be seen between these two records during the deglaciation and the Holocene (19–1 kyr BP) (Fig. 4g, h). Since this $\delta^{18}O_{SW}$ record is interpreted as reflecting changes in salinity conditions in surface waters overlying site MD77-176 (Marzin et al., 2013), it appears that PP peaks are related to low SSS intervals before the LGM, and high SSS intervals over the last 19 kyr. The latter relationship is particularly~~

~~obvious during HS1 and BA. From 19 to 14.8 kyr BP, the dramatic increase in PP (~70 gC m^{-2} yr^{-1} in amplitude) is associated with a ~6 psu increase of SSS (estimated using the modern δ^{18}Osw/salinity relationship that exists in the Northern Indian Ocean; Singh et al., 2010; Sijinkumar et al., 2016). On the contrary, the sharp decrease in PP (~40 gC m^{-2} yr^{-1} in amplitude) after 14.8 kyr BP, is accompanied by a significant drop in SSS (~5 psu in amplitude).~~

4.2 Simulated PP and physicochemical profiles~~Influence of North Atlantic climate and Indian Summer Monsoon on PP~~

~~4.2.1 Last glacial: 26 to 19 kyr BP~~

Simulated annual and seasonal (summer and winter) patterns of PP (gC m^{-2} yr^{-1}) are shown for the BoB and the Andaman Sea in Figure 3, where the MH and LGMc simulations are compared to the CTRL one, and where the LGMf simulation is compared to the LGMc one, highlighting the effects of the AMOC slowdown. According to the CTRL simulation, the coastal northern BoB and Andaman Sea as well as the southwestern BoB appear to be the most productive areas under pre-industrial conditions, which is in accordance with the Vertical Generalized Production Model (VGPM), representing in situ PP distribution based on satellite derived Chlorophyll concentration (Fig. 1h, i; Behrenfeld and Falkowski, 1997). In all cases, high PP (> 220 gC m^{-2} yr^{-1}) is related to high nutrient contents in the upper column, thanks to the influence of river discharges (northern coastal BoB and Andaman Sea) or the development of coastal upwelling (southwestern BoB; Vinayachandran et al., 2004). Hence, despite its coarse spatial resolution, the IPSL-CM5A model is able to represent the main area of high PP and their seasonal cycles. The differences of annual PP between MH and CTRL reveal a dipole structure in the studied area, with slightly lower PP in the western part of the BoB and slightly higher PP in the eastern part including the Andaman Sea. Strong signal of lower PP is found in the southwestern BoB during summer, and in the northern BoB during winter. Slightly higher PP is found in the eastern BoB and the Andaman Sea, mainly during summer. The overall increase in annual PP simulated within the center part of the BoB during LGM compared to preindustrial (LGMc–CTRL), reflects well the general PP increase simulated during the summer season. This area is an extension of the high PP found by the CTRL simulation within the southwestern BoB. One of the most striking pattern highlighted by this comparison is the important increase in annual PP in the northeastern part of the BoB at the junction with the Andaman Sea, that reflects significant increases of PP during both summer and winter seasons, while PP in the northern BoB and the whole Andaman Sea is lower. This pattern highlights the CTRL river mouth grids shift toward the northeastern BoB during the LGM (section 3.3.1), and its most probable location closer to the MD77-176 site at that period. Between LMGf and LGMc, PP is lower in the entire BoB, except in the northeastern part of the BoB in winter, for which a higher annual PP is simulated.

Summer and winter vertical profiles are extracted from grids at the GBM and the IS river mouths for CTRL and MH (Fig. 4), and from grids at the northeastern BoB, near the location where core MD77-176 has been retrieved, for CTRL, MH, LGMc and LGMf (Fig. 5).

CTRL and MH river mouth profiles depict PP maxima within the surface layers (0–50 m), where reduced salinity and density conditions help maintaining a nutricline around 50 m water depth in both seasons (Fig. 4). In all cases, temperatures and SSS are lower during the MH compared to CTRL. The most striking difference is observed for the GBM river mouth system, where salinity is clearly lower within the surface layer (0–30 m) during MH compared to CTRL, especially during winter, while temperature change is limited. Such pattern results in lower density in the surface layer and stronger density gradient within the upper 200 m of the seawater (i.e. stronger salinity-related stratification) during winter season of MH. Under such conditions, nutrient content and thus PP, are lower in the upper 30 m water depth.

For the CTRL profiles of the northeastern BoB, PP maxima are found at ~75 m water depth, just above the nutricline, in both seasons (Fig. 5). Such a pattern reflects well what is found in the open sea environment of the BoB at present (Madhupratap et al., 2003). MH PP profiles show no large difference compared to the CTRL ones. It is only during winter, that salinity is significantly lower between 0 and 50 m water depth, and that the associated increase in the density gradient within the photic zone is related to slightly lower PP.

PP profiles of LGMc and LGMf are very different from those of CTRL and MH. They are associated with generally saltier and/or colder surface waters. Interestingly, high PP is found in the surface layers (0–50 m) where nutrient contents are higher than CTRL and MH conditions (Fig. 5). Such distributions show that nutrient content and PP are comparable to those found in the CTRL river mouth profiles, and particularly case during winter, where LGMc and LGMf simulations of salinity gradient show a shallower halocline that rises the density gradient of surface layers and is thus accompanied by a shallower pycnocline. It indicates that PP reacts to the shift from the open sea environment configuration during CTRL and MH simulations to the more coastal one during LGMc and LGMf simulations, as previously documented in section 3.3.1. Interestingly, during the winter, PP and nutrients contents between 0 and 30 water depths of LGMf are higher than those of LGMc. Such patterns are associated with higher salinity in surface waters and a reduced density gradient that might promote upper layer mixing. Overall, the LMGc, LMGf and MH simulations do not show strong difference in the vertical variation of temperature compared to the MH. Changes in PP and nutrient contents are rather associated to modifications in density gradient, thanks to salinity changes which highlight the importance of salinity-related stratification vs mixing in the PP distribution in the past.

~~Several pieces of evidence suggest that millennial-scale variations of PP between 26 and 19 kyr (i.e. before the LGM) chiefly resulted from wind-driven mixing. First, high PP values are reached during intervals of low surface water salinity. If these PP variations (and upper water column stratification) were primarily driven by precipitation – evaporation changes, the opposite relationship would be expected, and PP would peak at periods of higher salinity because of the weaker barrier layer effect. Besides, according to the record of δ18OSW difference between surface and subsurface seawaters obtained in the ADS, which is used as an upper water vertical stratification proxy, it appears that no significant variations occurred in upper ocean salinity stratification before the LGM (Gebregiorgis et al., 2016). Second, the speleothem δ18O signal in North India (Fig. 4c; Dutt et al., 2015), the δDalkanes record in the N-BoB (Fig. 4d; Contreras-Rosales et al., 2014), as well as the Ba/CaG. sacculifer record in the Andaman Sea (Fig. 4f, Gebregiorgis et al., 2016) all document a long-lasting dry phase and heavily reduced river runoff in the area before the LGM, implying a subdued influence of freshwater inputs within the BoB and the ADS, either directly (decreased precipitation over the sea) or from reduced river runoff. Third, the relationship between PP and SSS is similar to that observed in western and northern Arabian Sea, where PP pattern is primarily controlled by surface wind strength (Fig. 4i–k; Ivanochko et al., 2005; Schulz et al. 1998; Anand et al., 2008). Indeed, over the last 26 kyr, enrichments of organic carbon and Ba in sediments appear to reflect strong-southwesterly wind-induced biological productivity, when δ18O values document low SSS conditions (Fig.4i–k). At last, this is in line with overall ISM reconstructions documenting cool and dry conditions in the northern Indian Ocean during the strong glaciation period (Cullens, 1981; Duplessy, 1982; Kudrass et al., 2001; Contreras-Rosales et al., 2014; Dutt et al., 2015) due to enhanced snow accumulation and relatively low temperatures in the Tibetan Plateau and Himalaya (Shi Y, 2002; Mark et al., 2005) that cause a weakened meridional thermal land-sea gradient and an equatorward shift of the ITCZ mean position (Kudrass et al., 2001; Overpeck et al., 1996; Sirocko et al., 1996; Cai et al., 2012).~~

5. Discussion: Forcing factors behind PP variations over the last 26 kyr as revealed by a model-data comparison~~4.2.2 Last deglaciation to present (19 – 1 kyr BP)~~

5.1 The last glacial period

~~Several pieces of evidence suggest that millennial-scale variations of PP between 26 and 19 kyr (i.e. before the LGM) chiefly resulted from wind-driven mixing. First, high PP values are reached during intervals of low surface water salinity. If these PP variations (and upper water column stratification) were primarily driven by precipitation – evaporation changes, the opposite relationship would be expected, and PP would peak at periods of higher salinity because of the weaker barrier layer effect. Besides, according to the record of~~ $\delta^{18}O_{SW}$ ~~difference between surface and subsurface seawaters obtained in the ADS, which is used as an upper water vertical stratification proxy, it appears that no significant variations occurred in upper ocean salinity stratification before the LGM (Gebregiorgis et al., 2016). Second, the speleothem~~ $\delta^{18}O$ ~~signal in North India (Fig. 4c; Dutt et al., 2015), the~~ $\delta D_{alkanes}$ ~~record in the N-BoB (Fig. 4d; Contreras-Rosales et al., 2014), as well as the~~ $Ba/Ca_{G. sacculifer}$ ~~record in the Andaman Sea (Fig. 4f, Gebregiorgis et al., 2016) all document a long-lasting dry phase and heavily reduced river runoff in the area before the LGM, implying a subdued influence of freshwater inputs within the BoB and the ADS, either directly (decreased precipitation over the sea) or from reduced river runoff. Third, the relationship between PP and SSS is similar to that observed in western and northern Arabian Sea, where PP pattern is primarily controlled by surface wind strength (Fig. 4i–k; Ivanochko et al., 2005; Schulz et al. 1998; Anand et al., 2008). Indeed, over the last 26 kyr, enrichments of organic carbon and Ba in sediments appear to reflect strong-southwesterly wind-induced biological productivity, when~~ $\delta^{18}O$ ~~values document low SSS conditions (Fig.4i–k). At last, this is in line with overall ISM reconstructions documenting cool and dry conditions in the northern Indian Ocean during the strong glaciation period (Cullens, 1981; Duplessy, 1982; Kudrass et al., 2001; Contreras-Rosales et al., 2014; Dutt et al., 2015) due to enhanced snow accumulation and relatively low temperatures in the Tibetan Plateau and Himalaya (Shi Y, 2002; Mark et al., 2005) that cause a weakened meridional thermal land-sea gradient and an equatorward shift of the ITCZ mean position (Kudrass et al., 2001; Overpeck et al., 1996; Sirocko et al., 1996; Cai et al., 2012).~~During the LGM (23–19 kyr BP), i.e. when drier conditions prevailed in the area, our reconstructed PP estimates average ~120 gC m^{-2} yr^{-1}, which is nearly the same value as the one reconstructed for the late Holocene (2–1 kyr BP) (Figs. 6i and 7f, g). An important discovery is the high-amplitude millennial-scale variations that PP depicts from 26 to 19 kyr BP. Such variations mirror those of SSS (seawater $\delta^{18}O$ anomaly signal) obtained on the same core (Fig. 6h), and to some extent in the Andaman Sea (Fig. 6e, g), thus documenting high PP intervals at times of low SSS pulses and vice versa. In such a context, the most plausible explanation for higher PP coeval with low SSS deals with higher nutrient inputs from rivers. Indeed, during the LGM and relatively low sea-level, more proximal IS river mouth system might promote freshwater and terrigenous nutrient transfer to our core site, thus decreasing (increasing) SSS and increasing (decreasing) nutrient content and PP, according to South Asia precipitation and riverine flux dynamics. Such millennial-scale variations are readily seen in the record of South Asian monsoonal precipitation, thus confirming our assumption. Indeed, despite long-term aridity during the LMG, as documented by the net precipitation results of the TraCE simulation together with $\delta^{18}O$ and δD alkane signals from cave speleothems and marine sediments respectively (Fig. 6c, d), rapid SSS decreases at our core site are in phase with short-term increases in precipitation and vice versa (Figs. 6h). They are also found in IPSL-CM5A simulations where higher PP and higher nutrient contents within the upper 50 m of the photic zone during LGMf and LGMc compared to MH and CTRL, reflect higher terrigenous nutrient inputs to the studied site, as the the IS river mouth system migrates probably northward, i.e closer to our core site (section 4.2). Interestingly, the highest reconstructed PP (~160 gC m^{-2} yr^{-1}) remains lower than the simulated PP at river mouths (>220 gC m^{-2} yr^{-1}), thus suggesting that core MD77-176 is not within the coastal environment during the LGM, but is rather influenced by the nutrient enriched-river system plume. The local specificities of the area have in part been highlighted by Sijinkumar et al. (2016) that reported lower SSS compared to the modern time in the northern Andaman Sea due to major changes in basin morphologies between both periods, thanks to the sea-level significantly lower during the LGM compared to modern times. Therefore, in such contexts, one cannot exclude that both, the low sea-level conditions and the migration of the IS river mouth system, might result in the specific SSS and PP records obtained at our core site. In all cases, it appears that between 26 and 19 kyr BP, the IS river system renders MD77-176 PP sensitive to millennial-scale variations in South Asian monsoonal precipitation, as it modulates riverine flux and the extent of the nutrient-rich riverine plume in the area.

5.2 The last deglaciation

~~The factors controlling PP on the millennial-scale over the last 19 kyr, appear to differ from those acting before the LGM. A strong impact of wind-related changes on vertical stratification is unlikely given that river runoff (Gebregiorgis et al., 2016), together with the precipitation (Dutt et al., 2015; Contreras-Rosales et al., 2014), gradually strengthened in this area during the last deglaciation up to the mid-Holocene, due to stronger southwest monsoon circulation (Fig. 4e–g). Since site MD77-176 is directly influenced by river discharges and because PP positively covaries with SSS during that time interval (Fig. 4g, h), it seems reasonable to propose that those PP variations are driven by ISM dynamic through changes in upper water column stratification associated to SSS variations (Govil and Naidu, 2011). In such a scenario, we suggest that the gradual increases of PP during HS1 and YD reflect the shoaling of the nutricline in response to increased salinity of the mixed layer resulting from a weaker summer (wet) southwest monsoon and strongly reduced river runoff (Sinha et al., 2005; Govil and Naidu, 2011;~~

~~Dutt et al., 2015; Contreras-Rosales et al., 2014, Phillips et al., 2014; Gebregiorgis et al., 2016). On the contrary, PP minima observed during the B-A and the early to mid-Holocene testify for a stronger stratification and a deeper nutricline, due to stronger South Asian Monsoon precipitation (Sinha et al., 2005).~~

~~Some influence from the North Atlantic climate is also likely, given that, during the last deglaciation, events of high (low) PP and SSS in the BoB (Rashid et al., 2007; Marzin et al., 2013), i.e. weak (strong) ISM, correspond to cold HS1 and YD (warm B-A) events in the North Atlantic, as defined by the GISP2 Greenland ice core δ18O record on Fig. 2. The abrupt changes in the North Atlantic climate have been widely associated with changes in the AMOC (Elliot et al., 2002; McManus et al., 2004; Stocker and Johnsen, 2003). A widely held explanation for these rapid climatic changes involves the supply of fresh water to the northern Atlantic Ocean and its direct effect on the transport of heat to mid and low latitudes, via a decrease and even a collapse, of the AMOC (Heinrich, 1988). In such a scenario, the AMOC is usually seen as a conveyor belt involved in interhemispheric transport of heat (e.g. Liu et al., 2009; Buckley and Marshall, 2016), whose changes have a specific influence on tropical Atlantic rainfall (Wang et al., 2004; Peterson et al., 2000; Peterson and Haug, 2006; Swingedouw et al., 2009), and ISM (Overpeck et al., 1996; Barber et al., 1999; Fleitmann et al., 2003; Gupta et al., 2003; Murton et al., 2010; Yu et al., 2010; Cai et al., 2012; Marzin et al., 2013). Therefore, it is not excluded that our PP record is sensitive to such processes. However, as anti-phase relationships between our PP record and those in the N- and W-AS are observed, it implies that the mechanism involving the influence of AMOC on PP in the northeastern BoB, is different from that in the AS related to wind-induced upwelling and mixing (Schultz et al., 1998; Altabet et al., 2002; Ivanochko et al., 2005). One plausible explanation is that during HS1 and YD, releases of meltwaters in the northern Atlantic Ocean subdued or disrupted the AMOC, thus triggering a southward shift of the ITCZ, a large decrease in Indian Monsoon precipitation (Gupta et al., 2003; Goswami et al., 2006; Li et al., 2008; Pausata et al., 2011), and leading to an increased PP in the BoB due to saltier surface sea waters. However, even if our record supports the scenario of a major role of the AMOC in rapid deglacial PP changes, there are still major unresolved issues regarding the mechanisms at play. In particular, the evidence linking PP changes with upper water column stratification in the context of past ISM and AMOC variabilities is still incomplete.The largest PP variations occur during the deglaciation. The outputs of MWF experiment also show strong responses of SSS and ΔPD_200-5 to the changes of AMOC strength forced by meltwater discharge in the North Atlantic (Fig. S8). Therefore, we analyzed how PP in the northeastern BoB responds to AMOC changes in the ESM including the marine biogeochemical component PISCES.~~

~~We analyzed the LGMc and LGMf experiments (section 3.3.2), and the results shown here are the mean of winter months, from December to February (DJF) in the northern BoB (Fig. S7 shows the grids from which the results~~

~~have been extracted). In the LGMf, the AMOC is progressively getting weaker during the duration of the run (Fig. 3b). Under weakening AMOC conditions, SSS in the northern BoB is getting higher (Fig. 6d). Similar to the results of TraCE, the change of SSS contributes to the change of stratification in CM5A (Fig. 6d). The smaller ΔPD_200-5 (weaker stratification) causes the integrated nitrate content of the upper 50 m (NO3_0-50 for short) to increase, and a negative correlation can be seen between them (Fig. 6b). The increasing upper nitrate content results in an increase of the integrated PP, and a positive correlation can be seen between them (Fig. 6a). Consequently, the increased PP is related to weakened stratification caused by higher SSS (Fig. 6c).~~

~~Vertical profiles of the four parameters discussed above (namely: salinity, density, NO3 and PP) were also investigated (Figs. 7 and 8). They show the contrasted response of nitrate concentration in the upper water column (above 40 m) and the lower water column (below 60 m) associated to AMOC reduction. While the upper-water nitrate content increases, the lower-water nitrate content decreases, and the increase is much lower than the decrease (Fig. 8a). Conversely, the PP increase in the upper layer is larger than the decrease in the subsurface (Fig. 8b). This is because photosynthesis rate is much higher in the upper euphotic layer than in the lower euphotic layer, but the upper seawater is nutrient limited. Therefore, PP variations in the NE-BoB driven by changes of AMOC intensity are linked to the upper nutrient availability, which is controlled by the salinity-related stratification.~~

~~The results discussed above are for the DJF mean because modern data show that the highest PP takes place in winter, which contributes about half of the annual gross PP (Fig. 1m). We propose that this mechanism revealed by the DJF mean results of the experiments run with CM5A involving the changed AMOC explains the PP changes in the deglaciation given by our PP record reconstructed by coccoliths assemblages.~~During the last deglaciation (19–11 kyr BP), the most striking changes of reconstructed PP covary positively with SSS, especially after the 19-17 kyr BP transient period, when high PP intervals correspond to high SSS ones, and vice versa (Fig. 6h, i). Both signals show three stages that correspond to abrupt temperature changes in the North Atlantic Ocean, i.e. the cold Heinrich Stadial 1 (HS1; 17–14.8 kyr BP), the warm Bølling-Allerød (B-A; 14.8–12.9 kyr BP) and the cold Younger Dryas (YD; 12.9–11.8 kyr BP), which are characterized by changes in AMOC strength (Fig. 6b, h, i; Elliot et al., 2002; McManus et al., 2004). The AMOC is a component in inter-hemispheric transport of heat (e.g. Liu et al., 2009; Buckley and Marshall, 2016) and its changes in intensity, which are related to inter-hemisphere temperature gradient, have a strong influence on tropical Atlantic (Wang et al., 2004; Peterson et al., 2000; Peterson and Huaug, 2006; Swingedouw et al., 2009), and South Asia rainfalls (Overpeck et al., 1996; Barber et al., 1999; Fleitmann et al., 2003; Gupta et al., 2003; Murton et al., 2010; Yu et al., 2010; Cai et al., 2012; Marzin et al., 2013). Cold periods in the North Atlantic are associated with relatively weak AMOC and low monsoon precipitation, and vice versa. The relationship between South Asian rainfall and AMOC during the last deglaciation has been studied by Marzin et al., (2013), based on several water hosing experiments run with IPSL-CM4 model. They found a strong positive correlation between the AMOC strength and South Asian summer precipitation rates and pointed out that temperature anomalies over the tropical Atlantic Ocean are key elements in modulating the tele-connection mechanisms between the AMOC and South Asian rainfall. It has been proposed that a southward shift of the ITCZ was triggered by low tropical Atlantic Ocean temperatures and weakened AMOC during HS1 and possibly the YD (Stocker and Johnsen, 2003; Gupta et al., 2003; Goswami et al., 2006; Li et al., 2008; Pausata et al., 2011; McGee et al., 2014; Schneider et al., 2014). Such variations of moisture are simulated here, in the IPSL-CM5A housing simulation (LGMf), that shows weaker summer winds and drier climate over the AS and South Asia when AMOC is weakened compared to the LGMc simulation (Fig. 7k, n). They are also observed in the TraCE simulation over the deglaciation, with millennial-scale variations of net precipitation being mainly forced by changes in AMOC strength, and the colder periods (HS1 and YD) being associated with weaker precipitation (Figs. 6d, S4). More importantly, the reconstructed records and TraCE results, together show that weaker net precipitation intervals correspond to higher SSS ones, which indicates that South Asian net precipitation controls the salinity budget in the BoB and Andaman Sea (Figs. 6d, h). Since SSS and PP variations of MD77-176 site are highly correlated to upper seawater density gradient (stratification) while SST remains relatively stable (Figs. 6f, h, i), it seems reasonable to propose that during the last deglaciation, PP variations are directly driven by precipitation dynamics through changes in upper water column stratification associated to SSS variations (the so-called “barrier layer” effect). An important finding is that millennial-scale variations of MD77-176 PP are anti-phased with those in the western and northern AS (Fig. 6j, k), which are indicators of local summer wind strength. We interpret this anti-phased PP patterns by the fact that weaker summer winds (i.e. reduced PP) over AS, by bringing less moisture to South Asia, result in subdued freshwater inputs within the NE-BoB, that weaken stratification and increase PP. To the opposite, stronger summer winds (i.e. higher PP) over AS, reinforce precipitation over South Asia, enhance freshwater inputs within the NE-BOB, and ultimately decrease PP through enhanced stratification.

The relationships between ITCZ, southwesterly winds over the AS, South Asian rainfall, SSS, and stratification over the northern BoB and Andaman Sea, are confirmed by IPSL-CM5A. Compared to LGMc, LGMf clearly show higher SSS and weaker stratification, especially in the northeastern BoB, under weakened AMOC condition (Fig. 7k–o). The areas with higher PP in the northeastern BoB, that corresponds to the LGMc river mouth grids, match well those with the largest increase of SSS (Figs. 3j and 7m), indicating that salinity-stratification controls PP, even under unchanged amount of nutrient inputs from rivers (section 3.3.1). The relationship that exists between the salinity-stratification and PP of these grids is shown in Fig. 8. It clearly shows a positive correlation between PP and nitrate contents and between nitrate contents in the upper photic zone (0–50 water depth) and SSS. In such a context, PP is therefore inversely correlated to the stratification, with high PP being associated to high nutrients, high SSS and reduced vertical density gradient. Moreover, the annual simulated PP increase is mainly associated to PP increase during winter (Fig. 3l), which mirrors well the winter peak of PP observed in modern times (Fig. 1m).

Although LGMf is not set under the complete conditions of HS1 or YD (higher atmospheric pCO_2 and sea-level compared to the LGM), it helps deciphering the control that salinity-stratification exerts on PP in the northeastern BoB under weakened AMOC condition and lower South Asian rainfall. Together with the robust relationships that exist between reconstructed PP, SSS, South Asia rainfall, and AS southwesterly winds, we can conclude that as the sea-level rises during the last deglaciation, the location of MD77-176 is less influenced by nutrient inputs from the IS river mouth system than during the last glacial period, and that the "barrier layer" effect dominates. Therefore, PP variability is highly controlled by the changes of salinity-stratification that is linked to the changes of AMOC strength and monsoon precipitation.

~~4.3 PP dynamics over the last 19 kyr: data-model combined arguments~~

~~As mentioned above, PP variations in the northeastern BoB over the last 19 kyr have a close linkage to local SSS changes related to Indian Monsoon precipitation. In order to better understand the mechanisms behind PP response, we analyzed climate model outputs (section 3.3). We focused on the Holocene and the deglaciation to investigate the effect of insolation and AMOC strength on the Indian Monsoon and try and understand how the Indian Monsoon influences PP in the northeastern BoB during a period of AMOC change.~~

~~4.3.1 Impacts of insolation and AMOC on the Indian Summer Monsoon and local hydrological conditions~~

5.3 The Holocene

~~During the Holocene, insolation is the main climate forcing factor since other forcing (i.e. greenhouse gas, ice volume, coastlines, vegetation) are relatively stable after the deglaciation. The mechanisms that force monsoon climate to change were studied by many modeling works (Kutzbach, 1981; Kutzbach and Street-Perrott, 1985; Braconnot et al., 2007a, 2007b; Marzin and Braconnot, 2009; Zhao and Harrison, 2012; Kageyama et al., 2013). During the last deglaciation, the AMOC strength showed large fluctuations (McManus et al., 2004) and modeling studies focused on the impact of AMOC variations on the Asian Monsoon (e.g. Zhang and Delworth, 2005; Lu et al., 2006; Marzin et al., 2013; Liu et al., 2014; Wen et al., 2016). Regarding precipitation changes over South Asia,~~

~~Marzin et al. (2013) proposed that AMOC can remotely impact the Indian monsoon via perturbations of the subtropical jet over Africa and Eurasia triggered by atmospheric and oceanic changes over the tropical Atlantic.~~

~~Here, to illustrate the general impacts of insolation on the Indian Monsoon and local hydrological changes, we studied the differences of summer wind vectors, annual mean precipitation and annual mean SSS between the MH and the CTRL experiment run with CM5A (Fig. S3c, d), and between the MH (6.5–5.5 kyr BP mean) and LH (1.5–0.5 kyr BP mean) in the TraCE and ORB experiments (section 3.3; Fig. S4). To test the impact of AMOC variation, we studied the differences of the same parameters between the LGMc and LGMf (Figs. 3a and S3a, b), between the LGM (21–19 kyr BP mean) and HS1 (17–15.5 kyr BP mean), and between the B-A (14.8–14 kyr BP mean) and HS1 in the TraCE and MWF experiments (section 3.3; Figs. 3a, S5 and S6). The results of CM5A show increased South Asia precipitation and decreased SSS in BoB and ADS in the MH compared to the CTRL, while such trends are less obvious in the TraCE and ORB experiments (Fig. S4). The experiments involving changes of AMOC conditions depict similar results. They both show that enhanced (weakened) AMOC conditions observed during the LGM and the B-A (HS1) are associated with decreased (increased) SSS and increased (decreased) stratification in the studied area (Fig. 5), while no striking trends may be highlighted for SST during these time intervals.~~

~~In the TraCE simulation, we first investigated the changes in annual mean seawater salinity at 5m (SSS), seawater temperature at 5m (SST), and upper seawater stratification in the northeastern BoB over the last 19 kyr (Fig. 5 and S7). The density difference between the surface (5 m) and 200 m is a useful measure of stratification (ΔPD_200-5; Behrenfeld et al., 2006). Such numerical results clearly support our PP results and previous interpretations and is in good accordance with the modern “barrier effect” associated to low SSS conditions. Similarly, a good correlation exists between the simulated SSS changes and the SSS record of MD77-176 during the deglaciation. The oscillations of simulated ΔPD_200-5 and SSS in the deglaciation are chiefly accounted for by the MWF forcing as shown by the outputs of the MWF sensitivity experiment (Fig. S8). However, during the Holocene, the simulated ΔPD_200-5 and SSS in the TraCE simulation fail to reproduce the successive decreasing and then increasing trends observed in PP and SSS records from core MD77-176 (Fig. 5), which we have attributed to orbital forcing. The outputs of the ORB sensitivity experiment show limited and even opposite trends to what we observed (Fig. S8). As mentioned above, the results of IPSL show large differences of SSS between the MH and the pre-industrial period, which is identical to what the sedimentary reconstruction of SSS shows (Sijinkumar et al., 2016). This indicates that the CM5A has probably a higher sensitivity to the orbital insolation forcing than the CCSM3. Moreover, the difference of precipitation between MH and CTRL experiments in the eastern BoB (ADS) is negative, which is opposite to the difference occurring in the South Asia (Fig. S3c). However, the SSS decreased in the whole~~

~~BoB (ADS) during the MH compared to the CTRL, which means that river runoff is a much larger contributor of freshwater input than direct rainfall on the sea, and is thus the main driver of SSS changes in the BoB and ADS (Behara and Vinayachandran, 2016).~~During the Holocene (11–1 kyr), long-term decreasing trends in reconstructed PP match long-term decreasing trends in SSS, increasing trends in South Asian precipitation, and increasing trends in AS PP, while simulated SST show a gradual increase of ~1°C across the area (Fig. 6). Therefore, the relationships between these parameters are similar to those we observed over the last deglaciation. The most obvious pattern is found during the early–middle Holocene (8–6 kyr BP) when PP and SSS minima correspond to South Asian precipitation and AS PP maxima. This time interval, also called the Early Holocene Climatic Optimum (EHCO; e.g. Ciais et al., 1992; Contreras-Rosales et al., 2014), is characterized by higher North Hemisphere (NH) summer insolation compared to present, as highlighted by a maximum in the 30°N August mean insolation (Fig. 6a), and the peak of insolation difference between 6 kyr BP and present day over low- and mid-latitude areas (Marzin and Braconnot, 2009). Under enhanced boreal summer insolation, the MH simulation reveals stronger southwesterly summer winds over the AS and enhanced net precipitation over South Asia (Fig. 7p, s), thanks to the northward shift of the ITCZ system (Bassinot et al., 2011; McGee et al., 2014; Schneider et al., 2014). Lower SSS and higher density gradient (stronger stratification) are concomitantly documented over the entire BoB, but they are particularly obvious in the northern BoB (Fig. 7q, r), that are directly influenced by freshwater budget and input from the GBM river system (Behara and Vinayachandran, 2016). All these elements suggest that during the Holocene PP changes in the northeastern BoB were most probably driven by salinity-stratification associated to the changes in precipitation. This is confirmed by the comparison between the MH and CTRL profiles of the GMB river mouth system, that highlights lower nutrient contents and PP in the upper seawater associated with reduced SSS and increased density gradient between 0 and 30 m water depths (section 4.2, Fig. 4).

~~4.3.2 PP response to hydrological changes~~

~~The largest PP variations occur during the deglaciation. The outputs of MWF experiment also show strong responses of SSS and ΔPD_200-5 to the changes of AMOC strength forced by meltwater discharge in the North Atlantic (Fig. S8). Therefore, we analyzed how PP in the northeastern BoB responds to AMOC changes in the ESM including the marine biogeochemical component PISCES.~~

~~We analyzed the LGMc and LGMf experiments (section 3.3.2), and the results shown here are the mean of winter months, from December to February (DJF) in the northern BoB (Fig. S7 shows the grids from which the results have been extracted). In the LGMf, the AMOC is progressively getting weaker during the duration of the run (Fig. 3b). Under weakening AMOC conditions, SSS in the northern BoB is getting higher (Fig. 6d). Similar to the results~~

~~of TraCE, the change of SSS contributes to the change of stratification in CM5A (Fig. 6d). The smaller ΔPD_200-5 (weaker stratification) causes the integrated nitrate content of the upper 50 m (NO3_0-50 for short) to increase, and a negative correlation can be seen between them (Fig. 6b). The increasing upper nitrate content results in an increase of the integrated PP, and a positive correlation can be seen between them (Fig. 6a). Consequently, the increased PP is related to weakened stratification caused by higher SSS (Fig. 6c).~~

~~Vertical profiles of the four parameters discussed above (namely: salinity, density, NO3 and PP) were also investigated (Figs. 7 and 8). They show the contrasted response of nitrate concentration in the upper water column (above 40 m) and the lower water column (below 60 m) associated to AMOC reduction. While the upper-water nitrate content increases, the lower-water nitrate content decreases, and the increase is much lower than the decrease (Fig. 8a). Conversely, the PP increase in the upper layer is larger than the decrease in the subsurface (Fig. 8b). This is because photosynthesis rate is much higher in the upper euphotic layer than in the lower euphotic layer, but the upper seawater is nutrient limited. Therefore, PP variations in the NE-BoB driven by changes of AMOC intensity are linked to the upper nutrient availability, which is controlled by the salinity-related stratification.~~

~~The results discussed above are for the DJF mean because modern data show that the highest PP takes place in winter, which contributes about half of the annual gross PP (Fig. 1m). We propose that this mechanism revealed by the DJF mean results of the experiments run with CM5A involving the changed AMOC explains the PP changes in the deglaciation given by our PP record reconstructed by coccoliths assemblages.~~

6~~5~~. Conclusion

We document for the first time,~~We have reconstructed~~ a 26 kyr PP record for the northeastern BoB ~~over the last 26 kyr,~~ using an empirical equation relating Fp% to PP. Comparisons of this PP signal with previous geochemical data and new model outputs helped us proposing two coherent scenarios behind PP distribution during 26–19 kyr BP and 19–1 kyr BP intervals, respectively. In all cases, PP is related to nutrient content and distribution in sea surface. From 26 to 19 kyr BP, when drier and lower sea-level conditions prevailed, millennial-scale PP changes are most probably related to nutrient discharges from the Irrawaddy-Salween river mouth system, that are paced by South Asian monsoon precipitation changes. ~~(including the LGM), data suggest that PP in the northeastern BoB was probably controlled by upper water wind mixing, while relatively dry climate conditions and reduced freshwater inputs to the ocean, prevailed.~~ Over the last 19 kyr, while the sea-level rise and more humid conditions prevailed, millennial-scale PP variations over the deglaciation and long-term trend over the Holovene are rather controlled by salinity-related-stratification that monitor nutrient distribution within the photic zone and is therefore less influenced by nutrient inputs from the IS river mouth system. We demonstrate more generally that stratification dynamic during that period, is driven by Indian Monsoon precipitation changes, that generates changes in freshwater supplies to the ocean. The analysis of climate model outputs provides additional evidences for that salinity-stratification hypothesis and help demonstrating that palaeoceanographic changes are forced by AMOC dynamic during the last deglaciation, and insolation during the Holocene. ~~the PP variations in the NE-BoB are anti-phased with those previously reconstructed for the western and northern AS, and with SSS reconstructions obtained on the same core. Such relationships point that, as for modern setting, the BoB received generally heavier annual precipitations than the AS, and that salinity-related-stratification controlled PP. Stratification changes are driven by Indian Monsoon precipitation dynamic, that generates variations in freshwater supplies to the ocean. The analysis of climate model outputs provides additional evidences for that salinity-stratification mechanism. Together with our PP record and published paleo-climatological and paleo-hydrological records, it demonstrates that during the deglaciation, salinity stratification is related to monsoon precipitation dynamics, which is chiefly forced by insolation and the strength of AMOC. The dramatic decrease of PP in the B-A compare to the HS1 is mainly due to the recovered AMOC which strengthen ISM and upper seawater stratification.~~

Data avalibility

Coccolith data of core MD77-176 can be found in the supplementary materials.~~Data to this paper can be required. Please contact the X. Zhou or S. Duchamp-Alphonse.~~

Supplement

The supplement related to this article is available online

Author contribution

XZ, SDA, MK and CC developed the idea. CC and FB provided sediment samples. XZ did coccolith analysis and visualization of the climate modelling results. The datasets of climate model IPSL-CM5A-LR were provided by MK. FB and LB joined the discussion and gave additional ideas for the manuscript. All authors contribute to the manuscript writing.

Competing interests

The authors declare that they have no conflict of interest.

Acknowledgements

X. Zhou was supported by a PhD scholarship from the China Scholarship Council (CSC) and thank Laboratoire des Sciences du Climat et de l'Environnement (LSCE) for admitting his study related to climate model. He also thanks Hongrui Zhang for personal communication. Th~~e work in this manuscript~~is research was supported by the French Centre national de la recherche scientifique (CNRS).

Reference

Akhil, V. P., Durand, F., Lengaigne, M., Vialard, J., Keerthi, M. G., Gopalakrishna, V. V., Deltel, C., Papa, F. and de Boyer Montegut, C.: A modeling study of the processes of surface salinity seasonal cycle in the Bay of Bengal., Journal of Geophysical Research: Oceans, 119, 3926–3947, 2014.

~~Altabet, M. A., Higginson, M. J. and Murray, D. W.: The effect of millennial-scale changes in Arabian Sea denitrification on atmospheric~~ ~~CO_2~~~~, Nature, 415, 159–162, 2002.~~

~~Anand, P., Kroon, D., Singh, A. D., Ganeshram, R. S., Ganssen, G and Elderfield, H.: Coupled sea surface temperature seawater~~ ~~$\delta^{18}O$~~ ~~reconstructions in the Arabian Sea at the millennial scale for the last 35 ka, Paleoceanography, 23, PA4207, 2008.~~

Anderson, D. M. and Prell, W. L.: The structure of the southwest monsoon winds over the Arabian Sea during the late Quaternary: observation, simulations, and marine geologic evidence, Journal of Geophysical Research, 97, 15481–15487, 1992.

Ashok, K., Guan, Z., Saji, N. H. and Yamagata, T.: Individual and combined inflences of ENSO and the Indian Ocean Dipole on the Indian Summer Monsoon, Journal of Climate, 17, 3141–3155, 2004.

Aumont, O. and Bopp, L.: Globalizing results from ocean in situ iron fertilization studies, Global Biogeochemical Cycle, 20, GB2017, 2006.

Barber, D. C., Dyke, A., Hillaire-Marcel, C., Jennings, A. E., Andrews, J. T., Kerwin, M. W., Bilodeau, G., McNeely, R., Southon, J., Morehead, M. D. and Gagnon, J.-M.: Forcing of the cold event of 8,200 years ago by catastrophic drainage of Laurentide lakes, Nature, 400, 344–348, 1999.

Bassinot, F. C., Marzin, C., Braconnot, P., Marti, O., Mathien-Blard, E., Lombard, F. and Bopp, L.: Holocene evolution of summer winds and marine productivity in the tropical Indian Ocean in response to insolation forcing: data-model comparison, Climate of the Past, 7, 815–829, 2011.

Beaufort, L., Lancelot, Y., Camberlin, P., Cayre, O., Vincent, E., Bassinot, F. and Labeyrie, L.: Insolation cycles as a major control of Equatorial Indian Ocean primary production, Science, 278, 1451–1454, 1997.

Beaufort, L., Barbarin, N. and Gally, Y.: Optical measurements to determine the thickness of calcite crystals and the mass of thin carbon particles such as coccoliths, Nature Protocols, 9, 633–642, 2014.

Behara, A. and Vinayachandran, P. N.: An OGCM study of the impact of rain and river water forcing on the Bay of Bengal, Journal of Geophysical Research: Oceans, 121, 2425–2446, 2016.

Behrenfeld, M. J. and Falkowski, P. G.: Photosynthetic rates derived from satellite-based chlorophyll concentration, Limnology and Oceanography, 42, 1–20, 1997.

Behrenfeld, M. J., O'Malley, R. T., Siegel, D. A., McClain, C. R., Sarmiento, J. L., Feldman, G. C., Milligan, A. J., Falkowski, P. G., Letelier, R. M. and Boss, E. S.: Climate-driven trends in contemporary ocean productivity, Nature, 444, 752–755, 2006.

Belyaeva, N. V. and Burmistrova, I. I.: Critical carbonate levels in the Indian Ocean, Journal of Foraminiferal Research, 15, 337–341, 1985.

Braconnot, P., Otto-Bliesner, B., Harrison, S., Joussaume, S., Peterchmitt, J.-Y., Abe-Ouchi, A., Crucifix, M., Driesschaert, E., Fichefet, Th., Hewitt, C. D., Kageyama, M., Kitoh, A., Laîné, A., Loutre, M.-F., Marti, O., Merkel, U., Ramstein, G., Valdes, P., Weber, S. L., Yu, Y., and Zhao, Y.: Results of PMIP2 coupled simulations of the Mid-Holocene and Last Glacial Maximum – Part 1: experiments and large-scale features, Climate of the Past, 3, 261–277, 2007a.

Braconnot, P., Otto-Bliesner, B., Harrison, S., Joussaume, S., Peterchmitt, J.-Y., Abe-Ouchi, A., Crucifix, M., Driesschaert, E., Fichefet, Th., Hewitt, C. D., Kageyama, M., Kitoh, A., Loutre, M.-F., Marti, O., Merkel, U., Ramstein, G., Valdes, P., Weber, L., Yu, Y., and Zhao, Y.: Results of PMIP2 coupled simulations of the Mid-Holocene and Last Glacial Maximum – Part 2: feedbacks with emphasis on the location of the ITCZ and mid- and high latitudes heat budget, Clim. Past, 3, 279–296, https://doi.org/10.5194/cp-3-279-2007, 2007b.

Braconnot, P., Harrison, S. P., Kageyama, M., Bartlein, P. J., Masson-Delmotte, V., Abe-Ouchi, A., Otto-Bliesner, B., and Zhao, Y.: Evaluation of climate models using palaeoclimatic data, Nature Climate Change, 2, 417–424, 2012.

Briegleb, B. P., Bitz, C. M., Hunke, E. C., Lipscomb, W. H., Holland, M., Schramm, J. L. and Moritz, R. E.: Scientific description of the sea ice component in the Community Climate System Model, Version 3, University Corporation for Atmospheric Research, 2004.

Buckley, M. W. and Marshall, J.: Observations, inferences, and mechanisms of the Atlantic Meridional Overturning Circulation: A review, Reviews of Geophysics, 54, 5–63, 2016.

Cai, Y., Zhang, H., Cheng, H., An, Z., Edwards, R. L., Wang, X., Tan, L., Liang, F., Wang, J. and Kelly, M.: The Holocene Indian Monsoon variablility over the southern Tibetan Plateau and its teleconnections, Earth and Planetary Science Letter, 335–336, 135–144, 2012.

Chen, T.-C.: Maintenance of summer monsoon circulations: a planetary-scale perspective, Journal of Climate, 16, 2022–2037, 2003.

Chiba, S., Ono, T., Tadokoro, K. and Midorikawa, T.: Increased stratification and decreased lower trophic level productivity in the Oyashio Region of the North Pacific: A 30-year retrospective study, Journal of Oceanography, 60, 149–162, 2004.

Ciais, P., Petit., J. R., Jouzel, J., Lorius, C., Barkov, N. I., Lipenkov. V. and Nicolaiev, V.: Evidence for an early Holocene climatic optimum in the Antarctic deep ice-core record, Climate Dynamics, 6, 169–177, 1992.

Clark, P. U., Shakun, J. D., Baker, P. A.: Global climate evolution during the last deglaciation: PNAS, 109, E1134–E1142, 2012.

Clement, A. C. and Peterson, L. C.: Mechanisms of abrupt climate change of the last glacial period, Reviews of Geophysics, 46, RG4002, 2008.

~~Colin, C., Turpin, L., Blamart, D., Frank, N., Kissel, C. and Duchamp, S.: Evolution of weathering patterns in the Indo-Burman Ranges over the last 280 kyrs: Effect of sediment provenance on 87Sr/86Sr ratios tracer, Geochemistry, Geophysics, Geosystems, 7, Q03007. 2006.~~

Collins, W. D., Bitz, C. M., Blackmon, M. L., Bonan, G. B., Bretheton, C. S., Carton, J. A., Chang, P., Doney, S. C., Hack, J. J., Henderson, T. B., Kiehl, J. T., Large, W. G., McKenna, D. S., Santer, B. D. and Smith, R. D.: The Community Climate System Model Version 3 (CCSM3), Journal of Climate, 19, 2122–2143, 2006a.

Collins, W. D., Rasch, P. J., Boville, B. A., Hack, J. J., McCaa, J. R., Williamson, D. L. and Briegleb, B. P.: The formulation and atmospheric simulation of the Community Atmosphere Model Version 3 (CAM3), Journal of Climate, 19, 2144–2161, 2006b.

Contreras-Rosales, Jennerjahn, T., Tharammal, T., Meyer, V., L. A., Lückge, A., Paul, A. and Schefuß, E.: Evolution of the Indian Summer Monsoon and terrestrial vegetation in the Bay of Bengal region during the past 18 ka, Quaternary Science Reviews, 102, 133–148, 2014.

~~Cullen, J. L.: Microfossil evidence for changes salinity patterns in the Bay of Bengal over the last 20 000 years, Palaeogeography, Palaeoclimatology, Palaeoecology, 35, 315–356, 1981.~~

Cullen, J. L and Prell, W. L.: Planktonic foraminifera of the northern Indian Ocean: Distribution and preservation in surface sediments, Marine Micropaleontology, 9, 1–52, 1984.

Currie, J. C., Lengaigne, M., Vialard, J., Kaplan, D. M., Aumont, O., Naqvi, S. W. A. and Maury, O.: Indian Ocean Dipole and El Niño/Southern Oscillation impacts on regional chlorophyll anomalies in the Indian Ocean, Biogeosciences, 10, 6677–6698, 2013.

Da Silva, R., Mazumdar, A., Mapder, T., Peketi, A., Joshi, R. K., Shaji, A., Mahalashmi, P., Sawant, B., Naik, B. G.., Carvalho, M. A. and Molletti, S. K.: Salinity stratification controlled productivity variation over 300 ky in the Bay of Bengal, Scientific Reports, 7, 14439, 2017.

Dey, S., Singh, R. P.: Comparison of chlorophyll distribution in the northeastern Arabian Sea and southern Bay of Bengal using IRS-P4 Ocean Color Monitor data, Remote Sensing of Environment, 85, 424–428, 2003.

Dickinson, R. E., Oleson, K. W., Bonan, G., Hoffman, F., Thirnton, P., Vertenstein, M., Yang, Z.-L. and Zeng, X.: The Community Land Model and its climate statistics as a component of the Community Climate System Model, Journal of Climate, 19, 2302–2324, 2006.

Duchamp-Alphonse, S., Siani, G, Michel, E., Beaufort, L, Gally, Y. and Jaccard, S. L.: Enhanced ocean-atmosphere carbon partitioning via the carbonate counter pump during the last deglacial, Nature Communications, 9, 2396, 2018.

Dutt, S., Gupta, A. K., Clemens, S. C., Cheng, H., Singh, R. K., Kathayat, G and Edwards, R. L.: Abrupt changes in Indian summer monsoon strength during 33,800 to 5500 years B.P., Geophysical Research Letters, 42, 5526–5532, 2015.

Dufresne, J.-L., Foujols, M.-A., Denvil, S., et al: Climate change projections us- ing the IPSL-CM5 Earth System Model: from CMIP3 to CMIP5, Climate Dynamics, 40, 2123–2165, 2013.

~~Duplessy, J. C.: Glacial to interglacial contrasts in the northern Indian Ocean, Nature, 195, 494–498, 1982.~~

Elliot, M., Labeyrie, L. and Duplessy, J.-C.: Changes in North Atlantic deep-water formation associated with the Dansgaard-Oeschger temperature oscillations (60–10 ka), Quaternary Science Reviews, 21, 1153–1165, 2002.

Fichefet, T. and Maqueda, M. A. M.: Sensitivity of a global sea ice model to the treatment of ice thermodynamics and dynamics, Journal of Geophysical Research-Ocean, 102, 12609–12646, 1997.

Fleitmann, D., Burns, S. J., Mudelsee, M., Neff, U., Kramers, J., Mangini, A. and Matter, A.: Holocene forcing of the Indian Monsoon recored in a stalagmite from southern Oman, Science, 300, 1737–1739, 2003.

Fournier, S., Vialard, F., Lengaigne, M., Lee, T., Gierach, M. M. and Chaitanya, A. V. S.: Modulation of the Ganges-Brahmaputra River Plume by the Indian Ocean Dipole and Eddies inferred from satellite observations, Journal of Geophysical Research: Ocean, 122, 9591–9604, 2017.

Gadgil, S.: The Indian Monsoon and its variability, Annual Review of Earth Planetary Science, 31, 429–467, 2003.

Gardner, W. D., Gundersen, J. S., Richardson, M. J. and Walsh.: The role of seasonal and diel changes in mixed-layer depth on carbon and chlorophyll distributions in the Arabian Sea, Deep-Sea Research Ⅱ, 46, 1833–1858, 1999.

Gauns, M., Madhupratap, M., Ramaiah, N., Jyothibabu, R., Fernandes, V., Paul, J. T. and Prasanna Kumar, S.: Comparative accounts of biological productivity characteristics and estimates of carbon fluxes in the Arabian Sea and the Bay of Bengal, Deep-Sea Research Ⅱ, 52, 2003–2017, 2005.

Gebregiorgis, D., Hathorne, E. C., Sijinkumar, A. V., Nagender Nath, B., Nürnberg, D.: South Asian summer monsoon variability during the last ~54 kyrs inferred from surface salinity and river runoff proxies, Quaternary Science Reviews, 138, 6–15, 2016.

Goswami, B. N., Madhusoodanan, M. S., Neema, C. P. and Sengupta, D.: A physical mechanism for North Atlantic SST influence on the Indian summer monsoon, Geophysical Research Letters, 33, L02706, 2006.

~~Govil, P. and Naidu, P. D.: Variations of Indian monsoon precipitation during the last 32 kyr reflected in the surface hydrography of the Western Bay of Bengal, Quaternary Science Reviews, 30, 3871–3879, 2011.~~

Gupta, A. K., Andrews, D. M. and Overpeck, J. T.: Abrupt changes in the Asian southwest monsoon during the Holocene and their links to the North Atlantic Ocean, Nature, 421, 354–357, 2003.

He, F.: Simulating transient climate evolution of the last deglaciation with CCSM3, PhD. dissertation, University of Wisconsin-Madison, 2008.

Heinrich, H.: Origin and consequences of cyclic ice rafting in the northeast Atlantic Ocean during the past 130,000 years, Quaternary Research, 29, 142–152, 1988.

Hernández-Almeida, I., Ausín, B., Saavedra-Pellitero, M., Baumann, K.-H. and Stoll, H. M.: Quantitative reconstruction of primary productivity in low latitudes during the last glacial maximum and the mid-to-late Holocene from a global *Florisphaera profunda* calibration dataset, Quaternary Science Reviews, 205, 166–181, 2019.

Hourdin, F., Foujols, M.-A., Codron, F., Guemas, V., Dufresne, J.- L., Bony, S., Denvil, S., Guez, L., Lott, F., Ghattas, J., Braconnot, P., Marti, O., Meurdesoif, Y., and Bopp, L.: Impact of the LMDZ atmospheric grid configuration on the climate and sensitivity of the IPSL-CM5A coupled model, Clim. Dynam., 40, 2167–2192, https://doi.org/10.1007/s00382-012-1411-3, 2013.

Ivanochko, T. S., Ganeshram, R. S., Brummer, G. A., Ganssen, G., Jung, S. J. A., Moreton, S. G. and Kroon, D.: Variations in tropical convection as an amplifier of global climate change at the millennial scale, Earth and Planetary Science Letters, 235, 302–314, 2005.

Ivanova, E., Schiebel, R., Singh, A. D., Schmiedl, G., Niebler, H.-S. and Hemleben, C.: Primary production in the Arabian Sea during the last 135 000 years, 197, 61–82, 2003.

Jourdain, N. C., Gupta, A. S., Taschetto, A. S., Ummenhofer, C. C., Moise, A. F. and Ashok, K.: The Indo-Australian monsoon and its relationship to ENSO and IOD in reanalysis data and the CMIP3/CMIP5 simulations, Climate Dynamics, 41, 3073–3102, 2013.

Kageyama, M., Merkel, U., Otto-Bliesner, B., Prange, M., Abe-Ouchi, A., Lohmann, G., Ohgaito, R., Roche, D. M., Singarayer, J., Swingedouw, D. and Zhang, X.: Climatic impacts of fresh water hosing under Last Glacial Maximum conditions: a multi-model study, Climate of the Past, 9, 935–953, 2013.

~~Keen, T. R., Kindle, J. C. and Young, D. K: The interaction of southwest monsoon upwelling, advection and primary production in the northwest Arabian Sea, Journal of Marine Systems, 61–82, 1997.~~

Krinner, G., Viovy, N., de Noblet-Ducoudré, N., Ogée, J., Polcher, J., Friedlingstein, P., Ciais, P., Sitch, S., and Prentice, I. C.: A dynamic global vegetation model for studies of the cou- pled atmosphere-biosphere system, Global Biogeochemistry Cycle, 19, GB1015, 2005.

~~Kudrass, H. R., Hofmann, A., Doose, H., Emeis, K. and Erlenkeuser, H.: Modulation and amplification of climatic changes in the Northern Hemisphere by the Indian summer monsoon during the past 80 k.y., Geology, 29, 63–66, 2001.~~

~~Kutzbach, J. E.: Monsoon Climate of the Early Holocene: Climate Experiment with the Earth's Orbital Parameters for 9000 Years Ago, Science, 214, 59–61, 1981.~~

~~Kutzbach, J. E. and Street-Perrott, F. A: Milankovitch forcing of fluctuations in the level of tropical lakes from 18 to 0 kyr BP, Nature, 317, 130–134, 1985.~~

Lau, K.-M., Kim, K.-M., Yang, S.: Dynamicsal and boundary forcing characteristics of regional components of the Asian Summer Monsoon, Journal of Climate, 13, 2461–2482, 2000.

Le Mézo, P., Beaufort, L., Bopp, L., Braconnot, P and Kageyama, M.: From monsoon to marine productivity in the Arabian Sea: insights from glacial and interglacial climates, Climate of the Past, 13, 759–778, 2017.

Lévy, M., Klein, P and Treguier, A.-M.: Impact of sub-mesoscale physics on production and subduction of phytoplankton in an oligotrophic regime, journal of Marine Research, 59, 535–565, 2001.

Li, S., Perlwitz, J., Quan, X. and Hoerling, M. P.: Modelling the influence of North Atlantic multidecadal warmth on the Indian summer rainfall, Geophysical Research Letters, 35, L05804, 2008.

Li, J., Liu, S., Shi, X., Zhang, H., Fang, X., Cao, P., Yang, G., Xue, X., Khokiattiwong, S. and Kornkanitnan, N.: Sedimentary responses to the sea level and Indian summer monsoon changes in the central Bay of Bengal since 40 ka, Marine Geology, 415, 105947, 2019.

Liu, Z., Otto-Bliesner, B. L., He, F., Brady, W. C., Tomas, R., Clark, P. U., Carlson, A. E., Lynch-Stieglitz, J., Curry, W., Brook, E., Erickson, D., Jacob, R., Kutzbach, J. and Cheng, J.: Transient Simulation of Last Deglaciaiton with a new mechanism for Bølling-Allerød Warming, Science, 325, 310–314, 2009.

~~Liu, Z., Wen, X., Brady, E. C., Otto-Bliesner, B., Yu, G., Lu, H., Cheng, H., Wang, Y., Zheng, W., Ding, Y., Edwards, R. L., Cheng, J., Liu, W. and Yang, H.: Chinese cave records and the East Asia Summer Monsoon, Quaternary Science Reviews, 83, 115–128, 2014.~~

Locarnini, R. A., Mishonov, A. V., Antonov, J. I., Boyer, T. P., Garcia, H. E., Baranova, O. K., Zweng, M. M., Johnson, D. R.: World ocean atlas 2009, In: Levitus, S. (Ed.), Temperature, 1. Government Printing Office, Washington, D.C., p. 184. NOAA Atlas NESDIS 68, 2010.

Ludwig, W., Probst, J, L. and Kempe, S.: Predicting the oceanic input of organic carbon by continental erosion, Global Biogeochemisry Cycle 10, 23–41, 1996.

Madec, G.: NEMO ocean engine, Note du pôle de modélisation, Institut Pierre-Simon Laplace (IPSL), France, No. 27 ISSN No. 1288-1619, 2008.

Madhupratap, M., Prasanna Kumar, S., Bhattathiri, P. M. A., Dileep Kumar, M., Raghukumar, S., Nair, K. K. C. and Ramaiah, N.: Mechanism of the biological response to winter cooling in the northeastern Arabian Sea, Nature, 384, 549–552, 1996.

~~Lu, R., Dong, B. and Ding, H.: Impact of the Atlantic Multidecadal Oscillation on the Asian summer monsoon, Geophysical Research Letters, 33, L24701, 2006.~~

Madhupratap, M., Gauns, M., Ramaiah, N., Prasanna Kumar, S., Muraleedharan, P. M., Sousa, S. N. and Muraleedharan, U.: Biogeochemistry of the Bay of Bengal: physical, chemical and primary productivity characteristics of the central and western Bay of Bengal during summer monsoon 2001, Deep-Sea Research Ⅱ, 50, 881–896, 2003.

~~Mark, B. G., Harrison, S. P., Spessa, A., New, M., Evans, D. J. A. and Helmens, K. F.: Tropical snowline changes at the last glacial maximum: A global assessment, Quaternary International, 138–139, 168–201, 2005.~~

Marzin, C. and Braconnot, P.: Variations of Indian and African monsoons induced by insolation changes a 6 and 9.5 kyr BP, Climate Dynamics, 33, 215–231, 2009.

Marzin, C., Kallel, N., Kageyama, M., Duplessy, J.-C. and Braconnot, P.: Glacial fluctuations of the Indian monsoon and their relationship with North Atlantic climate: new data and modeling experiments, Climate of the Past. 9, 2135–2151, 2013.

McCreary, J. P., Murtugudde, R., Vialard, J., Vinayachandran, P. N., Wiggert, J. D., Hood, R. R., Shankar, D. and Shetye, S.: Biophysical processes in the Indian Ocean, Geophysical Monograph Series, 2009.

McGee, D., Donohoe, A., Marshall, J. and Ferreira, D.: Changes in ITCZ location and cross-equatorial heat transport at the Last Glacial Maximum, Heinrich 1, and the mid-Holocene, Earth and Planetary Science Letters, 390, 69–79, 2014.

McManus, J. F., Francois, R., Gherardi, J.-M., Keigwin, L. D. and Brown-Leger, S.: Collapse and rapid resumption of Atlantic meridional circulation linked to deglacial climate changes, Nature, 834–837, 2004.

~~Madec, G.: NEMO ocean engine, Note du pôle de modélisation, Institut Pierre-Simon Laplace (IPSL), France, No. 27 ISSN No. 1288-1619, 2008.~~

Meehl, G. A.: Couple land-ocean-atmosphere processes and South Asian Monsoon variability, Science, 266, 263–267, 1994.

Meehl, G. A.: The South Asian Monsoon and the Tropospheric Biennial Oscillation, Journal of Climate, 10, 1921–1943, 1997.

~~McCreary, J. P., Murtugudde, R., Vialard, J., Vinayachandran, P. N., Wiggert, J. D., Hood, R. R., Shankar, D. and Shetye, S.: Biophysical processes in the Indian Ocean, Geophysical Monograph Series, 2009.~~

~~McManus, J. F., Francois, R., Gherardi, J.-M., Keigwin, L. D. and Brown-Leger, S.: Collapse and rapid resumption of Atlantic meridional circulation linked to deglacial climate changes, Nature, 834–837, 2004.~~

Molfino, B. and McIntyre, A.: Precessional forcing of nutricline dynamics in the Equatorial Atlantic, Science, 249, 766–769, 1990a.

Molfino, B. and McIntyre, A.: Nutricline variation in the Equatorial Atlantic coincident with the Younger Dryas, Paleoceanography, 5, 997–1008, 1990b.

Murton, J. B., Bateman, M. D., Dallimore, S. R., Teller, J. T. and Yang, Z.: Identification of Younger Dryas outburst flood path from Lake Agassiz to the Arctic Ocean, Nature, 464, 740–743, 2010.

Okada, H. and Honjo, S.: The distribution of oceanic coccolithophorids in the Pacific, Deep-Sea Research, 20, 355–374, 1973.

Overpeck, J., Anderson, D., Trumbore, S. and Prell, W.: The southwest Indian Monsoon over the last 18 000 year, Climate Dynamics, 12, 213–225, 1996.

Patterson, R. T., and Fishbein, E.: Re-examination of the statistical methods used to determine the number of point counts needed for micropaleontological quantitative research, J. Paleontol., 63(2), 245–248, 1984.

Pausata, F. S. R., Battusti, D. S., Nisancioglu, K. H. and Bitz, C. M.: Chinese stalagmite $\delta^{18}O$ controlled by changes in the Indian monsoon during a simulated Heinrich event, Nature Geoscience, 4, 474–480, 2011.

Peltier, W. R.: Global glacial isostasy and the surface of the ice-age earth: The ICE-5G (VM2) model and GRACE, Annual Review of Earth and Planetary Sciences, 32, 111–149, 2004.

Peterson, L. C., Haug, G. H., Hughen, K. A. and Röhl, U.: Rapid changes in the hydrologic cycle of the tropical Atlantic during the last Glacial, Science, 290, 1947–1951, 2000.

Peterson, L. C. and Huang, G. H.: Variability in mean latitude of the Atlantic Intertropical Convergence Zone as recorded by riverine input of sediments to the Cariaco Basin (Venezuela), Palaeogeography, Palaeoclimatology, Palaeoecology, 234, 97–113, 2006.

Phillips, S. C., Johnson, J. E., Giosan, L. and Rose, K.: Monsson-influenced variation in productivity and lithogenic sediment flux since 110 ka in the offshore Mahanadi Basin, northern Bay of Bengal, Marine and Petroleum Geology, 58, 502–525, 2014.

Prasad, T. G.: A comparison of mixed-layer dynamics between the Arabian Sea and Bay of Bengal: One-dimensional model results, Journal of Geophysical Research, 109, C03035, 2004.

Prasanna Kumar, S., Madhupratap, M., Dileep Kumar, M., Muraleedharan, P. M., de Souza, S. N., Gauns, M and Sarma, V. V. S. S.: High biological productivity in the central Arabian Sea during the summer monsoon driven by Ekman pumping and lateral advection, Current Science, 81, 1633–1638, 2001.

Prasanna Kumar, S., Muraleedharan, P. M., Prasad, T. G., Gauns, M., Ramaiah, N., de Souza, S. N., Sardesai, S. and Madhupratap, M.: Why is the Bay of Bengal less productive during summer monsoon compared to the Arabian Sea? Geophysical Research Letters, 29, 2235, 2002.

Prasanna Kumar, S., Narvekar, J., Nuncio, M. Ganus, M. and Sardesai, S.: What drives the biological productivity of the Northern Indian Ocean, Geophysical Monograph Series, 2009.

Randel, W. J. and Park, M.: Deep convective influence on the Asian summer monsoon anticyclone and associated tracer variability observed with Atmospheric Infrared Sounder (AIRS). J. Geophys. Res. Atmos., 111, D12314, 2006.

Rao, S. A., Saha, S. K., Pokhrel, S., Sundar, D., Dhakate, A. R., Mahapatra, S., Ali, S., Chaudhari, H. S., Shreeram, P., Vasimalla, S., Srikanth, A. S. and Suresh, R. R. V.: Modulation of SST, SSS over northern Bay of Bengal on ISO time scale, Journal of Geophysical Research, 116, C09026, 2011.

Rao, R. R. and Sivakumar, R.: Seasonal variability of sea surface salinity and salt budget of the mixed layer of the north Indian Ocean, Journal of Geophysical Research, 108, C13009, 2003.

Rashid, H., Flowe, B. P. Poore, R. Z. and Quinn, T. M.: A ~25ka Indian Ocean monsoon variability record from the Andaman Sea, Quaternary Science Reviews, 26, 2586–2597, 2007.

Schott, F.: Monsoon response of the Somali Current and associated upwelling, Progress in Oceanography, 12, 357–381, 1983.

Schott, F. A. and McCreary, J. P.: The monsoon circulation of the Indian Ocean, Progress in Oceanography, 51, 1–123, 2001.

Schneider, T., Bischoff, T. and Huang, G. H.: Migrations and dynamics of the intertropical convergence zone, Nature, 513, 45–53, 2014.

Schulz, H., von Rad, U. and Erlenkeuser, H.: Correlation between Arabian Sea and Greenland climate oscillations of the past 110,000 years, Nature, 393, 54–57, 1998.

Sengupta, D., Bharath Raj, G. N. and Shenoi, S. S. C.: Surface freshwater from Bay of Bengal runoff and Indonesian Throughflow in the tropical Indian Ocean, Geophysical Research Letters, 33, L22609, 2006.

Shankar, D., Vinayachandran, P. N. and Unnikrishnan, A. S.: The monsoon currents in the north Indian Ocean, Progress in Oceanography, 52, 63–120, 2002.

Shenoi, S. S. C., Shankar, D., Shetye, S. R.: Differences in heat budgets of the near-surface Arabian Sea and Bay of Bengal: Implications for the summer monsoon, Journal of Geophysical Research, 107, C63052, 2002.

~~Shi, Y.: Characteristics of late Quaternary monsoonal glaciation on the Tibetan Plateau and in East Asia, Quaternary International, 97–98, 79–91, 2002.~~

Shi, W, Morrison, J. M., Bryden, H. L.: Water, heat and freshwater flux out of northern Indian Ocean in September–October 1995, Deep-Sea Research II, 49, 1231–1252, 2002.

Sijinkumar, A. V., Clemens, S., Nath, B. N., Prell, W., Benshila, R. and Lengaigne, M.: $\delta^{18}O$ and salinity variability from the Last Glacial Maximum to Recent in the Bay of Bengal and Andaman Sea, Quaternary Science Reviews, 135, 79–91, 2016.

~~Sinha, A., Cannariato, K. G., Stott, L. D., Li, H.-C., You, C.-F., Cheng, H., Edwards, R. L. and Singh, I. B.: Variability of Southwest Indian summer monsoon precipitation during Bølling-Ållerød, Geology, 33, 813–816, 2005.~~

~~Singh, A. and Jani, R. A. and Ramesh, R.: Saptiotemporal variations of the $\delta^{18}O$-salinity relation in the northern Indian Ocean, Deep-Sea Research I, 57, 1422–1431, 2010.~~

Singh, A. D., Jung, S. J. A., Darling, K., Ganeshram, R., Ivanochko, T, and Kroon, D.: Productivity collapses in the Arabian Sea during glacial cold phases, Paleoceanography, 26, PA3210, 2011.

~~Sirocko, F., Garbe-Schönberg, D., McIntyre, A. and Molfino, B.: Teleconnections between the subtropical monsoons and high-latitude climates during the Last Deglaciation, Science, 272, 526–529, 1996.~~

Smith, R. D. and Gent, P. R.: Reference manual for the Parallel Ocean Program (POP), ocean component of the Community Climate System Model (CCSM2.0 and 3.0), Los Alamos National Laboratory, LAUR-02-2484, 2002.

Spiro Jaeger, G. and Mahadevan, A.: Submesoscale-selective compensation of fronts in a salinity-stratified ocean, Science Advance, 4, e1701504, 2018.

~~Stuiver, M. and Grootes, P. M.: GISP2 oxygen isotope ratios, Quaternary Research, 53, 277–284, 2000.~~

Stocker, T. F. and Johnsen, S. J.: A minimum thermodynamics model for the bipolar seesaw, Paleoceanography, 18, 1087, 2003.

Stoll H. M., Arevalos, A., Burke, A., Ziveri, P., Mortyn, G., Shimizu, N. and Unger, D.: Seasonal cycles in biogenic production and export in Northern Bay of Bengal sediments traps, Deep-Sea Research Ⅱ, 54, 558–580, 2007.

Swingedouw, D., Mignot, J., Braconnot, P., Mosquet, E., Kageyama, M. and Alkama, R.: Impact of freshwater release in the North Atlantic under different climate conditions in an OAGCM, Journal of Climate, 22, 6377–6403, 2009.

Taylor, K. E., Stouffer, R. J. and Meehl, G. A.: An overview of CMIP5 and the experiment design, BAMS, 93, 485–498, 2012.

van de Poll, W. H., Kulk, G., Timmermans, K. R., Brussaard, C. P. D., van der Woerd, H. J., Kehoe, M. J., Mojica, K. D. A., Visser, R. J. W., Rozema, P. D. and Buma, A. G. J.: Phytoplankton chlorophyll α biomass, composition, and productivity along a temperature and stratification gradient in the northeast Atlantic Ocean, Biogeosciences, 10, 4227–4240, 2013.

~~Veldhuis, M. J. W.: Seasonal and spatial variability in phytoplankton biomass, productivity and growth in the northwestern Indian Ocean: the southwest and northeast monsoon, 1992–1993, Deep-Sea Research, 44, 425–449, 1997.~~

Vinayachandran, P. N., Murty, V. S. N., Ramesh Bahu, V.: Observations of barrier layer formation in the Bay of Bengal during summer monsoon, Journal of Geophysical Research, 107, 8018, 2002.

Vinayachandran, P. N., Chauhan, P, Mohan, M. and Nayak, S.: Biological response of the sea around Sri Lanka to summer monsoon, Geophysical Rearch Letter, 31, L01302, 2004.

Wang, B., Clemens, S. C and Liu, P.: Contrasting the Indian and East Asian monsoons: implications on geologic timescales, Marine Geology, 201, 5–21, 2003.

Wang, B., Yang, J., Zhou, T. and Wang, B.: Interdecadal changes in the major modes of Asian-Australian Monsoon variability: strengthening relationship with ENSO since the late 1970s, Journal of Climate, 21, 1771–1788, 2008.

Wang, X., Auler, A. S., Edwards, R. L., Cheng, H., Cristalli, P. S., Smart, P. L., Richards, D. A. and Shen, C.-C.: Wet periods in northeastern Brazil over the past 210 kyr linked to distant climate anomalies, Nature, 432, 740–743, 2004.

Webster, P. J., Magaña, V. O., Palmer, T. N., Shukla, J. Tmas, R. A., Yanai, M. and Yasunari, T.: Monsoons: Processes, predictability, and the prospects for prediction, Journal of Geophysical Research, 103, 14451–14510, 1998.

~~Wen, X., Liu, Z., Wang, S., Cheng, J. and Zhu, J.: Correlation and anti-correlation of the East Asian summer and winter monsoons during the last 21,000 years, Nature Communications, 7, 11999, 2016.~~

Wolff, E. W., Chappellaz, J., Blunier, T., Rasmussen, S. O. and Svensson, A.: Millennial-scale variability during the last glacial: The ice core record, Quaternary Science Reviews, 29, 2828–2838, 2010.

Yu, S.-Y., Colman, S. M. Lowell, T. V., Milne, G. A., Fisher, T. G., Breckenridge, A., Boyd, M. and Teller, J. T.: Freshwater ourbrust from Lake Superior as a trigger for the cold event 9300 years ago, Science, 328, 1262–1266, 2010.

Zhang, H., Liu, C., Jin, X., Shi, J., Zhao, S. and Jian, Z.: Dynamics of primary productivity in the northern South China Sea over the past 24,000 years, Geochemistry, Geophysics, Geosystems, 17, 4878–4891, 2016.

~~Zhang, R. and Delworth, T. L.: Simulated tropical response to a substantial weakening of the Atlantic thermohaline circulation, Journal of Climate, 18, 1853–1860, 2005.~~

~~Zhao, Y. and Harrison, S. P.: Mid-Holocene monsoons: a muti-model analysis of the inter-hemispheric differences in the responses to orbital forcing and ocean feedbacks, Climate Dynamics, 39, 1457–1487, 2012.~~

Figures

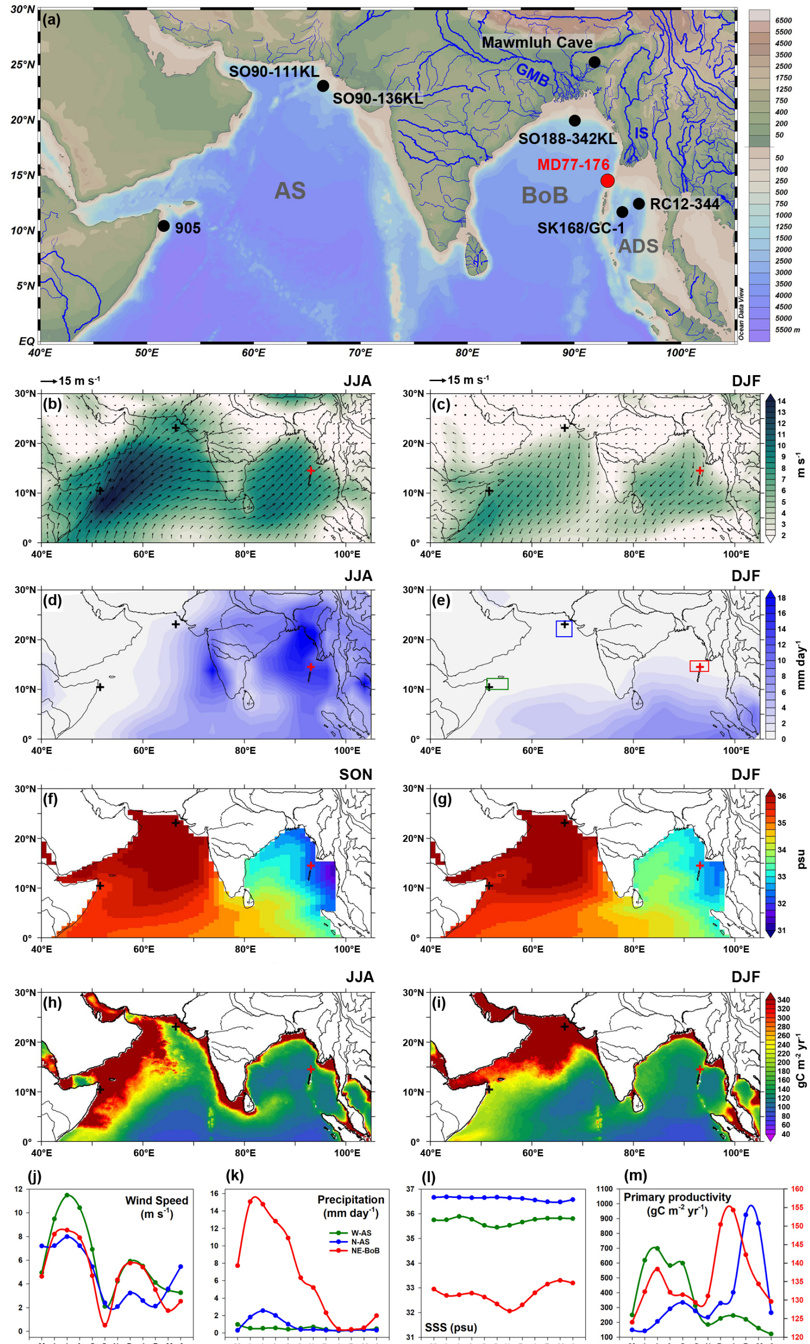

(a)
Mawmluh Cave
SO90-111KL
SO90-136KL
GMB
SO188-342KL
IS
MD77-176
AS
BoB
RC12-344
905
SK168/GC-1
ADS
Ocean Data View
(b)
JJA
15 m s-1
(c)
DJF
m s-1
(d)
JJA
(e)
DJF
mm day-1
(f)
SON
(g)
DJF
psu
(h)
JJA
(i)
DJF
gC m-2 yr-1
(j)
Wind Speed (m s-1)
(k)
Precipitation (mm day-1)
W-AS
N-AS
NE-BoB
(l)
SSS (psu)
(m)
Primary productivity (gC m-2 yr-1)

Fig. 1. (a) Geographic setting and bathymetric map of Indian Monsoon climate zone including the Arabian Sea (AS), the Bay of Bengal (BoB) and the Andaman Sea (ADS),~~.~~ the Ganges-Brahmaputra-Meghna river system (GMB), and the Irrawaddy-Salween river system (IS). The map was created by the Ocean Data View software (©Reiner Schlitzer, Alfred Wegener Institute) with its built-in global high resolution bathymetric data (GlobHR). Location of the sediment core ~~of~~ MD77-176~~the current study~~ is marked by the red circle. Black circles mark the locations of published records shown in Fig. 6~~4~~. (b) and (c) Mean (from 1979 to 2018) surface wind speed and wind vectors for north hemisphere (NH) summer (June~~,~~ July~~,~~ August, JJA) and winter (December~~,~~ January~~,~~ February, DJF), respectively. Data is from NCEP-DOE Reanalysis 2 (http:// esrl.noaa.bov/psd/data/grided/data.ncep.reanalysis2.html). (d) and (e) Mean (from 1979 to 2018) precipitation rate for NH winter and summer respectively. Data is from CPC Merged Analysis of Precipitation (http:// esrl.noaa.bov/psd/data/grided/data.ncep.camp.html). (f) and (g) Mean (from 1979 to 2018) surface seawater salinity (SSS) for NH autumn (September, October, November, SON) and winter respectively. Data is from NCEP Global Ocean Data Assimilation System (http:// esrl.noaa.bov/psd/data/grided/data.godas.html). (h) and (i) Mean (from 2003 to 2018) net primary productivity for NH summer and winter respectively. PP data is based on MODIS chlorophyll-a and calculated using the Vertical Generalized Production Model (VGPM; Behrenfeld and Falkowski, 1997)~~ model~~ (http:// science.oregonstate.edu/ocean.productivity). (j), (k), (l) and (m) Regional climatology and oceanography in the western AS, northern AS and northeastern BoB. The~~ selected~~ regions of data extracting are marked by color rectangles in (e). Data sources are the same with above.

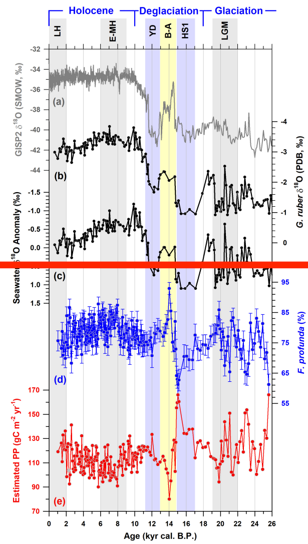

~~**Fig. 2.** (a) GISP2 Greenland ice core δ^{18}O signal (Stuiver and Grootes, 2000). (b) *Globigerinoides ruber* δ^{18}O record of core MD77-176 (Marzin et al., 2013). (c) Seawater δ^{18}O anomaly obtained on core MD77-176 (Marzin et al., 2013). (d) *F. profunda* relative abundance (Fp%) of core MD77-176 (this study). The error bars mark the 95% intervals. (e) Primary productivity calculated by MD77-176 Fp% using the tropical Indian Ocean empirical equation (Hernández-Almeida et al., 2019).~~

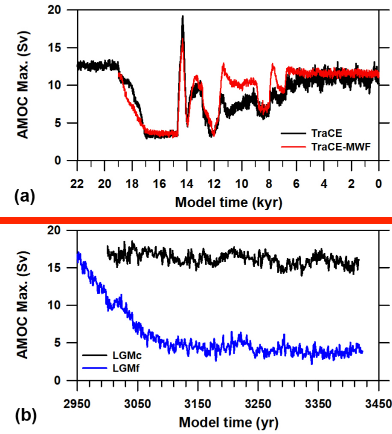

AMOC Max. (Sv)
TraCE
TraCE-MWF
Model time (kyr)
(a)
AMOC Max. (Sv)
LGMc
LGMf
Model time (yr)
(b)

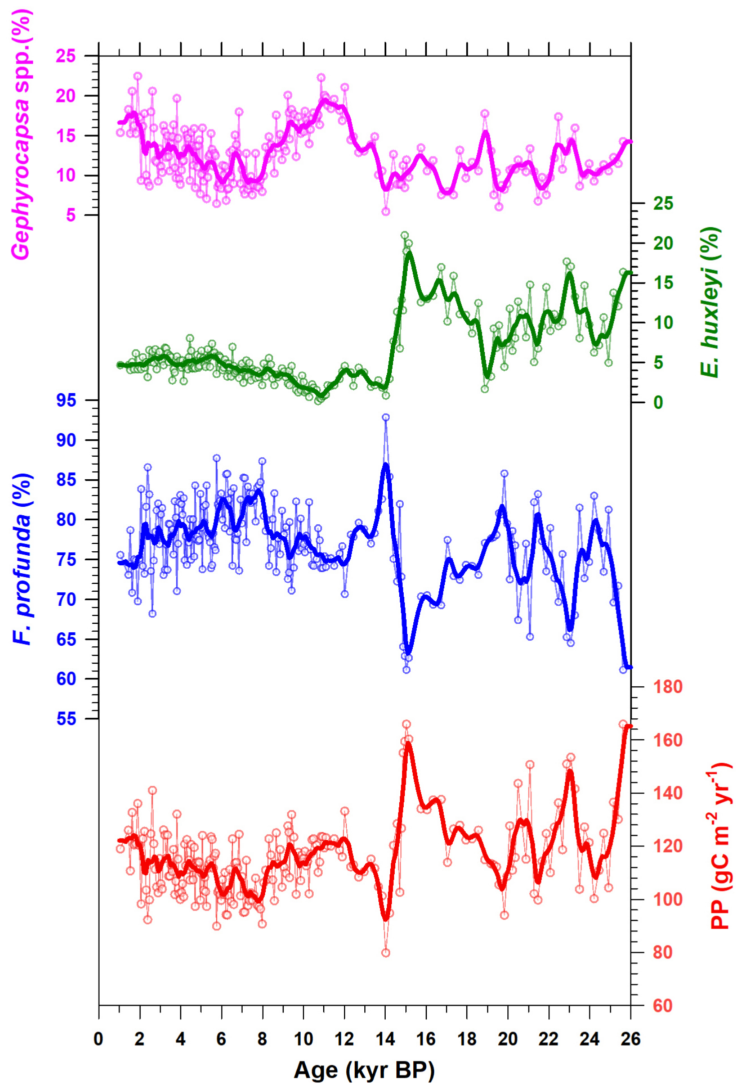

Fig. 2.– Relative abundance changes (%) of main coccolith species and reconstructed PP of core MD77-176: *Gephyrocapsa* spp. (pink), *Emiliania huxleyi* (green), *Florisphaera profunda* (blue), PP (red). The curves are smoothed results (five-point moving average of 0.1 kyr interpolation of original data).~~The changes of the maximum in the AMOC streamfunction below 500 m (AMOC strength) in (a) TraCE and TraCE-MWF experiments, and in (b) LGMc and LGMf experiments run with IPSL-CM5A-LR.~~

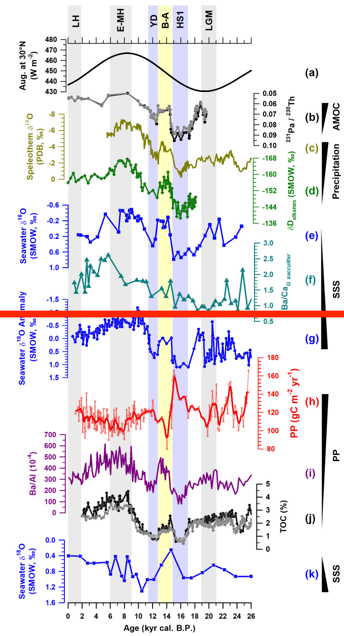
LH
E-MH
YD
B-A
HS1
LGM
Aug. at 30°N (W m-2)
(a)
231Pa / 230Th
(b)
AMOC
Speleothem δ18O (PDB, ‰)
(c)
Precipitation
(d)
Seawater δ18O (SMOW, ‰)
(e)
(f)
SSS
(g)
PP (gC m-2 yr-1)
(h)
Ba/Al (10-4)
(i)
PP
TOC (%)
(j)
Seawater δ18O (SMOW, ‰)
(k)
SSS
Age (kyr cal. B.P.)

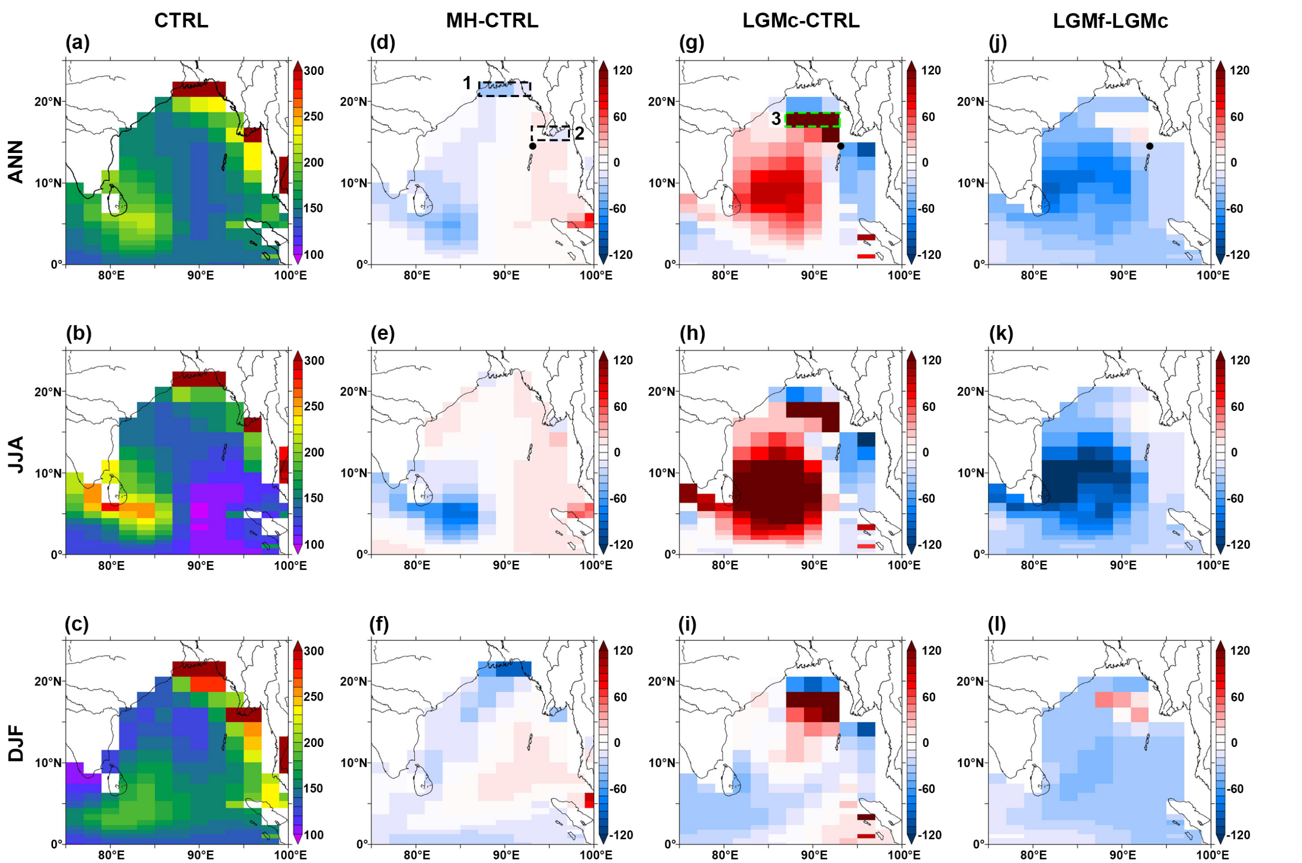

Fig. 3. IPSL-CM5A-LR simulated integrated PP of the full water column (in gC m^{-2} yr^{-1}) of the pre-industrial (CTRL) (a–c), and PP differences between the mid-Holocene (MH) and CTRL (d–f), the Last Glacial Maximum (LGMc) and CTRL (g–i), and the Last Glacial Maximum under AMOC shutdown (LGMf) and LGMc (j–l). Results are shown for annual mean (ANN), summer (June–July–August, JJA) and winter (December–January–February, DJF) seasons. The rectangles 1 and 2 on (d), mark the grids from which the vertical profiles on Fig. 4 are extracted. The rectangle 3 on (e), marks the grids from which the vertical profiles on Fig. 5 are extracted. The black dots mark the location of core MD77-176.~~(a) August mean insolation at 30°N. (b) AMOC strength indicated by $^{231}Pa/^{230}Th$ ratio of marine sediment from the western subtropical Atlantic Ocean (McManus et al., 2004). (c) Mawmluh Cave speleothem $\delta^{18}O$ (Dutt et al., 2015). (d) Alkane δD in marine sediment, core SO188-342 (Contreras-Rosales et al., 2016). (e) Seawater $\delta^{18}O$ record of core RC12-344 (Rashid et al., 2007). (f) Ba/Ca ratios derived from mixed layer foraminifer species *Globigerinoides sacculifer* from core SK 168/GC-1(Gebregiogis et al., 2016). (g) Seawater $\delta^{18}O$ anomaly record of core MD77-176 (Marzin et al., 2013). (h) Estimated PP record of core MD77-176 (this study). The thick red curve shows the result of a 500-year smoothing.~~

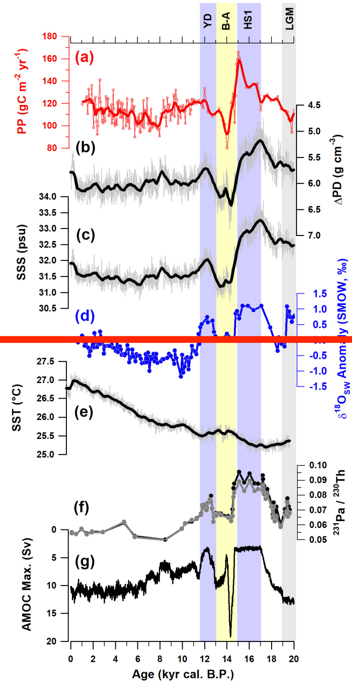

YD
B-A
HS1
LGM
PP (gC m-2 yr-1)
(a)
(b)
ΔPD (g cm-3)
SSS (psu)
(c)
(d)
δ18Osw Anomaly (SMOW, ‰)
SST (°C)
(e)
(f)
231Pa / 230Th
(g)
AMOC Max. (Sv)
Age (kyr cal. B.P.)

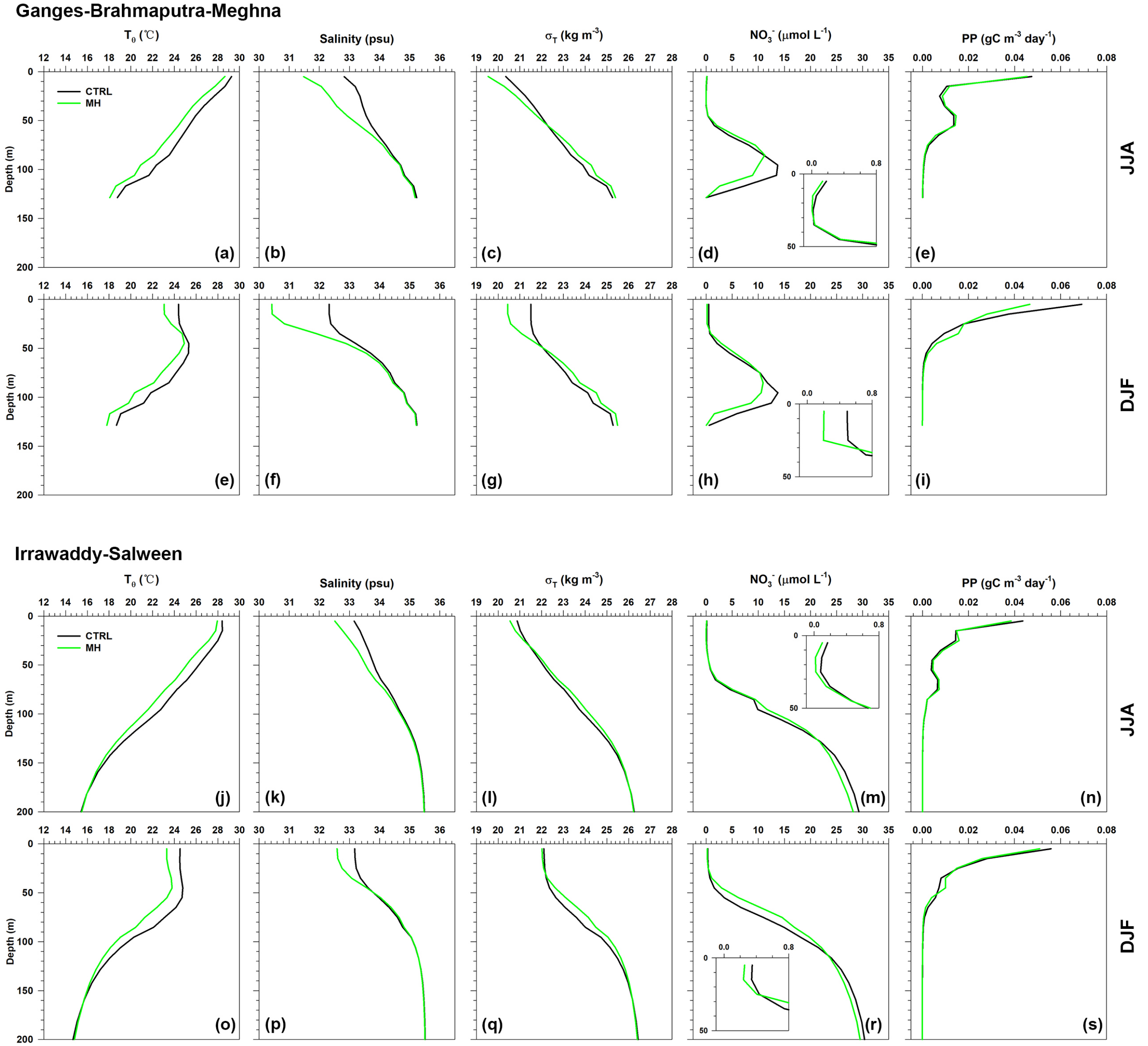

Fig. 4. Simulated ocean profiles between 0 and 200 water depths, in the MH and CTRL simulations run with IPSL-CM5A-LR. Data of (a)–(i) have been extracted from the grids located in the Ganges-Brahmanputra-Meghna river mouth (the rectangle 1 on Fig. 3d). (a)–(e) Results of summer (June–July–August, JJA). (f)–(i) Results of winter (December–January–February, DJF). Data of (j)–(s) have been extracted from the grids located in the Irrawaddy-

Salween river mouth (the rectangle 2 on Fig. 3d). (j)–(n) Results of summer (JJA). (o)–(s) Results of winter (DJF). The parameters shown here are potential temperature (T_θ), salinity, potential density (sigma-t, σ_T), nitrate concentration of seawater representing seawater nutrient content (NO_3^-), and total primary productivity (PP). Nutricline, halocline, pycnocline are the depths with largest vertical gradients of nutrient content, potential density and salinity under the upper seawater layers. ~~(a) Estimated-PP of core MD77-176 (this study). (b), (c), (e) and (g) are the results of the TraCE-21 simulation outputs of oceanic parameters in the northeastern BoB (the data grids are marked in Fig. S7). (b) Annual mean potential density difference between 200 and 5 m water depth (ΔPD). (c) Annual mean SSS (5m); (d) Seawater $\delta^{18}O$ anomaly record of core MD77-176 (Marzin et al., 2013). (e) Annual mean SST (5m). (f) AMOC strength indicated by $^{231}Pa/^{230}Th$ ratio of marine sediment from the western subtropical Atlantic Ocean (McManus et al., 2004). (g) Maximum flux of the AMOC in the TraCE-21 simulation.~~

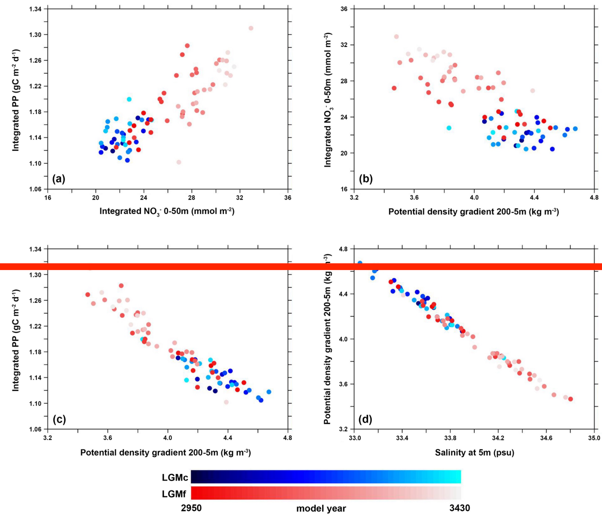
(a)
Integrated PP (gC m-2 d-1)
Integrated NO3- 0-50m (mmol m-2)
(b)
Integrated NO3- 0-50m (mmol m-2)
Potential density gradient 200-5m (kg m-3)
(c)
Integrated PP (gC m-2 d-1)
Potential density gradient 200-5m (kg m-3)
(d)
Potential density gradient 200-5m (kg m-3)
Salinity at 5m (psu)
LGMc
LGMf
2950
model year
3430

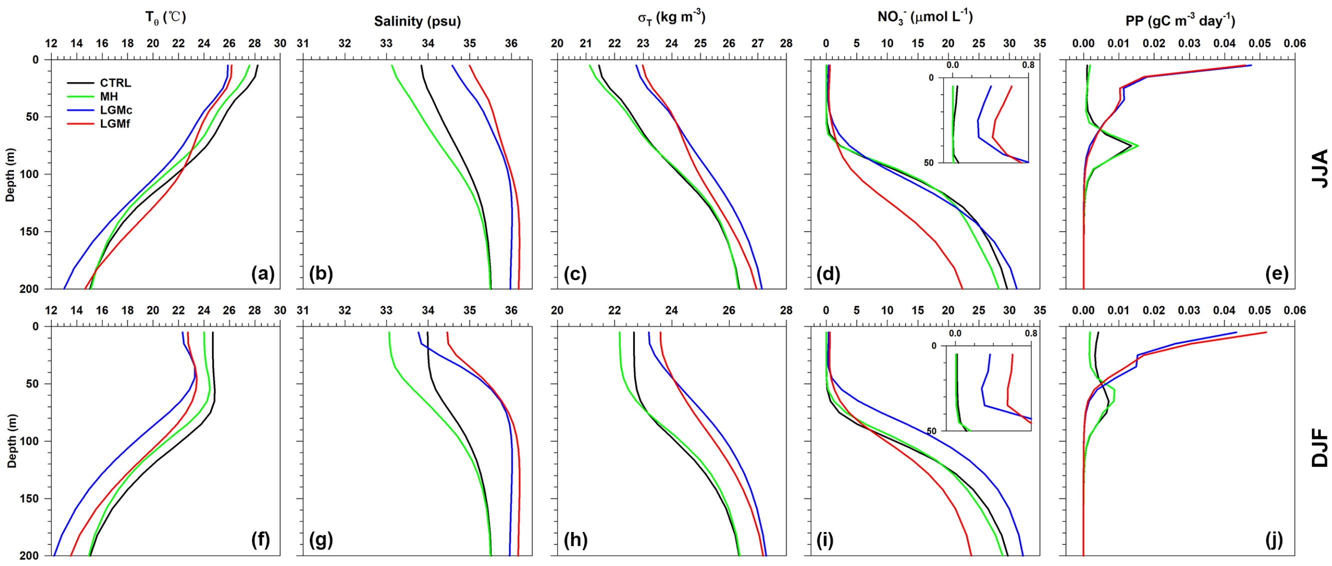

Fig. 5. Simulated ocean profiles between 0 and 200 water depth, in four experiments run with IPSL-CM5A-LR. (a)–(e) Results of summer (June–July–August, JJA). (f)–(j) Results of winter (December–January–February, DJF). Data have been extracted from the grids located in the northeastern part of the BoB closed to the MD77-176 core site (the rectangle 3 on Fig. 3e). The parameters shown here are potential temperature (T_θ), salinity, potential density (sigma-t, σ_T), nitrate concentration of seawater representing seawater nutrient content (NO_3^-), and total primary productivity (PP). Nutricline, halocline, pycnocline are the depths with largest vertical gradients of nutrient content, potential density and salinity under the upper seawater layers.~~Correlations between different oceanic parameters computed with the IPSL-CM5-LR model in experiments LGMc and LGMf for the northern BoB (the data grids are marked in Fig. S7). The results are DJF mean and every dot represents an average of ten model years (section 3.3; Fig. 3b). (a) Integrated nitrate content of the upper 50 m vs integrated PP of the whole seawater column. (b) Potential density difference between 200 and 5 m vs integrated nitrate content of the upper 50 m. (c) Potential density difference between 200 and 5 m vs integrated PP of the whole seawater column. (d) Salinity at 5 m vs potential density difference between 200 and 5 m seawater.~~

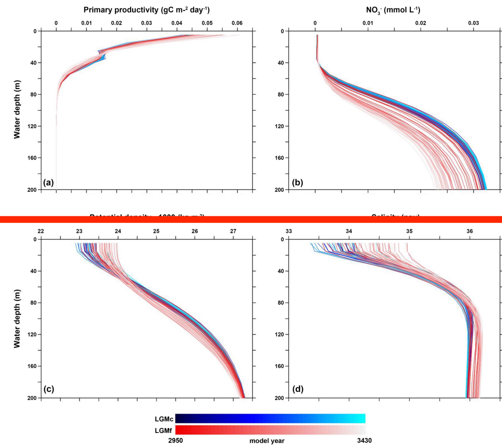

Primary productivity (gC m-2 day-1)
NO3- (mmol L-1)
Water depth (m)
(a)
(b)
(c)
(d)
LGMc
LGMf
2950
model year
3430

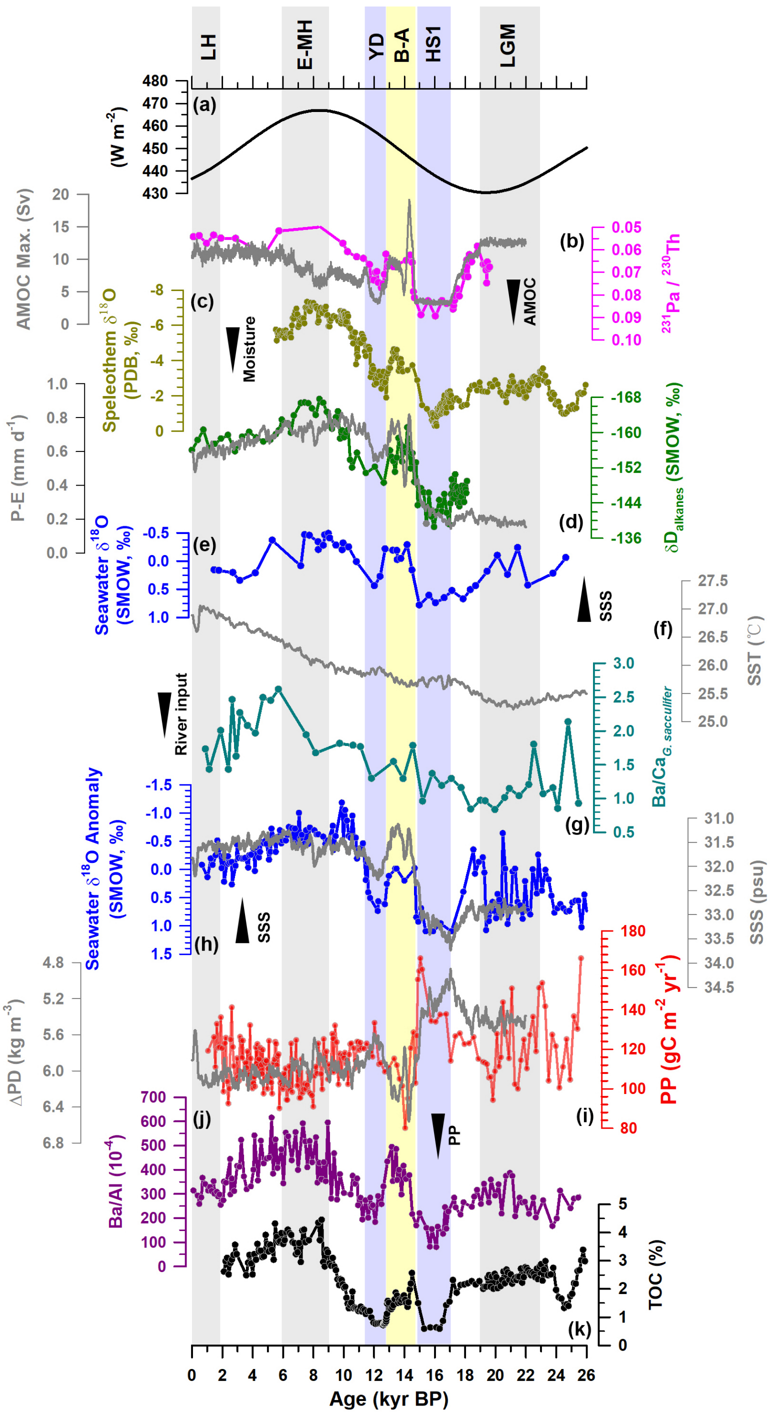

LH
E-MH
YD
B-A
HS1
LGM
(a)
(W m-2)
AMOC Max. (Sv)
(b)
231Pa / 230Th
(c)
Speleothem δ18O (PDB, ‰)
Moisture
AMOC
P-E (mm d-1)
(d)
δDalkanes (SMOW, ‰)
(e)
Seawater δ18O (SMOW, ‰)
SSS
(f)
SST (℃)
River input
Ba/CaG. sacculifer
(g)
Seawater δ18O Anomaly (SMOW, ‰)
(h)
SSS (psu)
ΔPD (kg m-3)
(i)
PP (gC m-2 yr-1)
PP
(j)
Ba/Al (10-4)
(k)
TOC (%)
Age (kyr BP)

Fig. 6. (a) 30°N August insolation (Laskar et al., 2004). (b) AMOC strength indicated by $^{231}Pa/^{230}Th$ ratio of marine sediment from the western subtropical Atlantic Ocean (in pink, McManus et al., 2004). The changes of the maximum in the AMOC stream function below 500 m (AMOC strength) in TraCE-21 (in gray). (c) Mawmluh Cave speleothem $\delta^{18}O$ signal (Dutt et al., 2015). (d) Alkane δD signal in marine core SO188-342 (in green, Contreras-Rosales et al., 2014) and simulated annual mean precipitation minus evaporation of TraCE-21 (in gray). (e) Seawater $\delta^{18}O$ record of core RC12-344 (Rashid et al., 2007). (f) Simulated annual mean SST in the NE-BoB. (g) Ba/Ca ratio derived from mixed layer foraminifer species *Globigerinoides sacculifer* from core SK 168/GC-1 (Gebregiogis et al., 2016). (h) Seawater $\delta^{18}O$ anomaly record of core MD77-176 (Marzin et al., 2013). (i) Estimated PP record of core MD77-176 (this study, in red) and simulated annual mean potential density gradient between 200 and 5 m of TraCE-21 (in gray), that reflect the stratification of the upper seawater (Behrenfeld et al., 2006). (j) Ba/Al ratio of sediment core 905 (Ivanochko et al., 2005). (k) Total organic carbon weight percentage of core SO90-136KL (Schulz et al., 1998). TraCE curves are shown using 100-yr averaged results. The results of single forcing experiments are shown in Fig. S4. Core locations of all these records above are marked in Fig. 1a. Grids of extracted TraCE data are shown in Fig. S5. High-resolution reconstructed and Trace21 data provide coherent climate patterns: i) For 26–19 kyr BP when higher PP is associated with lower SSS and lower moister conditions and vice versa, highlighting the control that river mouth system exert on PP; ii) for 19–11 kyr BP, when higher PP, in phase with AMOC strength, is associated with higher SSS and reduced precipitation, highlighting the impact of high-latitude climate on South Asian precipitation, salinity-related stratification and PP; iii) for 11-1 kyr BP, when higher PP, in phase with August insolation, is associated with higher SSS and reduced precipitation, highlighting the impact of insolation on South Asian precipitation on salinity-related stratification and PP, during the Holocene, and more particularly during the Early Holocene Climatic Optimum (~8–6 kyr BP)~~Vertical profiles of oceanic parameters of the IPSL-CM5-LR experiments LGMc and LGMf in the northern BoB (the data grids are marked in Fig. S7). The results are DJF mean and every curve represents an average of ten model years (section 3.3; Fig. 3b). (a) Primary productivity. (b) Nitrate concentration. (c) Potential density. (d) Salinity~~.

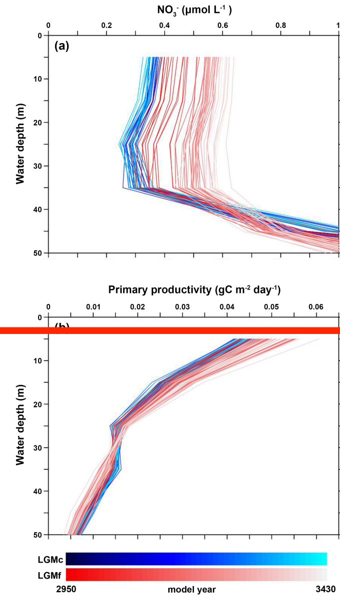
NO3- (µmol L-1)
(a)
Water depth (m)
Primary productivity (gC m-2 day-1)
Water depth (m)
LGMc
LGMf
2950
model year
3430

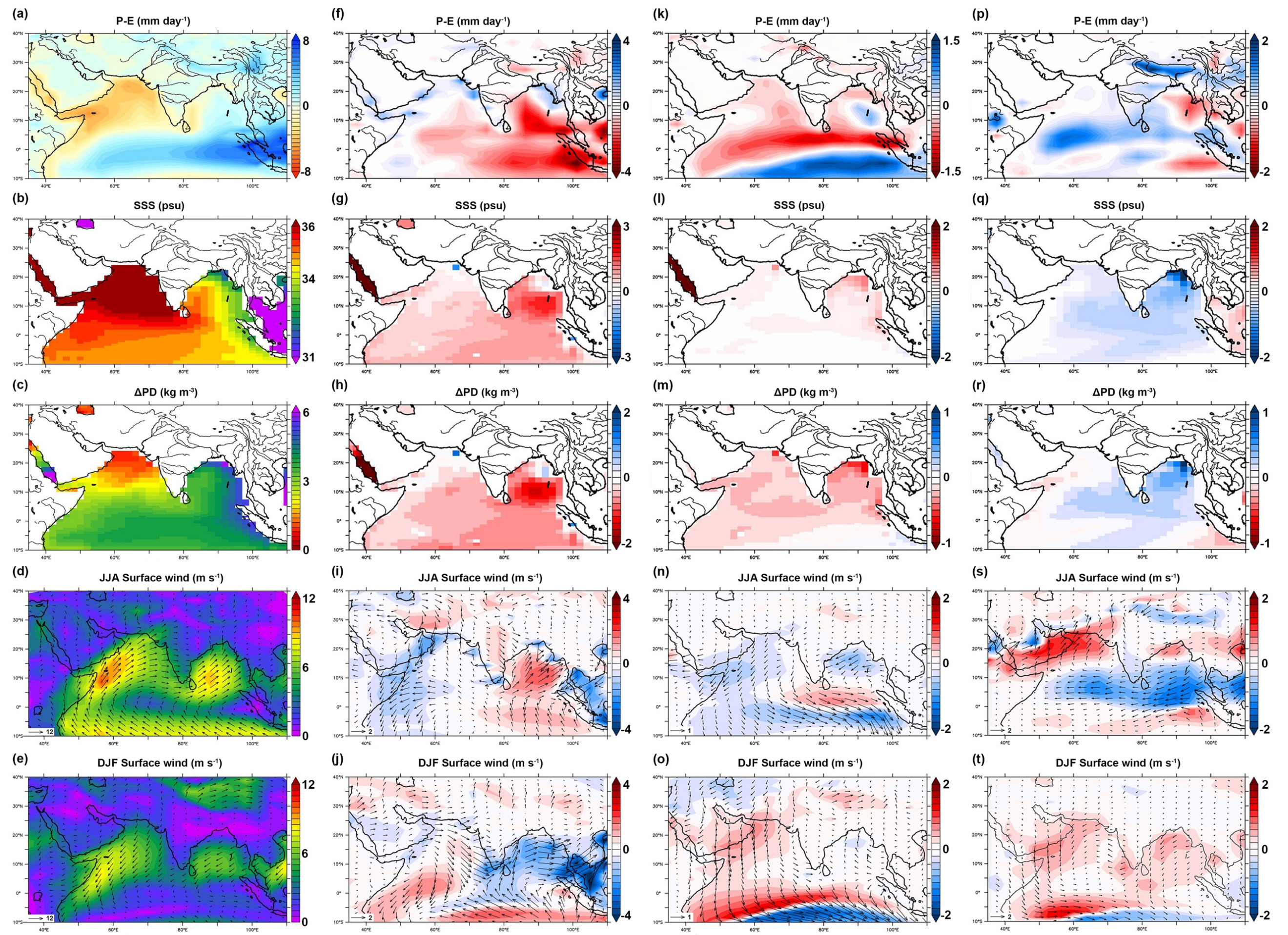

Fig. 7. IPSL-CM5A-LR outputs. (a)–(e) Results of CTRL. (f)–(j) Differences between LGMc and CTRL. (k)–(o) Differences between LGMf and LGMc. (p)–(t) Differences between MH and CTRL. The parameters are annual mean precipitation minus evaporation (P-E, net precipitation), sea surface salinity (SSS), potential density gradient between 200 and 5 m (stratification of the upper seawater; Behrenfeld et al., 2006), summer (June–July–August, JJA) and winter (December–January–February, DJF) surface wind speed and vectors. These figures give the results of simulated changes of climates and oceanic conditions over South Asia and the northern Indian Ocean. Stronger net precipitation is marked by blu color, higher SSS is marked by red color, stronger stratification is marked by blue color and stronger surface wind is marked by red color.

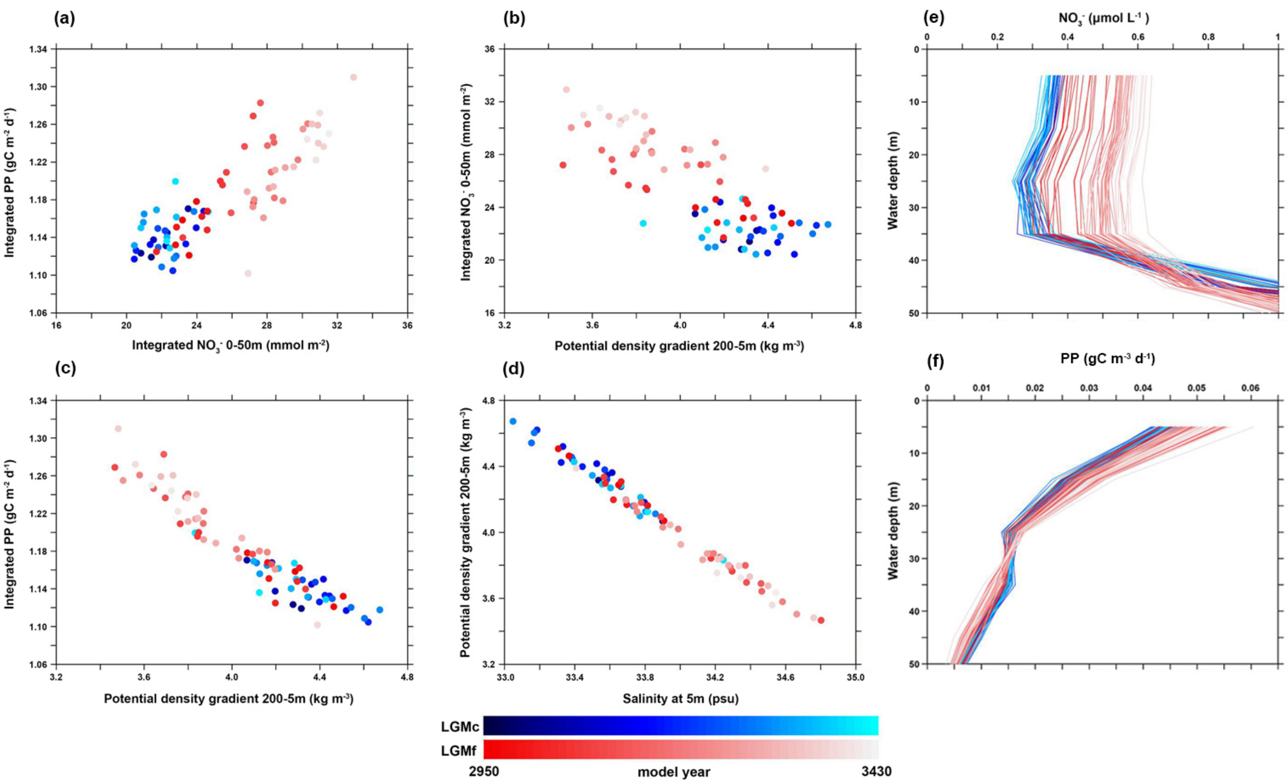

Fig. 8. IPSL-CM5A-LR outputs. (a)–(d) Crossplots between different oceanic parameters of LGMc and LGMf. (e) and (f) Vertical profiles of nitrate content and PP of LGMc and LGMf. All the results are from winter (December–January–February) and every curve represents an average of ten model years. Data have been extracted from the grids located in the northeastern part of the BoB closed to the MD77-176 core site (the rectangle 3 on Fig. 3e). They highlight the control salinity stratification exerts on upper layer nutrient content and integrated PP: higher PP is found when higher SSS drive weaker stratification.~~Vertical profiles of oceanic parameters of the IPSL-CM5-LR experiments LGMc and LGMf in the northern BoB (the data grids are marked in Fig. S7). The results are DJF mean and every curve represents an average of 10 model years (section 3.3; Fig. 3b). (a) Nitrate concentration. (b) Primary productivity.~~